

A Study on Monthly Marine Heatwave Forecasts in New Zealand: An Investigation of Imbalanced Regression Loss Functions with Neural Network Models

Ding Ning^{*1}, Varvara Vetrova¹, Sébastien Delaux², Rachael Tappenden¹, Karin R. Bryan³, and Yun Sing Koh⁴

¹School of Mathematics and Statistics, University of Canterbury

²Oceanum

³School of Environment, University of Auckland

⁴School of Computer Science, University of Auckland

Abstract

Marine heatwaves (MHWs) are extreme ocean-temperature events with significant impacts on marine ecosystems and related industries. Accurate forecasts (one to six months ahead) of MHWs would aid in mitigating these impacts. However, forecasting MHWs presents a challenging imbalanced regression task due to the rarity of extreme temperature anomalies in comparison to more frequent moderate conditions. In this study, we examine monthly MHW forecasts for 12 locations around New Zealand. We use a fully-connected neural network and compare standard and specialized regression loss functions, including the mean squared error (MSE), the mean absolute error (MAE), the Huber, the weighted MSE, the focal-R, the balanced MSE, and a proposed scaling-weighted MSE. Results show that (i) short lead times (one month) are considerably more predictable than three- and six-month leads, (ii) models trained with the standard MSE or MAE losses excel at forecasting average conditions but struggle to capture extremes, and (iii) specialized loss functions such as the balanced MSE and our scaling-weighted MSE substantially improve forecasting of MHW and suspected MHW events. These findings underscore the importance of tailored loss functions for imbalanced regression, particularly in forecasting rare but impactful events such as MHWs.

*Correspondence to: ding.ning@pg.canterbury.ac.nz

1 Introduction

This section provides an overview of marine heatwaves (MHWs), their impacts, and the significance of accurate forecasting methods. It sets the stage for exploring numerical and deep learning (DL) approaches to predict MHWs and related phenomena.

1.1 Marine Heatwaves

MHWs are observed around the world and have strong impacts on marine ecosystems. Such impacts include shifts in species ranges, local extinctions, and can have a follow-on economic impact on seafood industries (Hobday et al., 2016). The devastating impact on marine ecosystems caused by MHWs can bring irreversible loss of species or foundation habitats (Oliver et al., 2019), for example, mass coral bleaching and substantial declines in kelp forests and seagrass meadows (Holbrook et al., 2020). MHWs also affect aquaculture businesses and area-restricted fisheries because of the change of the distribution of sea life with follow on effects on production (Hobday et al., 2018), such as in mussel, oyster and salmon farms. Anthropogenic climate change is expected to cause an increase in both the intensity and frequency of MHWs (Hobday et al., 2016).

MHWs can be characterized using metrics, such as high maximum temperatures (Berkelmans et al., 2004), larger than normal or increasing temperature anomalies (Smale & Wernberg, 2013), and long degree heating days (Maynard et al., 2008). Even with the same metrics, different datasets might provide substantially different MHW information (Hobday et al., 2016). For example, MHWs from daily data show shorter and more intensive events than from monthly data (Hobday et al., 2016), and MHWs vary by location and season. In some related work (Ham et al., 2019; Pravallika et al., 2022; Taylor & Feng, 2022), the departures from the average sea surface temperature (SST) over a certain period were called “temperature anomalies” or “temperature variability”, and sometimes anomalies were called “outliers”. In this study, we define sea surface temperature anomalies (SSTAs) as the departures from the average sea surface temperature over a certain period. Spatially, SSTs or SSTAs at a specific location, as a pixel in gridded data, represent the average SSTs or SSTAs within the area that pixel covers. Referring to Hobday et al. (2016) that used the 90th percentile to define MHWs, we define monthly MHWs as events when the SSTAs greater than the 90th percentile of the SSTAs based on a monthly climatology. For example, a heatwave in January would be defined as an average SSTA for January that is greater than 90% of previous January SSTAs.

1.2 Numerical MHW Forecasts

The ability to accurately predict MHWs, six months in advance for instance, would allow mitigation of their potential impact, for example by collecting healthy samples for repopulation of impacted ecosystems, DNA sampling, and adjusting production beforehand. Dynamical prediction systems have been widely used for MHW forecasts (Merryfield et al., 2013; Saha et al., 2014; Vecchi et al., 2014). For example, a case study of the California Current System MHW of 2014-2016 used eight global coupled climate prediction systems to predict the MHW up to eight months ahead (Jacox et al., 2019). In this case, two of the four phases were predicted well by dynamic models but two others were missed. Moreover, numerical dynamic models are resource intensive, making it difficult to run enough simulations to perform probabilistic projections. At the same time, there have been more and more observations and completed hindcasts, so statistical explorations of the existing data to make forecasts might be a useful alternative to dynamic modeling. In the last ten years, statistical forecasts have become increasingly sophisticated, with innovations in machine learning (ML) methods, especially DL, being at the forefront.

1.3 Deep Learning for SST, SSTA, and MHW Forecasts

A number of ML techniques have been applied to predicting SSTAs and/or SSTA-related climate events. We focus on recent DL approaches to this task. Early work started with convolutional neural networks (CNNs), which have been widely used for spatiotemporal representation learning, and adopted some image and video learning techniques to environmental spatiotemporal data. Ham et al. (2019, 2021) used a CNN with SSTAs as one of the inputs to forecast the seasonal Nino3.4 SSTA index up to 18 months ahead, which is a climate index based on the SST field over the tropical eastern Pacific that characterizes the El Niño-Southern Oscillation (ENSO) in the equatorial Pacific Ocean. Another distinctive aspect of their work was the application of transfer learning to improve prediction, by leveraging two supplementary datasets. Then Cachay et al. (2021) used a graph neural network (GNN) to tackle the same ENSO forecasting task proposed by Ham et al. (2019) and outperformed the CNNs for one to six lead month forecasts. For other neural network classes for SSTA-related event forecasts, Ratnam et al. (2020) proposed a fully-connected neural network (FCN) to forecast SSTAs over the Indian Ocean, which are the indicators of the Indian Ocean Dipole (IOD). Also, the IOD forecasts have been made using an LSTM (Pravallika et al., 2022) and a CNN (Feng et al., 2022). Moreover, a CNN was developed to forecast SSTs and MHWs around Australia (Boschetti et al., 2022). Later work started to address the combination of multiple neural network classes for SST, SSTA, or SSTA-related climate event forecasts. Taylor &

Feng (2022) combined the U-Net (Ronneberger et al., 2015) with an LSTM to forecast SSTs up to 24 months ahead and validated the forecasts with a focus on specific SST variability-related oscillations (ENSO and IOD) and climate events (the Blob MHW). The U-Net-LSTM used SSTs as one of the inputs to predict SSTs, which then were converted into the Nino3.4 and Nino4 indices and the Blob index. The Blob index is the difference between the monthly average SST climatology (1980-2010) and the monthly average SST computed over the oceanic area off the west coast of the United States, as an indicator of MHWs. In this DL framework, to forecast SSTs, the spatial dependencies and the dependencies between variables were captured by the convolutional autoencoder, the short-term temporal dependencies were captured by the sliding window method, and the long-term temporal dependencies were captured by the LSTM. Taylor & Feng (2022) also mentioned the possible deficiency of transfer learning, which is insufficient to correct the inherent biases in the coupled models (Timmermann et al., 2018), and highlighted the feasibility of knowledge-based physics-informed ML (Karniadakis et al., 2021).

In terms of ML for SSTA-related oscillation or climate event forecasts, the majority of the attempts to predict SSTs or SSTAs have focused on reproducing the average conditions but not the extremes, such as the ENSO (Ham et al., 2019; Taylor & Feng, 2022; Boschetti et al., 2022) and IOD (Wu & Tang, 2019; Ratnam et al., 2020; Feng et al., 2022) forecasts. Nevertheless, the extremes, like MHWs, are much more damaging to ecosystems and productivity, and their forecasts are useful for the climate domain. For example, Ham et al. (2019); Pravallika et al. (2022); Taylor & Feng (2022) generally formulated the ML tasks for SST or SSTA-related event forecasts as a standard regression or classification task (using a standard loss function) and focused on reproducing the average conditions. However, forecasting SSTA anomalies or extremes calls for a different approach. A label, which is a continuous quantity or a category that a ML model aims to predict, is typically assumed to have a uniform distribution in most ML algorithms. However, label imbalance is common in real-world ML tasks, such as fraud detection, social media spam detection, disease diagnosis, and natural disaster forecasts, where the labels of interest are rare or underrepresented when compared to the other labels. In our proposed ML framework, we view the forecasting tasks as imbalanced regression (for imbalanced labels) to be able to explore the techniques to handle anomalies. We started with imbalanced regression because SSTAs are a continuous variable, and treating different continuous labels as distinct classes is unlikely to yield optimal results because it does not take advantage of the similarity between nearby continuous labels (Yang et al., 2021). However, Berg et al. (2021) pointed out that for deep ordinal regression, training a classifier, particularly when utilizing their proposed label devising approach, could outperform training a regressor in terms of accuracy. It is important to note that their approach

was not specifically designed for label imbalance tasks. Therefore, in this study, we still place emphasis on imbalanced regression for SSTA and MHW forecasts.

Approaches to tackle imbalanced regression were generally extended from those for imbalanced classification, which can be categorized into two groups: the data-based and the model-based. Data-based approaches to imbalanced classification include oversampling the minority class, undersampling the majority class, and combining both (Chawla et al., 2002; García & Herrera, 2009; He et al., 2008). These data re-sampling techniques were later introduced to imbalanced regression (Torgo et al., 2013; Branco et al., 2017; Yang et al., 2021). Model-based approaches include re-weighting or adjusting the loss function to compensate for class imbalance (Cao et al., 2019; Cui et al., 2019; Dong et al., 2018; Huang et al., 2016, 2019), and applying relevant auxiliary techniques, such as transfer learning (Yin et al., 2019), metric learning (Zhang et al., 2018), meta-learning (Shu et al., 2019), two-stage training (Kang et al., 2019), and semi-supervised learning and self-supervised learning (Yang & Xu, 2020). The loss function approaches were later introduced to imbalanced regression (Yang et al., 2021; Ren et al., 2022).

In all, we have defined SSTAs and MHWs for this study. We reviewed the numerical approaches and statistical DL approaches for SSTA-related oscillation and MHW forecasts, including different neural network classes with highlighted auxiliary techniques that tackled the forecasts. We then framed the task of forecasting MHWs in New Zealand as an imbalanced regression problem. Subsequently, we reviewed the approaches adapted from tackling imbalanced classification, which were specifically developed for imbalanced regression. In the next subsection, we will present the research questions of this study.

1.4 Research Questions

Having conducted a literature review on the DL approaches for SSTA and MHW forecasts, as well as the strategies for tackling imbalanced regression, we are now equipped to establish our research objectives. Alongside this review, we have also defined the essential concepts in this study, including SSTAs, MHWs, and the framed imbalanced regression task for forecasting monthly MHWs in New Zealand. Considering these elements, we propose a two-fold aim for this study.

First, this study aims to investigate the appropriate loss functions for a specific imbalanced regression task: monthly MHW forecasts in New Zealand. A loss function compares observed (target) values with predicted values and measures how well ML models the training data, and the choice of a loss function is a crucial factor that influences the performance of a ML model (Nie et al., 2018). A loss function for imbalanced regression accom-

modates the imbalanced training label distribution and leads to a better predictive performance on rare labels (Ren et al., 2022), which are the predicted values of the anomalies or extremes in this case study of MHWs. Related work can be divided into two categories: one is customizing a loss function for specific case studies, such as wind speed forecasts (Chen et al., 2020), COVID-19 diagnosis (Khakzar et al., 2021), and speech quality evaluation (Martin-Donas et al., 2018). The other is proposing a general loss function, such as the focal-R loss (Yang et al., 2021) and the balanced MSE loss (Ren et al., 2022). We synthesized the two approaches to propose a custom scaling-weighted loss function and compared it with the other commonly used regression loss functions for monthly MHW forecasts in New Zealand.

Second, this study aims to identify the degree to which the monthly MHWs at 12 selected New Zealand locations can be predicted by ML models based on regional data, for one, two, three, and six months in advance, especially using the loss functions investigated in the first aim. The formulated imbalanced regression task for forecasting MHWs, which focuses on extreme value or outlier prediction, is different from the balanced regression task for forecasting SSTs or SSTAs. We evaluated the predictions for extreme values and compared the ML models with the persistence models spatially and temporally. The second aim will provide a better understanding of the MHW’s predictability with appropriate predictors and models.

2 Data

This section outlines the dataset used in this study, detailing the preprocessing steps and the rationale behind the selection of specific data points. The goal is to ensure the data is suitable for developing and testing the proposed ML models for forecasting SSTAs and MHWs.

2.1 Dataset

The dataset we used in this study is the Simple Ocean Data Assimilation (SODA) (Carton & Giese, 2008), Version 2.2.4. It is global numerical modeling data available from January 1871 to December 2010, with a spatial resolution of 0.5×0.5 degrees. SODA is an ocean reanalysis dataset that describes the evolution of a number of ocean variables, including the ocean temperature, over a four dimensional grid (latitude, longitude, depth, and time). We used the version 2.2.4 of the dataset as it extends over a longer period and thus provides more training data than other more recent versions of the reanalysis. MHWs are found at any depth in the water column, but there has been a trend of observing MHWs at the surface because sea temperature measurements at the surface are much more abundant as only the temperature at the surface can be measured by satellites. Thus the MHWs

in our research is focused on surface MHWs, although in the future for better prediction it could be useful to explore the use of temperatures at other depths (often in the shape of heat content) and the use of other variables. We considered the temperature in the grid cells that are the nearest to the surface (depth of 5 meters) to represent the sea surface temperature (SST).

SODA 2.2.4 is available on the website of the Asia-Pacific Data-Research Center (APDRC) (Asia-Pacific Data Research Center, accessed 2022), a part of the International Pacific Research Center at the University of Hawai'i at Mānoa. The extracted multidimensional grid was of three dimensions (the longitude, 720 degrees from -179.75 to 179.75, the latitude, 330 degrees from -75.25 to 89.25, and the time, 1680 months from January 1871 to December 2010) and one channel (the temperature). We mainly used this SST grid for analysis and experiments.

2.2 Data Preprocessing

We preprocessed the extracted SST grid into separate sequences that are SST time series at 20 different ocean locations. The 12 locations in New Zealand were referred to the locations of interest for MHW forecasts in the Moana Project (MetOcean Solutions, accessed 2023), which uses numerical ocean models to forecast SSTs and MHWs up to seven days in advance. The aim of our research is to extend the MHW forecasts from a daily to a seasonal basis at these selected locations. The 12 locations, which are close to major human settlements and cover most of New Zealand's surrounding oceanic waters, provide MHW forecasts with greater socioeconomic value and representativeness. We also selected eight locations in the two areas where the movement of seawater potentially has an impact on the SSTs in New Zealand. The four locations are in the East Australian Current (Sutton & Bowen, 2019; Elzahaby et al., 2021) and the other four locations are in an area in the Central Pacific, east of North Cape (Sutton & Bowen, 2019). The SSTs in these two areas have been demonstrated to be highly correlated with the SSTs in New Zealand. Figure 1 shows the 20 locations, including 12 New Zealand locations and eight non-New Zealand locations. Tables 1 and 2 summarize the information of the time series of 20 locations. In addition, it is noticeable that the 20 sequences contain no missing values, because SODA 2.2.4 is modeling data.



Figure 1: 20 selected locations of interest for MHW forecasts in New Zealand. The SSTA time series of the locations in blue are both predictands and predictors. The SSTA time series of the locations in red are predictors only.

Table 1: Information and statistics of the 12 label and feature time series of the locations in New Zealand. The test for normal distribution is the Shapiro-Wilk Test (Shapiro & Wilk, 1965) at a significance level of 0.05, which was applied to each of the 12 complete time series that contains 1680 data points. “Abbr.” is the abbreviation and “Std.” is the standard deviation, applied to the other tables in this study.

Location	Abbr.	Coordinates	Mean	Std.	Is normally distributed
Bay of Plenty	BOP	37.25°S, 176.75°E	0.0539	0.8376	Yes
Bank Peninsula	BP	43.75°S, 173.25°E	-0.0291	0.8573	No
Chatham Island	CI	43.75°S, 176.75°W	-0.0170	0.9278	No
Cape Reinga	CR	34.25°S, 172.25°E	0.0652	0.8237	No
Cook Strait	CS	40.75°S, 174.25°E	0.0286	0.6657	Yes
Fiordland	F	44.25°S, 167.25°E	0.0519	0.9631	No
Hauraki Gulf	HG	36.75°S, 175.25°E	0.0490	0.8536	Yes
Otago Peninsula	OP	45.75°S, 170.75°E	-0.0091	0.7822	No
Raglan	R	37.75°S, 174.75°E	0.0792	0.8447	No
Stewart Island	SI	47.25°S, 167.75°E	0.0053	0.8000	No
Taranaki	T	38.75°S, 174.25°E	0.1074	0.9864	Yes
Wairarapa	W	41.25°S, 176.25°E	0.1052	1.0462	No

Table 2: Information of the other eight feature time series of the locations outside New Zealand.

Location	Abbr.	Coordinates
Location A in the East Australian Current	EAC A	29.25°S, 155.75°E
Location B in the East Australian Current	EAC B	36.25°S, 152.75°E
Location C in the East Australian Current	EAC C	38.25°S, 150.75°E
Location D in the East Australian Current	EAC D	40.25°S, 150.75°E
Location A in the Central Pacific east of North Cape	CP A	33.75°S, 156.75°W
Location B in the Central Pacific east of North Cape	CP B	33.75°S, 159.75°W
Location C in the Central Pacific east of North Cape	CP C	35.25°S, 152.75°W
Location D in the Central Pacific east of North Cape	CP D	35.25°S, 155.75°W

Each sequence has monthly data points over 140 years, totaling 1680 data points. Therefore, for each month from 1871 to 2010, there are 140 SSTs. To remove seasonality, we split the data temporally into the training (80%) and test (20%) sets without shuffling in order to keep temporal dependencies, and used the training set to obtain the mean SSTs by month. Taking January as an example, when we used the 112 years (80%) SSTs for training, we summed the 112 SSTs and averaged them to get the mean SST for January at each location. This mean SST is a reference value and then was applied to both the training and test sets. We subtracted the mean SST from the 140 January SSTs resulting in 140 SSTAs, where a positive SSTA means the SST was warmer than the reference value and a negative SSTA means the SST was cooler than the reference value. We repeated this step for the other 11 months providing in total 1680 SSTAs for each sequence.

The 12 SSTA time series of the New Zealand locations are the predic-tands, the labels, or the output of the ML model. Also, the 12 time series together with the eight time series of the non-New Zealand locations are the predictors, the features, or the input of the model. We applied the Shapiro-Wilk Test (Shapiro & Wilk, 1965) at a significance level of 0.05 to test whether the labels are normally distributed. The normally distributed labels follow a Gaussian distribution, where the majority of the labels are close to the mean and the rest taper off symmetrically towards both tails. If the labels are not normally distributed, the labels’ distribution deviates from a normal distribution and the statistical procedures that assume normality may not be appropriate, so additional techniques are required. It is worth noting that more outliers are likely to result in a non-normal distribution. Table 1 includes the basic statistics of the 12 label time series. Appendix A.1 provides the histograms of the 12 time series.

The preprocessed SSTA sequences are stored in the NumPy array files and are available for download. The hyperlink is in Appendix A.4.

3 Methods

This section describes the various methods and techniques employed in this study to develop and evaluate the proposed ML models for forecasting SSTAs and MHWs. The following subsections provide detailed explanations of the forecasting task, neural network architecture, loss functions, data re-sampling techniques, evaluation metrics, and model configurations.

3.1 Forecasting Task

The forecasting task is an imbalanced regression task performed by ML models and auxiliary computational techniques. The input consists of the SSTA time series of 12 locations in New Zealand and eight locations outside New Zealand. The output is the SSTA time series of the 12 New Zealand locations. The forecasting is conducted for lead times of one, two, three, and six months, resulting in output SSTA time series with one, two, three, and six lags respectively. In accordance with the definition of MHWs in Subsection 1.1, the forecasted SSTAs are further classified as MHWs or non-MHWs. The following subsections provide a detailed explanation of the methods used in this analysis.

3.2 Neural Network Class

The neural network class we used for this study is fully-connected neural networks (FCNs), a basic form of neural network architectures. Because this study investigates the loss functions for a specific imbalanced regression task, we aimed to focus on experimenting with relevant loss functions and exploring the predictability of monthly MHWs in New Zealand. FCNs can perform various common ML tasks, including regression, classification, detection, recommendation, etc., and FCNs can efficiently learn non-linear hidden representations from a small number of data in sequences, simplifying the hyperparameter experiments. In addition, FCNs have been used for SSTA-related event forecasts (Ratnam et al., 2020). However, FCNs are slow to train with large amounts of data and data in complex formats, and both conditions of data could be used for improving forecasts, so advanced architectures would be needed.

3.3 Loss Functions

The loss functions we selected for normal regression tasks are the mean squared error (MSE), the mean absolute error (MAE), and the Huber loss

(Huber, 1964). The Huber loss is expressed as

$$L(y, \hat{y}) = \frac{1}{N} \sum_{i=1}^N l_i, \quad (1)$$

$$l_i = \begin{cases} \frac{1}{2}(\hat{y}_i - y_i)^2; & \text{if } |\hat{y}_i - y_i| < \delta, \\ \delta(|\hat{y}_i - y_i| - \frac{\delta}{2}); & \text{otherwise,} \end{cases} \quad (2)$$

where N is the number of data points, y is the observed values, \hat{y} is the predicted values, and δ is a controllable scaling hyperparameter for the L1 part.

The first loss function for imbalanced regression is the weighted MSE. In the training process, we assigned a larger weight to the mean square errors for the observations greater than the 90th percentile and another larger weight for the mean square errors for the observations greater than the 80th percentile and smaller than or equal to the 90th. The former weight is larger than the latter weight to separate the importance of the MHW predictions. The observations between the 80th and 90th percentiles can be considered as suspected MHWs or MHW warnings. This weighted MSE is expressed as

$$L(y, \hat{y}) = \frac{1}{N} \sum_{i=1}^N l_i, \quad (3)$$

$$l_i = \begin{cases} w_{90\%}(\hat{y}_i - y_i)^2; & y_i > y_{90\%}, \\ w_{80\%}(\hat{y}_i - y_i)^2; & y_{80\%} < y_i \leq y_{90\%}, \\ (\hat{y}_i - y_i)^2; & \text{otherwise,} \end{cases} \quad (4)$$

where $y_{90\%}$ and $y_{80\%}$ are the 90th and 80th percentiles of y , and $w_{90\%}$ and $w_{80\%}$ ($w_{90\%} > w_{80\%}$) are the controllable weight hyperparameters.

In addition to the weighted MSE, we selected the focal-R (Yang et al., 2021) as the second loss function and the balanced MSE (Ren et al., 2022) as the third loss function for imbalanced regression. The two functions have been explicitly defined in the corresponding literature and are therefore not elaborated upon in this study.

In addition, we proposed a custom scaling-weighted MSE loss function that was designed for this specific imbalanced regression task, based on the distributions of the 12 SSTA time series. The loss function is defined as

$$L(y, \hat{y}) = \frac{1}{N} \sum_{i=1}^N l_i, \quad (5)$$

$$l_i = \begin{cases} (w_{90\%} \cdot |y_i|^\alpha)^\beta (\hat{y}_i - y_i)^2; & y_i > y_{90\%}, \\ (w_{80\%} \cdot |y_i|^\alpha)^\beta (\hat{y}_i - y_i)^2; & y_{80\%} < y_i \leq y_{90\%}, \\ (|y_i|^\alpha)^\beta (\hat{y}_i - y_i)^2; & \text{otherwise,} \end{cases} \quad (6)$$

where $(w \cdot |y|^\alpha)^\beta$ is a scaling weight term. α , β , $w_{90\%}$, and $w_{80\%}$ are the controllable hyperparameters, where $\alpha \in [1, +\infty]$, $\beta \in (0, 1]$, $w_{90\%} \in [1, +\infty]$, $w_{80\%} \in [1, +\infty]$, and $w_{90\%} > w_{80\%}$ are suggested. In this loss function, the weight scales with the observed values y and α controls the degree of scaling. The absolute value of y ensures the term to be a real number. Similar to the weighted MSE, an additional weight w is multiplied to separate the errors between MHW observations and predictions. Furthermore, β is added to the scaling weight to control the overestimation of extreme values (the Type I error) that leads to more false positive predictions in the classification context. When $\alpha \cdot \beta = 1$, the term scales linearly to y and the computational efficiency increases.

It is possible to simplify the scaling weight term $(w \cdot |y|^\alpha)^\beta$ to $(w' \cdot |y|)^\gamma$ with one hyperparameter γ , where $w' = w^{-\alpha}$ and $\gamma = \alpha \cdot \beta$. However, we kept the two hyperparameters for easy interpretation and convenient control of model performance. In the initial experiments, the weight w could directly use the weight value from the weighted MSE loss. β could be set as 1 initially, and depending on performance, β could be adjusted to a smaller value to control the number of Type I errors.

The custom scaling-weighted MSE has advantages over the standard weighted MSE by dynamically scaling with anomaly severity via incorporating anomaly magnitude, rather than applying the same values of weights across all cases. This approach allows for better representation of extreme values. Additionally, the controllable hyperparameters offer flexibility to balance the trade-off between false alarms and undetected positives, making the loss function well-suited to MHW prediction. For example, reducing α or β lowers the influence of extreme values, leading to more conservative predictions and fewer false positives.

3.4 Data Re-Sampling

Besides loss functions, we applied one data re-sampling technique for imbalanced regression: the SMOGN (Branco et al., 2017). There is one controllable hyperparameter k , the number of nearest neighbors. However, because the dataset has no missing values and the time series are relatively evenly distributed, these techniques designed for situations with substantial missing data in specific ranges may not improve the forecasts in this study.

3.5 Evaluation Metrics

We used the MSE to evaluate the overall prediction skill of the predicted SSTA time series.

To evaluate the predictions for MHWs, we used the critical success index (CSI) (Schaefer, 1990). The CSI is also called the threat score, which is equal to the total number of true positive predictions for extremes divided

by the sum of the predictions for extremes plus the number of misses. The examples of using the CSI as an evaluation includes rainfall prediction in weather forecasts (Pham et al., 2020) and disease diagnosis (Larner, 2021), where rainfalls and diseases were considered as critical or extreme events. We first used neural network models to predict SSTAs as a regression task. Then we categorized the predicted values by regression into three classes: the MHW ($\hat{y}_i > y_{90\%}$), the suspected MHW ($y_{80\%} < \hat{y}_i \leq y_{90\%}$), and the normal or not a MHW ($\hat{y}_i \leq y_{80\%}$). We used the CSI as the evaluation metrics for the predictions for the first two classes, denoted as “CSI” and “CSI 80” respectively.

The model’s training time is another metric of interest to demonstrate the different time efficiency of the loss functions, given the other conditions being the same. Also, we define perfect underfitting (PU) as the event that a model predicts only one value so the model has no ability to predict. We introduce this definition based on the experiments, where we noticed that some models with specific loss functions exhibited the PU phenomenon when performing longer lead forecasts. Therefore, as we trained multiple models using each configuration, we also recorded the ratio of the number of trained models with PU to all models per configuration, denoted as “PUR”. The scatter plots of one example model with PU are shown in Figure 2.

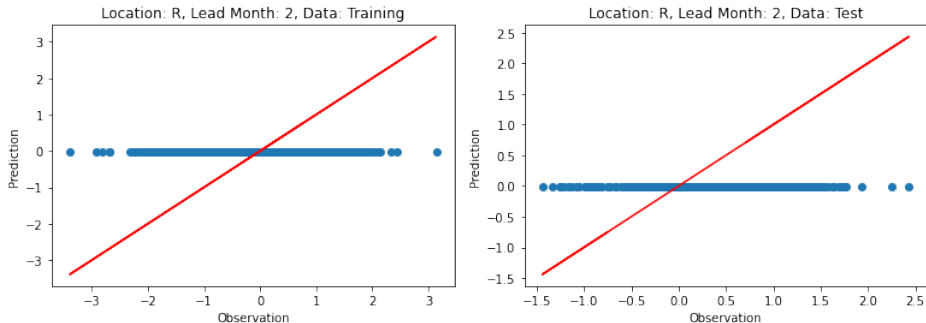


Figure 2: SSTA observation and prediction scatter plots of a model that shows perfect underfitting (PU) on the training and test data respectively, which indicates no ability to predict.

In addition, using the MSE and the CSI to compare the performance of models with different loss functions (different regressors) is only appropriate for evaluating on the single dataset. Although the input features are the same, the labels are different, which are time series of different locations. Therefore, the datasets are slightly different and a statistical test that assesses multiple models over multiple datasets is required. We used the non-parametric Friedman Test (Friedman, 1937, 1940) to compare the models and recommend the loss functions for SSTA forecasts, MHW forecasts,

and suspected MHW forecasts respectively.

Let r_i^j be the rank of j^{th} of k models in terms of an evaluation metric on the i^{th} of N datasets (locations). $R_j = \frac{1}{N} \sum_i r_i^j$ is the average ranks of models. The null-hypothesis states that all the models are equivalent so their ranks R_j should be equal. The Friedman Statistic is defined as

$$\chi_F^2 = \frac{12N}{k(k+1)} \left[\sum_j R_j^2 - \frac{k(k+1)^2}{4} \right]. \quad (7)$$

Iman & Davenport (1980) later showed that the Friedman Statistic was undesirably conservative. Therefore, a better statistic is defined as

$$F_F = \frac{(N-1)\chi_F^2}{N(k-1) - \chi_F^2}, \quad (8)$$

which is distributed according to the F-distribution with $k-1$ and $(k-1)(N-1)$ degrees of freedom. Demšar (2006) introduced the use of the Friedman Test to compare learning algorithms. In this study, we used F_F to assess the comparisons of the models across all locations with regards to SSTA, MHW, and suspected MHW forecasts.

3.6 Sliding Window

The sliding window method uses a subset of data points in the time series as inputs rather than all previous data points, and has been used in SST-related forecasts (Ham et al., 2019; Taylor & Feng, 2022). The corresponding hyperparameter, window size, determines the number of previous time steps as predictors. The SSTA in the selected sequences have short-term temporal dependencies and we suggest a window size of 3 or larger (three months or more) when using the same sequence as both predictors and predictands. For multiple predictors at monthly time steps, Ham et al. (2019) used a window size of 3 and Taylor & Feng (2022) used 12 (one year). The window size is a controllable hyperparameter and the values between 3 and 12 were trialed.

3.7 Model Configurations

In ML, a base model refers to the simplest form of a ML model. Because this study primarily focuses on investigating regression loss functions, we consider the FCN model with the MSE loss as the base model. Therefore, the configuration for the base FCN model: there are one input layer that takes 120 features (20×6 , the number of predictors multiplied by the window size) as input, one output layer that outputs one single value, two hidden layers with 100 neurons next to the input layer, and one hidden layer with 50 neurons next to the output layer. The loss function is the MSE. The L1 regularization with a weight of 0.01 is incorporated into the loss function.

All activations functions are the hyperbolic tangent. The optimizer is the stochastic gradient descent, with a learning rate of 0.01 and a weight decay of 0.01. The batch size is 64. The forecasting lead times include one, two, three, and six months. The ratio of training data to test data is 4:1. The number of training epochs is 400. We trained five models for the same configuration and we recorded the test MSE, test CSI, and the test CSI 80 of the average predictions by the five models and the average training time. We repeated the process for all 12 locations and obtained a final average result for each metric for all locations.

In designing the FCN architecture, we aimed to balance model complexity with generalization, ensuring it could capture patterns in the SSTA time series data. Preliminary experiments showed that the three-layer structure was sufficient to learn non-linear representations while avoiding overfitting. By incrementally reducing the number of neurons, the model was guided toward abstract features in the third layer, enhancing generalization. This study, however, focuses on evaluating various loss functions rather than refining the architecture. Hence, the chosen architecture was intended to be sufficient to capture non-linear patterns while being computationally efficient, enabling us to train a large number of models quickly for robust experimental comparisons across different loss functions.

In order to investigate the effectiveness of different loss functions, we fixed the other hyperparameters and only modified the loss function from the base model. This process aligns with the goal of ablation experiments, which involve removing or degrading specific components of ML to understand their contribution to the overall system. Because removing the loss function would make neural network training impossible, we replaced the original MSE loss function with the other loss functions to explore their impact. The alternative loss functions for investigation were the MAE, the Huber, the weighted MSE, the focal-R (Yang et al., 2021), the balanced MSE (Ren et al., 2022), and our proposed scaling-weighted MSE. For the hyperparameters associated with some loss functions, in the Huber loss, $\delta = 0.5$. In the weighted MSE and the scaling-weighted MSE, $w_{90\%} = 1.5$ and $w_{80\%} = 1.25$. In the focal-R, the error is the MSE (focal-R-MSE), $\beta = 2$, and $\gamma = 1$. In the balanced MSE, σ was optimized in training. In the scaling-weighted MSE, different sets of α and β were attempted. However, there is a potential problem: to reach the best performance, the other hyperparameters should be tuned to suit different loss functions. We will explain this problem with the results in the Discussion. To compare the models across all locations, the Friedman Statistics with regards to the MSE, the CSI, and the CSI 80 were reported.

4 Results

This section presents the results of the study, detailing the performance of various models and approaches used for forecasting SSTAs and MHWs. The focus is on evaluating the models based on different metrics to determine their effectiveness in handling the forecasting tasks.

4.1 One Lead Month Forecasts

The forecasts started from one month ahead prediction of SSTAs and MHWs, across the 12 selected locations in New Zealand, and the goal was to investigate the effectiveness of different loss functions and different predictions across the selected locations.

We used the MSE, the CSI, and the CSI 80 on the average of five sets of predictions on the test data to evaluate the models' performances. The training time and the PUR of the five trained models further evaluated the performances. We used the Friedman Test to assess these models across all locations.

4.1.1 Persistence Model

The persistence model was used for result comparison. The evaluation metrics of the persistence model for each location are in Table 3.

Table 3: Results of the persistence models for one lead month SSTA and MHW forecasts. A persistence model predicts the next observation the same as the current observation, so the model does not involve a training process.

Location	MSE↓	CSI↑	CSI 80↑
BOP	0.1690	0.3846	0.4717
BP	0.4665	0.1875	0.2949
CI	0.3095	0.2174	0.4211
CR	0.2468	0.3286	0.4959
CS	0.1247	0.4043	0.5327
F	0.3402	0.4699	0.5500
HG	0.2668	0.4386	0.3750
OP	0.3155	0.3478	0.4198
R	0.2377	0.5158	0.6259
SI	0.2440	0.4545	0.4646
T	0.3926	0.4595	0.5541
W	0.4578	0.4607	0.5541
Average	0.2976	0.3891	0.4800

4.1.2 Base Model

The base model was used as a baseline model, whose definition and configurations are in Subsection 3.7. The evaluation metrics of the base model for each location are in Table 4. The example observation and prediction scatter plots are in Appendix A.3, applied to the models with the other loss functions for one, two, three, and six lead month SSTA and MHW forecasts in this study.

Table 4: Results of the base models for one lead month SSTA and MHW forecasts. The results in bold are better than those of the persistence model, applied to the other tables in this study.

Location	MSE↓	CSI↑	CSI 80↑	Training Time↓	PUR↓
BOP	0.1528	0.0357	0.4211	18.3887	
BP	0.3831	0.1600	0.2899	18.3435	
CI	0.2592	0.1765	0.3824	18.6351	
CR	0.2327	0.1373	0.4224	18.6882	
CS	0.1235	0.3143	0.4737	18.4263	
F	0.3150	0.3611	0.5752	18.3620	0%
HG	0.2349	0.2045	0.3832	18.5357	
OP	0.2776	0.4103	0.4430	20.8010	
R	0.2275	0.2055	0.5859	18.6367	
SI	0.2281	0.4474	0.4646	18.3489	
T	0.3995	0.3735	0.5782	19.4791	
W	0.5109	0.2500	0.4789	18.6513	
Average	0.2787	0.2563	0.4582	18.7747	0%

4.1.3 Models with Different Loss Functions

To improve the forecasts for MHWs, i.e. improving CSI and CSI 80, we experimented with different loss functions other than the MSE. The evaluation metrics of the models with the MAE loss, the Huber loss, the weighted MSE loss, the focal-R loss, and the balanced MSE loss for each location are respectively in Tables 5, 6, 7, 8, and 9. The evaluation metrics of the models with our proposed scaling-weighted MSE loss with three sets of hyperparameters are respectively in Tables 10, 11, and 12.

Table 5: Results of the models with the MAE loss for one lead month SSTA and MHW forecasts.

Location	MSE↓	CSI↑	CSI 80↑	Training Time↓	PUR↓
BOP	0.1551	0.0357	0.4433	20.0169	0%
BP	0.3914	0.0	0.0	20.4129	40%
CI	0.2572	0.0714	0.4028	20.6211	0%
CR	0.2335	0.1346	0.4957	19.8763	0%
CS	0.1315	0.2703	0.5000	20.1543	0%
F	0.3202	0.2899	0.5714	20.0417	0%
HG	0.2415	0.0476	0.3982	20.4639	0%
OP	0.2778	0.3158	0.4805	20.1162	0%
R	0.2333	0.1096	0.5906	20.6929	0%
SI	0.2403	0.4444	0.4950	20.3889	0%
T	0.3975	0.2593	0.5714	20.1049	0%
W	0.4869	0.2754	0.5135	20.6761	0%
Average	0.2805	0.1878	0.4552	20.2972	3.3%

Table 6: Results of the models with the Huber loss with $\delta = 0.5$ for one lead month SSTA and MHW forecasts.

Location	MSE↓	CSI↑	CSI 80↑	Training Time↓	PUR↓
BOP	0.2137	0.1333	0.3333	18.1167	
BP	0.4538	0.0400	0.2424	18.5230	
CI	0.3455	0.3889	0.3286	18.8040	
CR	0.2798	0.1724	0.4407	18.7517	
CS	0.1678	0.3400	0.4583	18.8105	
F	0.4054	0.2778	0.4057	18.3605	0%
HG	0.3089	0.2885	0.3826	18.3977	
OP	0.3159	0.2500	0.4684	18.2076	
R	0.3139	0.1111	0.4113	18.2090	
SI	0.2930	0.5263	0.4639	18.4739	
T	0.5094	0.2903	0.4658	18.7340	
W	0.5528	0.2727	0.4295	18.5557	
Average	0.3467	0.2576	0.4025	18.4954	0%

Table 7: Results of the models with the weighted MSE loss with $w_{90\%} = 1.5$ and $w_{80\%} = 1.25$ for one lead month SSTA and MHW forecasts.

Location	MSE↓	CSI↑	CSI 80↑	Training Time↓	PUR↓
BOP	0.1527	0.0357	0.4316	29.4885	
BP	0.3829	0.1538	0.2899	30.3551	
CI	0.2612	0.1765	0.3768	29.8527	
CR	0.2333	0.1373	0.4397	31.4612	
CS	0.1228	0.3143	0.4912	30.2711	
F	0.3146	0.3750	0.5752	30.0870	0%
HG	0.2357	0.2273	0.3761	30.4401	
OP	0.2780	0.4000	0.4557	30.7987	
R	0.2266	0.2055	0.6000	31.8953	
SI	0.2304	0.4474	0.4747	30.9633	
T	0.3982	0.3735	0.5714	31.4724	
W	0.5075	0.2647	0.4722	29.2572	
Average	0.2787	0.2592	0.4629	30.5286	0%

Table 8: Results of the models with the focal-R-MSE loss with $\beta = 2$ and $\theta = 1$ for one lead month SSTA and MHW forecasts.

Location	MSE↓	CSI↑	CSI 80↑	Training Time↓	PUR↓
BOP	0.1506	0.0714	0.4271	24.7791	
BP	0.3848	0.1600	0.3000	25.6488	
CI	0.2587	0.1765	0.3824	26.4069	
CR	0.2317	0.0980	0.4174	25.7978	
CS	0.1243	0.2286	0.4821	25.4496	
F	0.3132	0.3611	0.5752	26.4808	0%
HG	0.2348	0.2273	0.3832	25.1393	
OP	0.2776	0.4103	0.4557	25.7948	
R	0.2263	0.2162	0.5814	25.4148	
SI	0.2277	0.4595	0.4646	25.4777	
T	0.3975	0.3780	0.5714	25.4651	
W	0.5148	0.2500	0.4786	25.1732	
Average	0.2785	0.2531	0.4599	25.5857	0%

Table 9: Results of the models with the balanced MSE loss with optimized σ for one lead month SSTA and MHW forecasts.

Location	MSE↓	CSI↑	CSI 80↑	Training Time↓	PUR↓
BOP	0.2587	0.2985	0.4779	25.9831	
BP	0.6484	0.1765	0.3431	25.2746	
CI	0.3446	0.1944	0.4524	24.7637	
CR	0.3636	0.3864	0.5102	26.1010	
CS	0.1443	0.3860	0.4692	26.8915	
F	0.4006	0.4949	0.5615	24.6535	0%
HG	0.3419	0.3247	0.4242	24.7438	
OP	0.3696	0.3226	0.4900	25.5400	
R	0.2934	0.4902	0.5789	27.2411	
SI	0.3119	0.4746	0.5214	26.5847	
T	0.4185	0.5088	0.6061	25.0011	
W	0.5245	0.4700	0.5671	24.6375	
Average	0.3683	0.3773	0.5002	25.6180	0%

Table 10: Results of the models with the scaling-weighted MSE loss with $\alpha = 1.5$, $\beta = 0.5$, $w_{90\%} = 1.5$, and $w_{80\%} = 1.25$ for one lead month SSTA and MHW forecasts.

Location	MSE↓	CSI↑	CSI 80↑	Training Time↓	PUR↓
BOP	0.1832	0.3415	0.4836	39.5585	
BP	0.4882	0.1667	0.3407	40.0110	
CI	0.3012	0.2222	0.4177	39.1581	
CR	0.2752	0.2879	0.4545	48.1067	
CS	0.1409	0.3818	0.4538	41.6232	
F	0.3510	0.4598	0.5772	40.1473	0%
HG	0.2781	0.3651	0.4242	40.2325	
OP	0.3270	0.3704	0.4898	41.3760	
R	0.2435	0.4300	0.5933	40.3831	
SI	0.2678	0.5094	0.5495	40.6573	
T	0.4032	0.4587	0.6101	41.2600	
W	0.5073	0.4556	0.5253	40.3576	
Average	0.3139	0.3708	0.4933	41.0726	0%

Table 11: Results of the models with the scaling-weighted MSE loss with $\alpha = 2$, $\beta = 0.5$, $w_{90\%} = 1.5$, and $w_{80\%} = 1.25$ for one lead month SSTA and MHW forecasts.

Location	MSE↓	CSI↑	CSI 80↑	Training Time↓	PUR↓
BOP	0.1989	0.3125	0.4959	29.1585	
BP	0.4959	0.1429	0.3483	30.1651	
CI	0.3183	0.2258	0.4250	29.1210	
CR	0.3068	0.3151	0.4694	30.3416	
CS	0.1471	0.3559	0.4627	29.2815	
F	0.4289	0.4783	0.5952	30.3365	0%
HG	0.2950	0.3636	0.4058	29.8237	
OP	0.3449	0.3621	0.4900	30.0989	
R	0.2570	0.4851	0.5882	29.5209	
SI	0.2942	0.4828	0.5294	30.8662	
T	0.4227	0.4655	0.5864	29.9534	
W	0.5233	0.4536	0.5466	30.2747	
Average	0.3361	0.3703	0.4952	29.9119	0%

Table 12: Results of the models with the scaling-weighted MSE loss with $\alpha = 2$, $\beta = 1$, $w_{90\%} = 1.5$, and $w_{80\%} = 1.25$ for one lead month SSTA and MHW forecasts.

Location	MSE↓	CSI↑	CSI 80↑	Training Time↓	PUR↓
BOP	0.3517	0.2500	0.4207	23.8322	
BP	0.6716	0.2353	0.2925	27.7756	
CI	0.4365	0.2105	0.4302	23.5380	
CR	0.5111	0.2743	0.4199	23.9643	
CS	0.1807	0.3288	0.4748	23.8340	
F	0.5689	0.4526	0.5615	23.9980	0%
HG	0.3687	0.3059	0.3716	25.1013	
OP	0.4653	0.3158	0.4348	24.5288	
R	0.3409	0.4750	0.5680	24.7397	
SI	0.4570	0.3636	0.4688	24.3617	
T	0.5511	0.4351	0.5805	24.5661	
W	0.7170	0.4160	0.5393	24.5252	
Average	0.4684	0.3386	0.4636	24.5638	0%

4.1.4 Comparison of Multiple Models Across Locations

We ranked the models based on the MSE, the CSI, and the CSI 80 respectively across all locations. Tables 13, 15, and 15 summarizes the ranks of all models including the persistence model. The Friedman test (Friedman, 1937, 1940; Demšar, 2006) was used to test the statistical significance of the comparison based on the ranks. The computed values of F_F (Demšar, 2006) were 65.8918, 11.2928, and 6.9737 for the ranks of the three metrics respectively. Because the number of datasets (locations) is 12 and the number

of models including the persistence model is 10, the value of F in the F -distribution with 9 and 99 degrees of freedom denoted as $F(9, 99)$ is 1.9758 at a significance of 0.05. $F_F > F(9, 99)$ so the null hypothesis is rejected.

We only assessed the models with the Friedman test across all locations for one lead month. Because the PU phenomenon widely existed in the long lead forecasts and the PUR must be combined with the MSE, the CSI, and the CSI 80 for model evaluation, ranking the models solely based on each of the three metrics is inappropriate.

Table 13: Ranks of the models based on the MSE. The three best average ranks are in bold. The acronym “WMSE” is “weighted MSE”, “FR” is “focal-R”, “BMSE” is “balanced MSE”, and “SWMSE” is “scaling-weighted MSE”. The numbers “1”, “2”, and “3” behind “SWMSE” indicate the hyperparameters $\alpha = 1.5$, $\beta = 0.5$, $\alpha = 2$, $\beta = 0.5$, and $\alpha = 2$, $\beta = 1$ respectively, applied to the other tables in this study.

Location	Persist	MSE	MAE	Huber	WMSE	FR	BMSE	SWMSE1	SWMSE2	SWMSE3
BOP	5	3	4	8	2	1	9	6	7	10
BP	6	3	4	5	1	2	9	7	8	10
CI	6	3	1	9	4	2	8	5	7	10
CR	5	2	4	7	3	1	9	6	8	10
CS	4	2	5	9	1	3	7	6	8	10
F	5	3	4	8	2	1	7	6	9	10
HG	5	2	4	8	3	1	9	6	7	10
OP	5	1.5	3	6	4	1.5	9	7	8	10
R	5	3	4	9	2	1	8	6	7	10
SI	5	2	4	7	3	1	9	6	8	10
T	1	5	2.5	9	4	2.5	7	6	8	10
W	1	5	2	9	4	6	8	3	7	10
Average	4.4167	2.875	3.4583	7.8333	2.75	1.9167	8.25	5.8333	7.6667	10

Table 14: Ranks of the models based on the CSI.

Location	Persist	MSE	MAE	Huber	WMSE	FR	BMSE	SWMSE1	SWMSE2	SWMSE3
BOP	1	9	9	6	9	7	4	2	3	5
BP	2	5.5	10	9	7	5.5	3	4	8	1
CI	4	8	10	1	8	8	6	3	2	5
CR	2	7.5	9	6	7.5	10	1	4	3	5
CS	1	7.5	9	6	7.5	10	2	3	4	5
F	8	6.5	9	10	5	6.5	1	3	2	4
HG	1	9	10	6	7.5	7.5	4	2	3	5
OP	9	1.5	7.5	10	3	1.5	6	4	5	7.5
R	1	7.5	10	9	7.5	6	2	5	3	4
SI	6	7.5	9	1	7.5	5	4	2	3	10
T	3	7.5	10	9	7.5	6	1	4	2	5
W	2	9.5	6	7	8	9.5	1	3	4	5
Average	3.3333	7.2083	9.0417	6.6667	7.0833	6.875	2.9167	3.25	3.5	5.125

Table 15: Ranks of the models based on the CSI 80.

Location	Persist	MSE	MAE	Huber	WMSE	FR	BMSE	SWMSE1	SWMSE2	SWMSE3
BOP	4	8	5	10	6	7	3	2	1	9
BP	5	7.5	10	9	7.5	4	2	3	1	6
CI	4	7.5	6	10	9	7.5	1	5	3	2
CR	2	8	3	6	7	10	1	5	4	9
CS	1	8	2	9	3	4	7	10	8	5
F	9	4	6	10	4	4	7.5	2	1	7.5
HG	9	5.5	4	7	8	5.5	1.5	1.5	3	10
OP	10	4	5	6.5	6.5	8	1.5	3	1.5	9
R	1	6	4	10	2	7	8	3	5	9
SI	8	8	4	10	5	8	3	1	2	6
T	9	5	7	10	7	7	2	1	3	4
W	2	7	6	10	9	8	1	5	3	4
Average	5.3333	6.375	5.1667	8.9583	6.1667	6.6667	3.2083	3.4583	2.9583	6.7083

4.1.5 Data Re-Sampling

We applied the SMOGN re-sampling (Branco et al., 2017) to the input data: the 20 predictor time series. However, because there are no missing values in the time series, after the SMOGN was applied, there were new feature vectors generated and some contained missing values. We used the mean to interpolate the missing values. We tested a range of values for the hyperparameter k , from 5 to 200. After inputting the re-sampled data to the base model, the performance deteriorated substantially. Therefore, we did not input the re-sampled data to the other models and we do not further report the results of the SMOGN re-sampling.

4.2 Longer Lead Time Forecasts

Extending the forecasting horizon, this subsection examines the performance of models predicting SSTAs and MHWs up to six months ahead. The objective is to evaluate the predictability and performance degradation as the lead time increases.

4.2.1 Fixed-Lag Model

The SSTA and MHW forecasts were extended up to six months in advance, across all New Zealand locations. We would like to investigate the predictability for longer lead times.

Referring to the persistence model that uses the observation at the last time step as the prediction at the current target time step, we define the model that uses the observation at the second, third, or sixth last time step as the prediction at the current target time step as a fixed-lag model. The persistence model is a one-lag model. We use two-lag, three-lag, and six-lag models to compare with the FCN models in terms of two, three, and six lead month forecasts.

For the longer lead time forecasts, the number of the trained models for each of two, three, and six lead months is the same as the number of the trained models for one lead month. We only report the average results across all 12 locations due to the length constraints of this study. The detailed results, presented in the same format as Subsection 4.1, can be found in Appendix A.2. The code and results are presented in Jupyter Notebooks and available for download. The hyperlink is in Appendix A.5.

Table 16: Average results of the fixed-lag models for two, three, and six lead months SSTA and MHW forecasts.

Across All Locations	MSE↓	CSI↑	CSI 80↑
Average (two lead months)	0.6240	0.2204	0.3173
Average (three lead months)	0.8089	0.1459	0.2602
Average (six lead months)	1.0178	0.1125	0.1882

4.2.2 Base Model

Table 17: Average results of the base models for two, three, and six lead months SSTA and MHW forecasts.

Across All Locations	MSE↓	CSI↑	CSI 80↑	Training Time↓	PUR↓
Average (two lead months)	0.5246	0.0	0.2197	22.5095	0%
Average (three lead months)	0.6370	0.0	0.0200	22.5024	38.3%
Average (six lead months)	0.7163	0.0	0.0	22.8932	95%

4.2.3 Models with Different Loss Functions

The average evaluation metrics across all locations of the models with the MAE loss, the Huber loss, the weighted MSE loss, the focal-R loss, and the balanced MSE loss for each location are respectively in Tables 18, 19, 20, 21, and 22. The average evaluation metrics across all locations of the models with our proposed scaling-weighted MSE loss with three sets of hyperparameters are respectively in Tables 23, 24, and 25.

Table 18: Average results of the models with the MAE loss for two, three, and six lead months SSTA and MHW forecasts.

Across All Locations	MSE↓	CSI↑	CSI 80↑	Training Time↓	PUR↓
Average (two lead months)	0.7122	0.0	0.0	18.5255	95%
Average (three lead months)	0.7376	0.0	0.0	18.3525	100%
Average (six lead months)	0.7383	0.0	0.0	18.2578	100%

Table 19: Average results of the models with the Huber loss with $\delta = 0.5$ for two, three, and six lead months SSTA and MHW forecasts.

Across All Locations	MSE↓	CSI↑	CSI 80↑	Training Time↓	PUR↓
Average (two lead months)	0.6137	0.0968	0.1970	21.1989	0%
Average (three lead months)	0.7474	0.0276	0.1151	21.9763	0%
Average (six lead months)	0.8570	0.0066	0.0643	21.1274	0%

Table 20: Average results of the models with the weighted MSE loss with $w_{90\%} = 1.5$ and $w_{80\%} = 1.25$ for two, three, and six lead months SSTA and MHW forecasts.

Across All Locations	MSE↓	CSI↑	CSI 80↑	Training Time↓	PUR↓
Average (two lead months)	0.5257	0.0	0.2222	30.7924	0%
Average (three lead months)	0.6323	0.0	0.0536	31.113	26.7%
Average (six lead months)	0.7036	0.0	0.0	30.1553	66.7%

Table 21: Average results of the models with the focal-R-MSE loss with $\beta = 2$ and $\theta = 1$ for two, three, and six lead months SSTA and MHW forecasts.

Across All Locations	MSE↓	CSI↑	CSI 80↑	Training Time↓	PUR↓
Average (two lead months)	0.5240	0.0	0.2202	26.128	0%
Average (three lead months)	0.6484	0.0	0.0151	26.3625	48.3%
Average (six lead months)	0.7209	0.0	0.0	26.1644	99.2%

Table 22: Results of the models with the balanced MSE loss with optimized σ for two, three, and six lead month SSTA and MHW forecasts.

Across All Locations	MSE↓	CSI↑	CSI 80↑	Training Time↓	PUR↓
Average (two lead months)	1.0370	0.2026	0.3127	25.5092	1.7%
Average (three lead months)	1.0233	0.0694	0.0998	25.8331	58.3%
Average (six lead months)	0.7136	0.0	0.0	26.0090	100%

Table 23: Results of the models with the scaling-weighted MSE loss with $\alpha = 1.5$, $\beta = 0.5$, $w_{90\%} = 1.5$, and $w_{80\%} = 1.25$ for two, three, and six lead month SSTA and MHW forecasts.

Across All Locations	MSE↓	CSI↑	CSI 80↑	Training Time↓	PUR↓
Average (two lead months)	0.6418	0.1926	0.3161	40.4254	0%
Average (three lead months)	0.7360	0.0866	0.2297	38.9710	0%
Average (six lead months)	0.8411	0.0223	0.1187	38.0058	15%

Table 24: Results of the models with the scaling-weighted MSE loss with $\alpha = 2$, $\beta = 0.5$, $w_{90\%} = 1.5$, and $w_{80\%} = 1.25$ for two, three, and six lead month SSTA and MHW forecasts.

Across All Locations	MSE↓	CSI↑	CSI 80↑	Training Time↓	PUR↓
Average (two lead months)	0.6988	0.1976	0.3213	29.6779	0%
Average (three lead months)	0.8176	0.1170	0.2300	30.1820	0%
Average (six lead months)	1.0395	0.0682	0.1913	30.3764	0%

Table 25: Results of the models with the scaling-weighted MSE loss with $\alpha = 2$, $\beta = 1$, $w_{90\%} = 1.5$, and $w_{80\%} = 1.25$ for two, three, and six lead month SSTA and MHW forecasts.

Across All Locations	MSE↓	CSI↑	CSI 80↑	Training Time↓	PUR↓
Average (two lead months)	1.0222	0.1761	0.2978	24.6314	0%
Average (three lead months)	1.2485	0.1356	0.2310	24.5649	0%
Average (six lead months)	1.5275	0.0970	0.1695	25.0025	0%

5 Discussion

This section provides an of the results, focusing on the performance of different loss functions and their impact on the predictive accuracy of SSTAs

and MHWs.

5.1 Loss Functions

Evaluating the effectiveness of various loss functions is crucial for understanding their impact on forecasting performance, especially for tasks involving extreme events like MHWs.

5.1.1 Average MSE, CSI and CSI 80

The base model with the MSE loss generally returned small test MSEs across most locations. The training time was short and the PUR was low. However, according to the CSI and the scatter plots, the MSE loss did not accurately predict the extreme values. The MSE loss was unable to learn hidden patterns when forecasting six months ahead using our FCN configuration.

The MAE loss returned slightly larger test MSEs than the MSE loss. When predicting suspected MHWs, the MAE loss performed almost the same as the MSE loss, but when predicting MHWs, the MAE loss demonstrated its lower sensitivity to the extreme values than the MSE loss. Also, the PUR was substantially high and the MAE loss was unable to forecast SSTAs and MHWs two, three, and six months ahead using our FCN configuration. Given these problems, we deduce that the MAE loss encouraged the models to make more conservative predictions and was unable to capture the complexity of the data, by being less sensitive to individual errors. For long lead time forecasts, the models had difficulties learning the hidden patterns from the current input data.

The Huber loss was generally outperformed by the MSE loss for one lead month forecasts in terms of the MSE and the CSI. However, the Huber loss had shorter training time and no underfitted models for all lead month forecasts. Therefore, the Huber loss could be used for two, three, and six lead month SSTA forecasts. As combining properties of the MSE and the MAE, the Huber loss is less influenced by outliers like the MAE while still providing meaningful gradients for backpropagation like the MSE.

The weighted MSE loss returned similar MSEs to the MSE loss but slightly better CSIs. The PURs of the weighted MSE were generally lower than the MSE loss. Compared with the Huber loss, the weighted MSE had better forecasts for both SSTAs and MHWs for one and two months ahead, which implies the effectiveness of the use of large weights for extreme values. However, considering the high PURs for three and six months, we do not suggest the weighted MSE loss for long lead forecasts. In addition, the weighted MSE was slow in training.

The performance of the focal-R loss was quite similar to the weighted MSE, referring to the evaluation metrics and scatter plots. The focal-R was

slightly faster than the weighted MSE in training, but for three and six lead months the focal-R had higher PURs. The focal-R was proposed for the situation where there are significant missing values in specific value ranges. The techniques introduced with the focal-R (Yang et al., 2021) attempts to amend the substantial data imbalance to the normal distribution and then perform learning. In this specific case of SSTA and MHW forecasts, the distributions of predictands and predictors are normally distributed or nearly normally distributed, with no missing values and limited outliers. Therefore, the focal-R loss performed similar to the standard MSE loss and the weighted MSE loss.

The balanced MSE loss outperformed the other loss functions and the persistence model on the one lead month MHW forecast with generally better CSIs. The trade-off was the high MSEs for SSTA forecasts. Compared with the fixed-lag models, the balanced MSE predicted suspected MHWs generally better and predicted MHWs slightly better at some locations. However, the PURs for three and six lead months were high, so we do not suggest using the balanced MSE for long lead forecasts, where the patterns learned from features are limited for prediction.

Our proposed scaling-weighted MSE loss was able to perform similarly to the balanced MSE, in terms of the MSE and the CSI. There was almost no perfect underfitting in training for all lead months. We noticed that the training time was long when the exponential hyperparameter $\alpha = 1.5$. When $\beta = 1$, there were more Type I errors. Also, our proposed loss function was able to balance the trade-off between the MSE and the CSI, returning similar CSIs without making MSEs larger. Our proposed loss was the only loss function that was able to forecast MHWs for longer lead times, although it has not generally outperformed the fixed-lag models.

In all, the results of this imbalanced task imply a trade-off between accurate prediction for normal values and accurate prediction for anomalies or extreme values. The regressors trained with the MSE loss and the focal-R endow larger weights to the normal, while the regressors trained with the balanced MSE and our scaling-weighted MSE adjust larger weights to anomalies. We suggest utilizing different loss functions to predict distinct classes of labels in the imbalanced regression task of SSTA and MHW forecasts.

5.1.2 Average Rank

Based on the ranks and the Friedman Test for all models across all locations for one lead month forecasts, we recommend the three most highly-ranked models: the MSE, the weighted MSE, and the focal-R for forecasting SSTAs, the persistence model, the balanced MSE, and our scaling-weighted MSE for forecasting MHWs, and the balanced MSE and our scaling-weighted MSE for forecasting suspected MHWs. For longer lead time forecasts, the situations

are more complicated and require evaluation with the PUR case by case. For forecasts at different locations, Figure 4 summarizes the three highest-ranked loss functions for each location.

5.2 Locations

We mainly discuss the one lead month forecasts by location.

In terms of the SSTA forecasts, the FCNs outperformed the persistence models at ten New Zealand locations, besides Taranaki and Wairarapa. According to the exploratory data analysis, the means of the SSTA time series at Taranaki and Wairarapa are around 0.1 instead of 0 and they have the two largest standard deviations, which might be the reasons for FCNs being unable to outperform the persistence model.

The forecasts of MHWs are generally more challenging than the forecasts of suspected MHWs. For MHW forecasts, the FCN models could outperform the persistence model at Bank Peninsula, Chatham Island, Cape Reinga, Fiordland, Otago Peninsula, Stewart Island, Taranaki, and Wairarapa. We noticed that among the four locations with the SSTA time series normally distributed, the FCN models did not outperform the persistence model at Bay of Plenty, Cook Strait, and Hauraki Gulf. For suspected MHW forecasts, only at two locations: Cook Strait and Raglan, the FCNs models did not outperform the persistence model. The balanced MSE and our scaling-weighted MSE generally had larger CSIs and CSI 80s than the persistence model at more locations than the other loss functions.

To further investigate the regional difference in predictability of the FCN models, we performed a Monte Carlo test. Cape Reinga, Hauraki Gulf, Bay of Plenty, Raglan, Taranaki, Cook Strait, and Wairarapa were the seven locations in the northern group. Bank Peninsula, Chatham Island, Fiordland, Otago Peninsula, and Stewart Island were the five locations in the southern group. We selected the regressors with the MSE loss and the balanced MSE loss for one lead month SSTA and MHW forecasts as examples. We calculated the differences between the average MSEs and the average CSIs of the two groups respectively. Then, we conducted a Monte Carlo test by randomly dividing the 12 locations into two groups of equal size and comparing the differences in the two metrics with the differences observed in the original two groups. After running 10000 simulations for each case, we observed that the probability of encountering counterexamples in all four cases exceeded 0.1. Considering a significance level of 0.01, the simulation results indicate that there is insufficient evidence to reject the null hypothesis, suggesting no significant difference in predictability between the two regions. The regressors exhibited similar performances in both regions, and it is unlikely that training different regressors for each region would result in a substantial improvement in predictability.

The results of the longer lead time forecasts by location were in the

Jupyter Notebooks accessible in Appendix A.5.

In general, the forecasts for southern locations were more accurate than those for northern locations. We deduce the reasons could be that SSTs in colder regions are more stable than those in warmer regions and especially in New Zealand, the southern oceanic part is less influenced by the East Australian Current.

5.3 Lead Times

The one lead month SSTA and suspected MHW forecasts were generally good, where the FCNs with the MSE, the MAE, the weighted MSE, and the focal-R loss mostly outperformed the persistence model in terms of the MSE, and the FCNs with the balanced MSE and our scaling-weighted MSE loss mostly outperformed the persistence model in terms of the CSI 80. For MHW forecasts, the persistence models mostly outperformed the FCNs. Typically, the occurrence of consecutive extreme values tends to result in good performance for persistence models in forecasting extremes, and vice versa. Also, there was almost no perfect underfitting in training.

The two lead month SSTA forecasts exhibit moderate performances, where the FCNs with the MSE, the Huber, the weighted MSE, and the focal-R loss mostly outperformed the fixed-lag model in terms of the MSE. Comparatively, the two lead month suspected MHW forecasts were not good, where only the FCNs with our scaling-weighted MSE mostly outperformed the fixed-lag model in terms of the CSI 80 metric. For MHW forecasts, the fixed-lag models outperformed the FCNs. Also, only the FCNs with the MAE loss had a large number of underfitted models.

For the three and six lead month SSTA forecasts, the models might simply predict one value to reach lower MSEs than the fixed-lag model. The FCNs with the MSE, the MAE, the weighted MSE, the focal-R, and the balanced MSE loss had large PURs and were unable to effectively learn hidden representations to make long lead forecasts given the current inputs and configurations. The FCNs with the Huber loss and our proposed scaling-weighted MSE loss were able to make forecasts, where the Huber loss generally returned lower MSEs and the scaling-weighted MSE generally returned lower CSI 80s than the fixed-lag model. The long lead SSTA and MHW forecasts are challenging.

Figure 3 summarizes the results by location and by lead time. Figure 4 summarizes the ranks of the loss functions in terms of one lead month forecasts only. In Appendix A.2, Table 56 summarizes the results by loss function, by location, and by lead time.

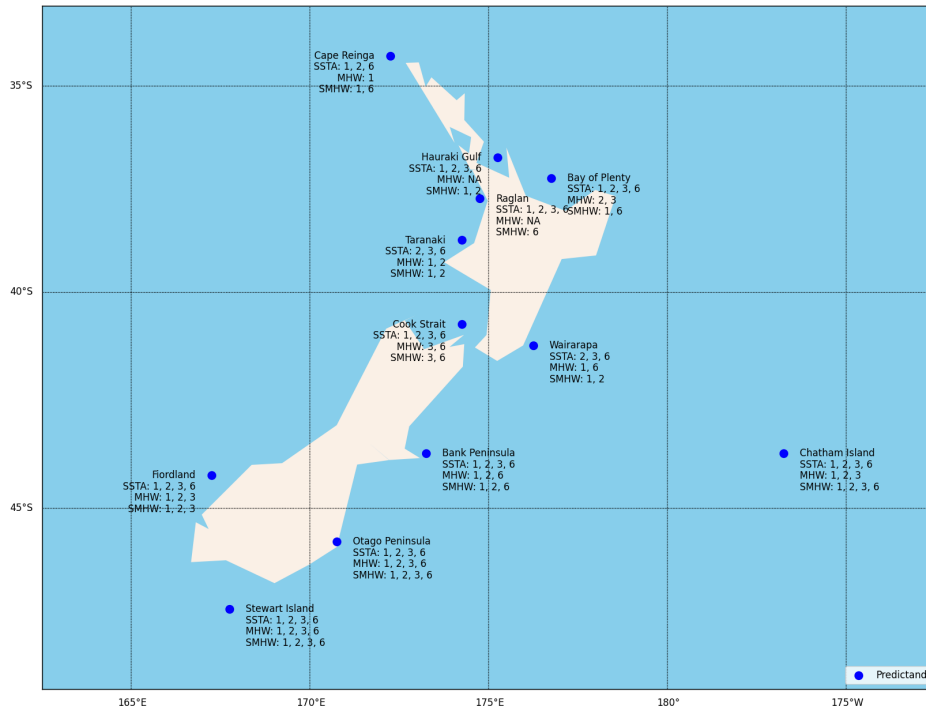


Figure 3: 12 selected locations with the corresponding results of monthly SSTA and MHW forecasts. The acronym “MHW” is “MHW” and “SMHW” is “suspected MHW”, applied to the other figures in this study. The numbers following each type of forecasts are the numbers of lead months. If at least one of the model outperformed the persistence or fixed-lag model at one location in terms of the MSE for SSTAs, the CSI for MHWs, and the CSI 80 for suspected MHWs with the PUR not greater than 20%, the corresponding type of forecasts and the lead month are added to the location.

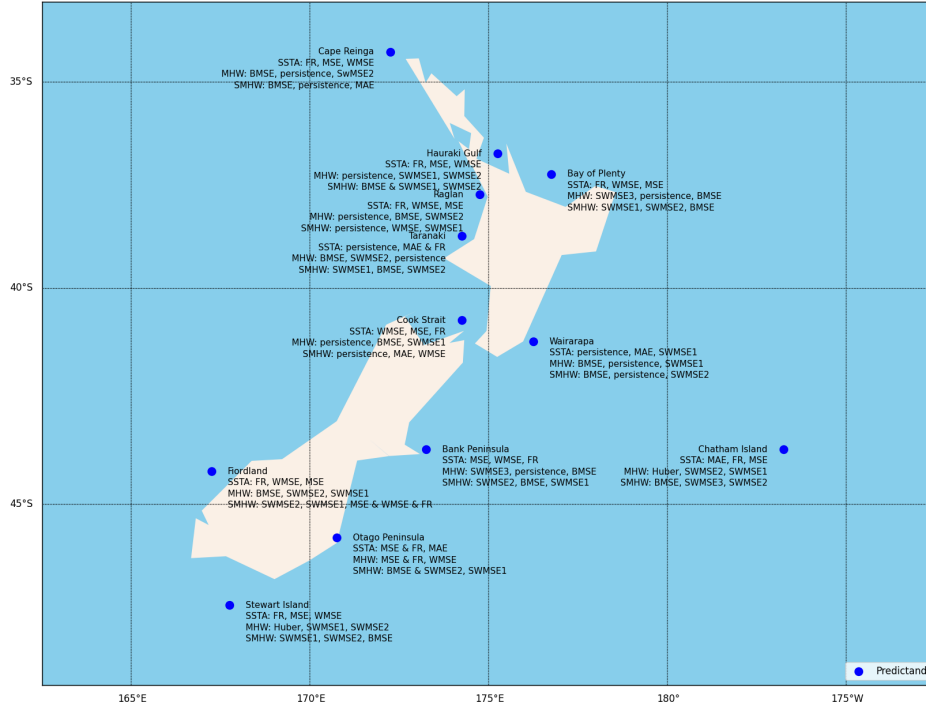


Figure 4: 12 selected locations with the corresponding ranks of the loss functions based on the Friedman test with regards to monthly SSTA and MHW forecasts. Only the top three ranked predictors for one lead month SSTA, MHW, and SMHW at each location are selected. “&” denotes the same rank.

6 Conclusion

This section summarizes the key contributions of this study and outlines directions for future work.

6.1 Contributions

This study makes three major contributions.

First, we assessed the predictability of SSTAs and MHWs using ML models for 12 New Zealand locations and for one, two, three, and six lead months. We analyzed the results by location and lead time, respectively. Generally, the forecasts for southern locations exhibit better performance compared to those for northern locations, possibly due to more stable changes in SSTAs in colder water. Six-month lead MHW forecasts remain challenging because the current data inputs are insufficient to learn the complex patterns for long lead time forecasts, and the randomness in the climate system might make long-lead statistical forecasts unattainable.

Second, we identified the influence of regression loss functions for monthly SSTA and MHW forecasts in New Zealand. For SSTA forecasts, we suggest using the standard MSE loss, the weighted MSE, and the focal-R loss. For MHW forecasts, we suggest using the persistence or fixed-lag model, the balanced MSE loss, and our proposed scaling-weighted MSE loss. For suspected MHW forecasts, we suggest using the balanced MSE loss and our scaling-weighted MSE loss. This finding can be extended to experiments on global SSTA and MHW forecasting.

Third, we proposed a scaling-weighted MSE loss function specifically designed for the imbalanced regression task of monthly MHW forecasts in New Zealand. The scaling-weighted loss function aims to achieve a balance between predictions for normal values and extreme values, offering flexibility in controlling predictions for extreme values and Type I errors, and preventing underfitting. Our proposed scaling-weighted MSE loss has demonstrated its effectiveness in forecasting MHWs at specific locations, including Chatham Island, Fiordland, Otago Peninsula, Stewart Island, and Taranaki, by outperforming the persistence or fixed-lag model.

6.2 Further Work

We plan to address the following aspects in subsequent studies.

First, the regional data inputs might not be sufficient for SSTA and MHW forecasts in New Zealand. We recommend increasing the number of inputs by expanding to global sources.

Second, given the substantial increase in inputs, we suggest using an alternative neural network class to perform representation learning on the large amount of data. While CNNs have been used for SST forecasts (Taylor & Feng, 2022), we propose experimenting with GNNs. Graph re-sampling provides flexibility in adjusting the number of inputs, and GNNs could potentially model climate teleconnections.

Third, relying on SSTAs as the only variable might not be sufficient for SSTA and MHW forecasts. Incorporating other ocean or climate variables could potentially enhance the forecasts by including them as either node attributes or edge attributes in graph re-sampling.

Fourth, the generalization of our proposed scaling-weighted MSE loss should be further justified through global SSTA and MHW forecasts and other imbalanced regression tasks. There is still room for improvement and generalization in the loss function.

References

Asia-Pacific Data Research Center. AVHRR Sea Surface Temperature Data. <http://apdrc.soest.hawaii.edu/las/v6/dataset?catitem=4781>, accessed 2022. Accessed on August 11, 2022.

- Berg, A., Oskarsson, M., and O'Connor, M. Deep ordinal regression with label diversity. In *2020 25th International Conference on Pattern Recognition (ICPR)*, pp. 2740–2747. IEEE, 2021.
- Berkelmans, R., De'ath, G., Kininmonth, S., and Skirving, W. J. A comparison of the 1998 and 2002 coral bleaching events on the great barrier reef: spatial correlation, patterns, and predictions. *Coral reefs*, 23(1):74–83, 2004.
- Boschetti, F., Feng, M., Hartog, J. R., Hobday, A. J., and Zhang, X. Sea surface temperature predictability at the interface between oceanographic modelling and machine learning. 2022.
- Branco, P., Torgo, L., and Ribeiro, R. P. Smogn: A pre-processing approach for imbalanced regression. In *First International Workshop on Learning with Imbalanced Domains: Theory and Applications*, pp. 36–50. PMLR, 2017.
- Cachay, S. R., Erickson, E., Bucker, A. F. C., Pokropek, E., Potosnak, W., Bire, S., Osei, S., and Lütjens, B. The world as a graph: Improving el niño forecasts with graph neural networks. *arXiv preprint arXiv:2104.05089*, 2021.
- Cao, K., Wei, C., Gaidon, A., Arechiga, N., and Ma, T. Learning imbalanced datasets with label-distribution-aware margin loss. *Advances in neural information processing systems*, 32, 2019.
- Carton, J. A. and Giese, B. S. A reanalysis of ocean climate using simple ocean data assimilation (soda). *Monthly weather review*, 136(8):2999–3017, 2008.
- Chawla, N. V., Bowyer, K. W., Hall, L. O., and Kegelmeyer, W. P. SMOTE: synthetic minority over-sampling technique. *Journal of artificial intelligence research*, 16:321–357, 2002.
- Chen, X., Yu, R., Ullah, S., Wu, D., Liu, M., Huang, Y., Gao, H., Jiang, J., and Nie, N. A new weighted mse loss for wind speed forecasting based on deep learning models. In *EGU General Assembly Conference Abstracts*, pp. 12899, 2020.
- Cui, Y., Jia, M., Lin, T.-Y., Song, Y., and Belongie, S. Class-balanced loss based on effective number of samples. In *Proceedings of the IEEE/CVF Conference on Computer Vision and Pattern Recognition*, pp. 9268–9277, 2019.
- Demšar, J. Statistical comparisons of classifiers over multiple data sets. *The Journal of Machine learning research*, 7:1–30, 2006.

- Dong, Q., Gong, S., and Zhu, X. Imbalanced deep learning by minority class incremental rectification. *IEEE transactions on pattern analysis and machine intelligence*, 41(6):1367–1381, 2018.
- Elzahaby, Y., Schaeffer, A., Roughan, M., and Delaux, S. Oceanic circulation drives the deepest and longest marine heatwaves in the east australian current system. *Geophysical Research Letters*, 48(17):e2021GL094785, 2021.
- Feng, M., Boschetti, F., Ling, F., Zhang, X., Hartog, J. R., Akhtar, M., Shi, L., Luo, J.-J., and Hobday, A. J. Predictability of sea surface temperature anomalies at the eastern pole of the indian ocean dipole-using a convolutional neural network model. *Frontiers in Climate*, pp. 143, 2022.
- Friedman, M. The use of ranks to avoid the assumption of normality implicit in the analysis of variance. *Journal of the american statistical association*, 32(200):675–701, 1937.
- Friedman, M. A comparison of alternative tests of significance for the problem of m rankings. *The Annals of Mathematical Statistics*, 11(1):86–92, 1940.
- García, S. and Herrera, F. Evolutionary undersampling for classification with imbalanced datasets: Proposals and taxonomy. *Evolutionary computation*, 17(3):275–306, 2009.
- Ham, Y.-G., Kim, J.-H., and Luo, J.-J. Deep learning for multi-year enso forecasts. *Nature*, 573(7775):568–572, 2019.
- Ham, Y.-G., Kim, J.-H., Kim, E.-S., and On, K.-W. Unified deep learning model for el niño/southern oscillation forecasts by incorporating seasonality in climate data. *Science Bulletin*, 66(13):1358–1366, 2021.
- He, H., Bai, Y., Garcia, E. A., and Li, S. Adasyn: Adaptive synthetic sampling approach for imbalanced learning. In *Proceedings of the IEEE International Joint Conference on Neural Networks (IEEE World Congress on Computational Intelligence)*, pp. 1322–1328. IEEE, 2008.
- Hobday, A. J., Alexander, L. V., Perkins, S. E., Smale, D. A., Straub, S. C., Oliver, E. C., Benthuisen, J. A., Burrows, M. T., Donat, M. G., Feng, M., et al. A hierarchical approach to defining marine heatwaves. *Progress in Oceanography*, 141:227–238, 2016.
- Hobday, A. J., Spillman, C. M., Eveson, J. P., Hartog, J. R., Zhang, X., and Brodie, S. A framework for combining seasonal forecasts and climate projections to aid risk management for fisheries and aquaculture. *Frontiers in Marine Science*, pp. 137, 2018.

- Holbrook, N. J., Sen Gupta, A., Oliver, E. C., Hobday, A. J., Benthuisen, J. A., Scannell, H. A., Smale, D. A., and Wernberg, T. Keeping pace with marine heatwaves. *Nature Reviews Earth & Environment*, 1(9):482–493, 2020.
- Huang, C., Li, Y., Loy, C. C., and Tang, X. Learning deep representation for imbalanced classification. In *Proceedings of the IEEE Conference on Computer Vision and Pattern Recognition*, pp. 5375–5384, 2016.
- Huang, C., Li, Y., Loy, C. C., and Tang, X. Deep imbalanced learning for face recognition and attribute prediction. *IEEE transactions on pattern analysis and machine intelligence*, 42(11):2781–2794, 2019.
- Huber, P. J. Robust estimation of a location parameter. *The Annals of Mathematical Statistics*, pp. 73–101, 1964.
- Iman, R. L. and Davenport, J. M. Approximations of the critical region of the fbietkan statistic. *Communications in Statistics-Theory and Methods*, 9(6):571–595, 1980.
- Jacox, M. G., Tommasi, D., Alexander, M. A., Hervieux, G., and Stock, C. A. Predicting the evolution of the 2014–2016 California current system marine heatwave from an ensemble of coupled global climate forecasts. *Frontiers in Marine Science*, 6:497, 2019.
- Kang, B., Xie, S., Rohrbach, M., Yan, Z., Gordo, A., Feng, J., and Kalantidis, Y. Decoupling representation and classifier for long-tailed recognition. In *International Conference on Learning Representations*, 2019.
- Karniadakis, G. E., Kevrekidis, I. G., Lu, L., Perdikaris, P., Wang, S., and Yang, L. Physics-informed machine learning. *Nature Reviews Physics*, 3(6):422–440, 2021.
- Khakzar, A., Musatian, S., Buchberger, J., Valeriano Quiroz, I., Pinger, N., Baselizadeh, S., Kim, S. T., and Navab, N. Towards semantic interpretation of thoracic disease and covid-19 diagnosis models. In *Proceedings of the International Conference on Medical Image Computing and Computer-Assisted Intervention*, pp. 499–508. Springer, 2021.
- Larner, A. Assessing cognitive screeners with the critical success index. *Progress in Neurology and Psychiatry*, 25(3):33–37, 2021.
- Martin-Donas, J. M., Gomez, A. M., Gonzalez, J. A., and Peinado, A. M. A deep learning loss function based on the perceptual evaluation of the speech quality. *IEEE Signal processing letters*, 25(11):1680–1684, 2018.
- Maynard, J. A., Turner, P. J., Anthony, K. R., Baird, A. H., Berkelmans, R., Eakin, C. M., Johnson, J., Marshall, P. A., Packer, G. R., Rea, A., et al.

- ReefTemp: An interactive monitoring system for coral bleaching using high-resolution SST and improved stress predictors. *Geophysical Research Letters*, 35(5), 2008.
- Merryfield, W. J., Lee, W.-S., Boer, G. J., Kharin, V. V., Scinocca, J. F., Flato, G. M., Ajayamohan, R., Fyfe, J. C., Tang, Y., and Polavarapu, S. The Canadian seasonal to interannual prediction system. part I: Models and initialization. *Monthly weather review*, 141(8):2910–2945, 2013.
- MetOcean Solutions. Marine Heatwave Forecast. <https://www.moanaproject.org/marine-heatwave-forecast>, accessed 2023. Accessed on February 18, 2023.
- Nie, F., Hu, Z., and Li, X. An investigation for loss functions widely used in machine learning. *Communications in Information and Systems*, 18(1): 37–52, 2018.
- Oliver, E. C., Burrows, M. T., Donat, M. G., Sen Gupta, A., Alexander, L. V., Perkins-Kirkpatrick, S. E., Benthuisen, J. A., Hobday, A. J., Holbrook, N. J., Moore, P. J., et al. Projected marine heatwaves in the 21st century and the potential for ecological impact. *Frontiers in Marine Science*, 6:734, 2019.
- Pham, B. T., Le, L. M., Le, T.-T., Bui, K.-T. T., Le, V. M., Ly, H.-B., and Prakash, I. Development of advanced artificial intelligence models for daily rainfall prediction. *Atmospheric Research*, 237:104845, 2020.
- Pravallika, M. S., Vasavi, S., and Vighneshwar, S. Prediction of temperature anomaly in Indian Ocean based on autoregressive long short-term memory neural network. *Neural Computing and Applications*, 34(10):7537–7545, 2022.
- Ratnam, J., Dijkstra, H., and Behera, S. K. A machine learning based prediction system for the Indian Ocean dipole. *Scientific reports*, 10(1): 1–11, 2020.
- Ren, J., Zhang, M., Yu, C., and Liu, Z. Balanced MSE for imbalanced visual regression. pp. 7926–7935, 2022.
- Ronneberger, O., Fischer, P., and Brox, T. U-net: Convolutional networks for biomedical image segmentation. In *Proceedings of the International Conference on Medical Image Computing and Computer-Assisted Intervention*, pp. 234–241. Springer, 2015.
- Saha, S., Moorthi, S., Wu, X., Wang, J., Nadiga, S., Tripp, P., Behringer, D., Hou, Y.-T., Chuang, H.-y., Iredell, M., et al. The NCEP climate forecast system version 2. *Journal of climate*, 27(6):2185–2208, 2014.

- Schaefer, J. T. The critical success index as an indicator of warning skill. *Weather and forecasting*, 5(4):570–575, 1990.
- Shapiro, S. S. and Wilk, M. B. An analysis of variance test for normality (complete samples). *Biometrika*, 52(3/4):591–611, 1965.
- Shu, J., Xie, Q., Yi, L., Zhao, Q., Zhou, S., Xu, Z., and Meng, D. Meta-weight-net: Learning an explicit mapping for sample weighting. *Advances in neural information processing systems*, 32, 2019.
- Smale, D. A. and Wernberg, T. Extreme climatic event drives range contraction of a habitat-forming species. *Proceedings of the Royal Society B: Biological Sciences*, 280(1754):20122829, 2013.
- Sutton, P. J. and Bowen, M. Ocean temperature change around new zealand over the last 36 years. *New Zealand Journal of Marine and Freshwater Research*, 53(3):305–326, 2019.
- Taylor, J. and Feng, M. A deep learning model for forecasting global monthly mean sea surface temperature anomalies. *Frontiers in Climate*, 4:178, 2022.
- Timmermann, A., An, S.-I., Kug, J.-S., Jin, F.-F., Cai, W., Capotondi, A., Cobb, K. M., Lengaigne, M., McPhaden, M. J., Stuecker, M. F., et al. El niño–southern oscillation complexity. *Nature*, 559(7715):535–545, 2018.
- Torgo, L., Ribeiro, R. P., Pfahringer, B., and Branco, P. SMOTE for regression. In *Proceedings of the Portuguese Conference on Artificial Intelligence*, pp. 378–389. Springer, 2013.
- Vecchi, G. A., Delworth, T., Gudgel, R., Kapnick, S., Rosati, A., Wittenberg, A. T., Zeng, F., Anderson, W., Balaji, V., Dixon, K., et al. On the seasonal forecasting of regional tropical cyclone activity. *Journal of Climate*, 27(21):7994–8016, 2014.
- Wu, Y. and Tang, Y. Seasonal predictability of the tropical indian ocean sst in the north american multimodel ensemble. *Climate Dynamics*, 53(5):3361–3372, 2019.
- Yang, Y. and Xu, Z. Rethinking the value of labels for improving class-imbalanced learning. *Advances in neural information processing systems*, 33:19290–19301, 2020.
- Yang, Y., Zha, K., Chen, Y., Wang, H., and Katabi, D. Delving into deep imbalanced regression. In *Proceedings of the 38th International Conference on Machine Learning*, pp. 11842–11851. PMLR, 2021.

- Yin, X., Yu, X., Sohn, K., Liu, X., and Chandraker, M. Feature transfer learning for face recognition with under-represented data. In *Proceedings of the IEEE/CVF Conference on Computer Vision and Pattern Recognition*, pp. 5704–5713, 2019.
- Zhang, H., Cisse, M., Dauphin, Y. N., and Lopez-Paz, D. mixup: Beyond empirical risk minimization. In *International Conference on Learning Representations*, 2018.

A Appendix

A.1 Histograms of SSTA Time Series

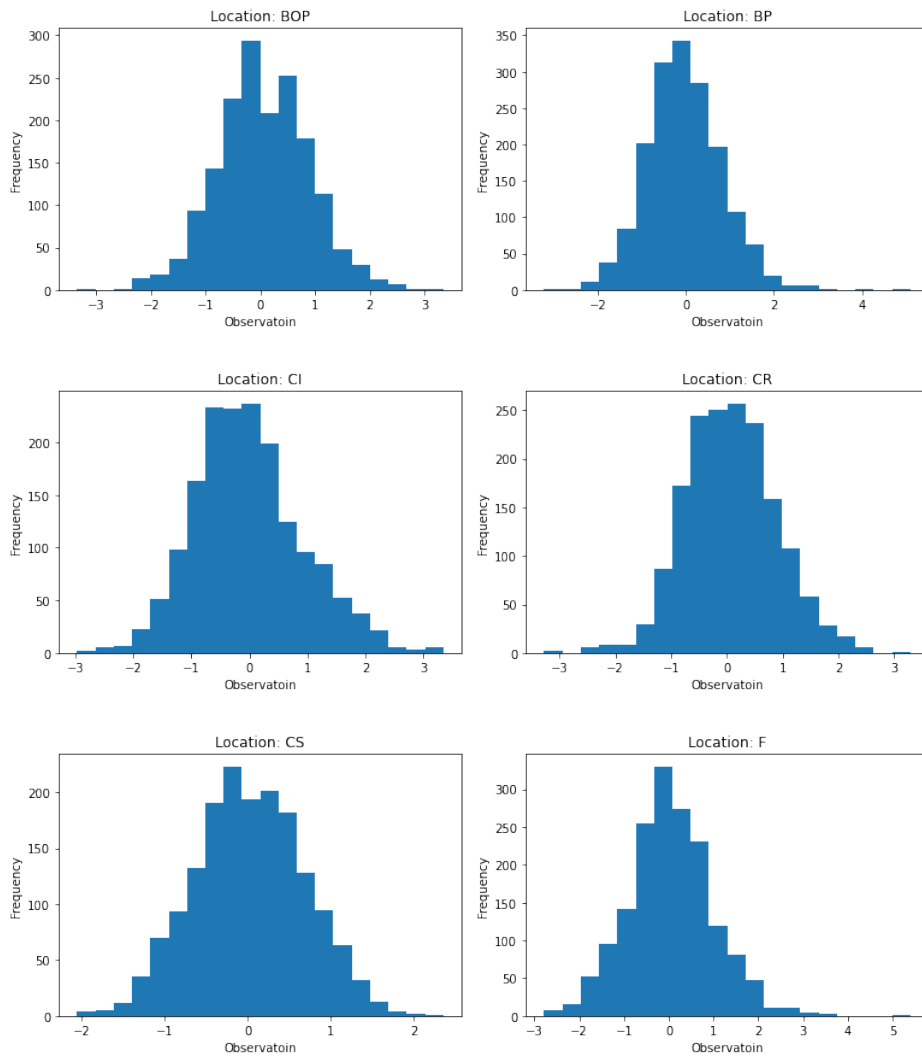


Figure 5: Histograms of the SSTA time series of the six selected NZ locations: Bay of Plenty, Bank Peninsula, Chatham Island, Cape Reinga, Cook Strait, and Fiordland.

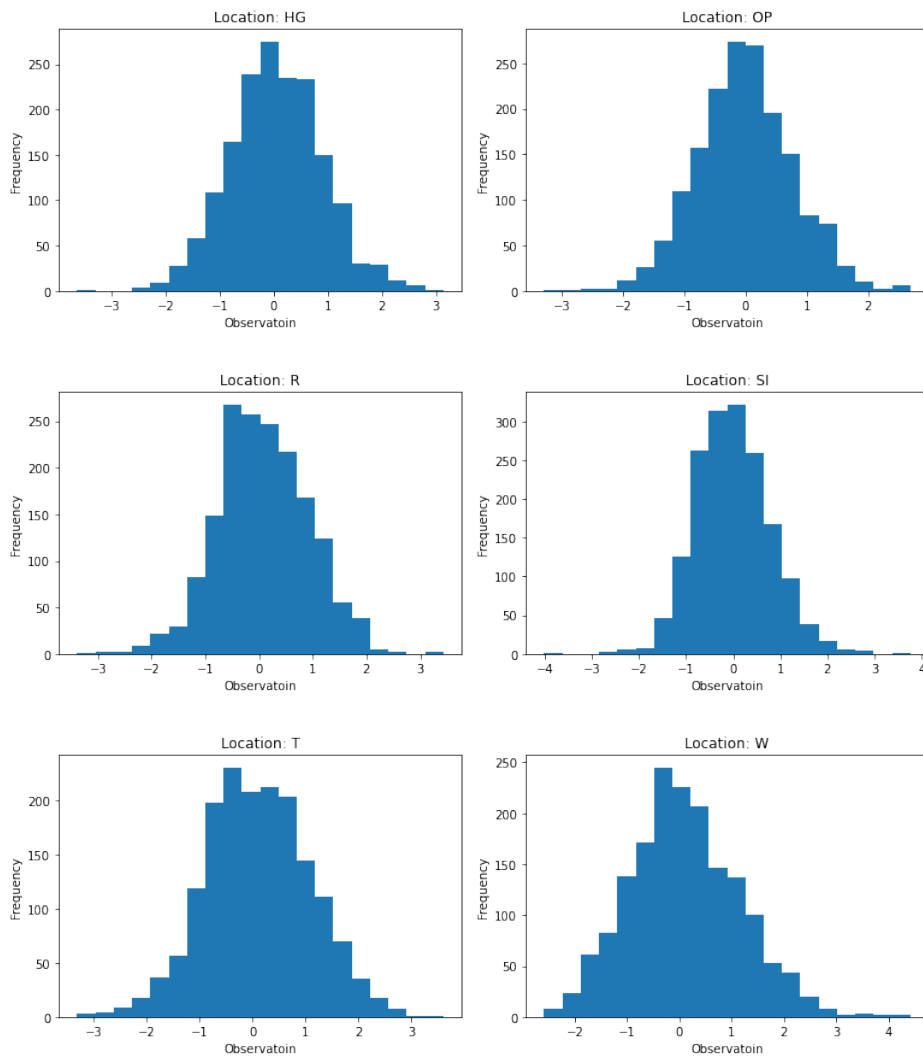


Figure 6: Histograms of the SSTA time series of the six selected NZ locations: Hauraki Gulf, Otago Peninsula, Raglan, Stewart Island, Taranaki, and Wairarapa.

A.2 Additional Results

A.2.1 Two Lead Month Forecasts

Table 26: Results of the two-lag models for two lead month SSTA and MHW forecasts.

Location	MSE↓	CSI↑	CSI 80↑
BOP	0.3339	0.2000	0.3684
BP	0.8608	0.0556	0.1477
CI	0.7036	0.0370	0.1868
CR	0.4255	0.2078	0.3636
CS	0.2569	0.2692	0.3898
F	0.7640	0.3407	0.4198
HG	0.5289	0.2812	0.2581
OP	0.6335	0.1923	0.1979
R	0.5123	0.3091	0.4586
SI	0.5382	0.2308	0.2832
T	0.8856	0.2462	0.3443
W	1.0450	0.2745	0.3898
Average	0.6240	0.2204	0.3173

Table 27: Results of the base models for two lead month SSTA and MHW forecasts. The results in bold are better than those of the corresponding fixed-lag model, applied to the other tables in this study.

Location	MSE↓	CSI↑	CSI 80↑	Training Time↓	PUR↓
BOP	0.2997	0.0	0.1818	22.3693	
BP	0.5798	0.0	0.1324	22.2763	
CI	0.5285	0.0	0.1406	22.5064	
CR	0.3740	0.0	0.1600	22.3860	
CS	0.2327	0.0	0.3426	22.4155	
F	0.6498	0.0	0.3084	22.3326	0%
HG	0.4216	0.0	0.2258	22.2642	
OP	0.5004	0.0	0.2564	22.6545	
R	0.4687	0.0	0.2049	23.5724	
SI	0.4346	0.0	0.2600	22.6813	
T	0.8610	0.0	0.2426	22.2724	
W	0.9448	0.0	0.1805	22.3836	
Average	0.5246	0.0	0.2197	22.5095	0%

Table 28: Results of the models with the MAE loss for two lead month SSTA and MHW forecasts.

Location	MSE↓	CSI↑	CSI 80↑	Training Time↓	PUR↓
BOP	0.4893	0.0	0.0	18.2881	0%
BP	0.6074	0.0	0.0	18.4212	100%
CI	0.6224	0.0	0.0	18.3987	100%
CR	0.5773	0.0	0.0	18.6549	100%
CS	0.3282	0.0	0.0	18.3463	80%
F	0.8867	0.0	0.0	18.3205	100%
HG	0.5620	0.0	0.0	18.1188	100%
OP	0.6101	0.0	0.0	18.5999	100%
R	0.7423	0.0	0.0	19.7982	100%
SI	0.6200	0.0	0.0	18.3323	100%
T	1.0200	0.0	0.0	18.8860	60%
W	1.4805	0.0	0.0	18.1411	100%
Average	0.7122	0.0	0.0	18.5255	95%

Table 29: Results of the models with the Huber loss with $\delta = 0.5$ for two lead month SSTA and MHW forecasts.

Location	MSE↓	CSI↑	CSI 80↑	Training Time↓	PUR↓
BOP	0.3595	0.0312	0.1900	20.7981	
BP	0.6079	0.0500	0.1186	20.6532	
CI	0.6373	0.0667	0.0690	21.5118	
CR	0.5063	0.0213	0.1364	20.7767	
CS	0.3087	0.2045	0.3008	20.9256	
F	0.8751	0.1077	0.1321	22.2434	0%
HG	0.4807	0.1489	0.2566	21.5380	
OP	0.4970	0.1795	0.2469	21.4226	
R	0.6063	0.0395	0.2283	21.9675	
SI	0.5284	0.1667	0.2637	20.9070	
T	0.9235	0.1047	0.2245	20.5573	
W	1.0339	0.0411	0.1972	21.0857	
Average	0.6137	0.0968	0.197	21.1989	0%

Table 30: Results of the models with the weighted MSE loss with $w_{90\%} = 1.5$ and $w_{80\%} = 1.25$ for two lead month SSTA and MHW forecasts.

Location	MSE↓	CSI↑	CSI 80↑	Training Time↓	PUR↓
BOP	0.3087	0.0	0.1889	30.1683	
BP	0.5794	0.0	0.1343	30.7600	
CI	0.5264	0.0	0.1406	30.9739	
CR	0.3774	0.0	0.1782	30.7878	
CS	0.2322	0.0	0.3426	30.8247	
F	0.6497	0.0	0.3178	30.3270	0%
HG	0.4262	0.0	0.2083	30.7889	
OP	0.5032	0.0	0.2532	30.9294	
R	0.4662	0.0	0.2195	31.4170	
SI	0.4386	0.0	0.2524	31.0867	
T	0.8623	0.0	0.2391	30.8594	
W	0.9384	0.0	0.1912	30.5861	
Average	0.5257	0.0	0.2222	30.7924	0%

Table 31: Results of the models with the focal-R-MSE loss with $\beta = 2$ and $\theta = 1$ for two lead month SSTA and MHW forecasts.

Location	MSE↓	CSI↑	CSI 80↑	Training Time↓	PUR↓
BOP	0.2952	0.0	0.1818	26.9496	
BP	0.5826	0.0	0.1343	27.1529	
CI	0.5315	0.0	0.1343	26.2288	
CR	0.3713	0.0	0.1531	25.1065	
CS	0.2322	0.0	0.3333	26.9141	
F	0.6489	0.0	0.3271	26.5709	0%
HG	0.4210	0.0	0.2022	26.2504	
OP	0.5010	0.0	0.2564	26.7791	
R	0.4656	0.0	0.2276	25.0567	
SI	0.4364	0.0	0.2549	26.9049	
T	0.8610	0.0	0.2391	24.5470	
W	0.9416	0.0	0.1985	25.0748	
Average	0.524	0.0	0.2202	26.128	0%

Table 32: Results of the models with the balanced MSE loss with optimized σ for two lead month SSTA and MHW forecasts.

Location	MSE↓	CSI↑	CSI 80↑	Training Time↓	PUR↓
BOP	0.8127	0.1429	0.2744	25.3428	0%
BP	1.4049	0.1404	0.1765	25.9395	0%
CI	1.1446	0.0727	0.2371	24.3099	0%
CR	0.6960	0.1786	0.2877	24.9177	20%
CS	0.3438	0.2152	0.3566	26.4798	0%
F	1.3362	0.3265	0.4275	25.0495	0%
HG	1.0137	0.1604	0.2455	24.8199	0%
OP	0.9222	0.1935	0.2992	25.7681	0%
R	0.9688	0.2520	0.3931	27.6355	0%
SI	0.8067	0.2706	0.3429	25.0878	0%
T	1.3473	0.2667	0.3750	25.3208	0%
W	1.6467	0.2119	0.3371	25.4387	0%
Average	1.037	0.2026	0.3127	25.5092	1.7%

Table 33: Results of the models with the scaling-weighted MSE loss with $\alpha = 1.5$, $\beta = 0.5$, $w_{90\%} = 1.5$, and $w_{80\%} = 1.25$ for two lead month SSTA and MHW forecasts.

Location	MSE↓	CSI↑	CSI 80↑	Training Time↓	PUR↓
BOP	0.4530	0.2143	0.2699	40.2966	
BP	0.7674	0.0930	0.1724	40.3910	
CI	0.6338	0.0769	0.2048	40.6418	
CR	0.4785	0.1167	0.2938	39.6368	
CS	0.2821	0.2143	0.3592	41.0330	
F	0.8256	0.2796	0.4462	40.0886	0%
HG	0.5925	0.2051	0.2629	41.3833	
OP	0.6089	0.2542	0.3186	41.1096	
R	0.5517	0.1667	0.4176	40.7052	
SI	0.5593	0.2308	0.3088	39.4776	
T	0.9751	0.2553	0.3580	40.3307	
W	0.9738	0.2039	0.3812	40.0105	
Average	0.6418	0.1926	0.3161	40.4254	0%

Table 34: Results of the models with the scaling-weighted MSE loss with $\alpha = 2$, $\beta = 0.5$, $w_{90\%} = 1.5$, and $w_{80\%} = 1.25$ for two lead month SSTA and MHW forecasts.

Location	MSE↓	CSI↑	CSI 80↑	Training Time↓	PUR↓
BOP	0.5167	0.2241	0.2743	29.4121	
BP	0.7908	0.0263	0.1538	29.7531	
CI	0.6844	0.1200	0.2195	29.5277	
CR	0.5194	0.1757	0.3214	29.7048	
CS	0.3011	0.2121	0.3517	29.9427	
F	0.9411	0.3535	0.4538	29.6311	0%
HG	0.6719	0.1765	0.2713	29.9946	
OP	0.6525	0.2254	0.3115	29.4866	
R	0.5853	0.1792	0.4350	29.5298	
SI	0.6548	0.2346	0.3020	29.7061	
T	1.0160	0.2212	0.3681	29.6716	
W	1.0517	0.2222	0.3927	29.7749	
Average	0.6988	0.1976	0.3213	29.6779	0%

Table 35: Results of the models with the scaling-weighted MSE loss with $\alpha = 2$, $\beta = 1$, $w_{90\%} = 1.5$, and $w_{80\%} = 1.25$ for two lead month SSTA and MHW forecasts.

Location	MSE↓	CSI↑	CSI 80↑	Training Time↓	PUR↓
BOP	0.8973	0.1452	0.2714	24.3832	
BP	1.2872	0.0769	0.1441	24.7838	
CI	0.9448	0.0833	0.2381	24.5354	
CR	0.9383	0.1304	0.2857	24.4787	
CS	0.4038	0.2062	0.3354	24.7088	
F	1.3063	0.2581	0.4154	24.7834	0%
HG	0.8998	0.1610	0.2316	24.5456	
OP	0.9796	0.2039	0.2819	24.6078	
R	0.8224	0.2697	0.4000	24.9198	
SI	1.1322	0.1825	0.2802	24.5594	
T	1.1858	0.2185	0.3920	24.6897	
W	1.4687	0.1770	0.2983	24.5811	
Average	1.0222	0.1761	0.2978	24.6314	0%

A.2.2 Three Lead Month Forecasts

Table 36: Results of the three-lag models for three lead month SSTA and MHW forecasts.

Location	MSE↓	CSI↑	CSI 80↑
BOP	0.4076	0.1250	0.3109
BP	1.0517	0.0	0.0860
CI	0.9345	0.0370	0.1134
CR	0.5004	0.1625	0.3358
CS	0.3439	0.1379	0.3016
F	1.0635	0.2079	0.3191
HG	0.6400	0.2239	0.2480
OP	0.7524	0.1273	0.1700
R	0.6558	0.2414	0.3713
SI	0.7586	0.1250	0.2414
T	1.1300	0.1912	0.2880
W	1.4679	0.1712	0.3370
Average	0.8089	0.1459	0.2602

Table 37: Results of the base models for three lead month SSTA and MHW forecasts.

Location	MSE↓	CSI↑	CSI 80↑	Training Time↓	PUR↓
BOP	0.1528	0.0357	0.4211	18.3887	
BP	0.3831	0.1600	0.2899	18.3435	
CI	0.2592	0.1765	0.3824	18.6351	
CR	0.2327	0.1373	0.4224	18.6882	
CS	0.1235	0.3143	0.4737	18.4263	
F	0.3150	0.3611	0.5752	18.3620	0%
HG	0.2349	0.2045	0.3832	18.5357	
OP	0.2776	0.4103	0.4430	20.8010	
R	0.2275	0.2055	0.5859	18.6367	
SI	0.2281	0.4474	0.4646	18.3489	
T	0.3995	0.3735	0.5782	19.4791	
W	0.5109	0.2500	0.4789	18.6513	
Average	0.2787	0.2563	0.4582	18.7747	0%

Table 38: Results of the models with the MAE loss for three lead month SSTA and MHW forecasts.

Location	MSE↓	CSI↑	CSI 80↑	Training Time↓	PUR↓
BOP	0.4894	0.0	0.0	18.4441	
BP	0.6071	0.0	0.0	18.1606	
CI	0.6225	0.0	0.0	19.0742	
CR	0.5772	0.0	0.0	18.1971	
CS	0.3861	0.0	0.0	18.1512	
F	0.8866	0.0	0.0	18.7150	100%
HG	0.5616	0.0	0.0	18.6446	
OP	0.6101	0.0	0.0	18.3353	
R	0.7437	0.0	0.0	18.1787	
SI	0.6202	0.0	0.0	18.0191	
T	1.2663	0.0	0.0	18.1565	
W	1.4805	0.0	0.0	18.1539	
Average	0.7376	0.0	0.0	18.3525	100%

Table 39: Results of the models with the Huber loss with $\delta = 0.5$ for three lead month SSTA and MHW forecasts.

Location	MSE↓	CSI↑	CSI 80↑	Training Time↓	PUR↓
BOP	0.4743	0.0	0.0957	23.1707	
BP	0.7335	0.0	0.0149	21.8572	
CI	0.6773	0.0	0.0308	22.2779	
CR	0.5270	0.0185	0.1565	21.9849	
CS	0.3624	0.0	0.1453	20.8197	
F	1.0469	0.0492	0.1031	22.3711	0%
HG	0.6138	0.0	0.1402	22.2079	
OP	0.6114	0.1282	0.1579	22.1079	
R	0.7207	0.0260	0.1143	21.4605	
SI	0.6563	0.0526	0.1573	20.9669	
T	1.2285	0.0123	0.1241	22.1980	
W	1.3167	0.0448	0.1408	22.2932	
Average	0.7474	0.0276	0.1151	21.9763	0%

Table 40: Results of the models with the weighted MSE loss with $w_{90\%} = 1.5$ and $w_{80\%} = 1.25$ for three lead month SSTA and MHW forecasts.

Location	MSE↓	CSI↑	CSI 80↑	Training Time↓	PUR↓
BOP	0.3554	0.0	0.0588	31.1222	0%
BP	0.6231	0.0	0.0	30.7661	100%
CI	0.6123	0.0	0.0161	31.1717	0%
CR	0.5545	0.0	0.0	30.8064	100%
CS	0.2825	0.0	0.1923	30.7800	0%
F	0.8189	0.0	0.1188	31.3309	0%
HG	0.4695	0.0	0.1124	31.5299	0%
OP	0.5739	0.0	0.0	31.2510	80%
R	0.5422	0.0	0.0	31.2416	0%
SI	0.5409	0.0	0.0	30.9479	40%
T	1.0727	0.0	0.0163	31.2068	0%
W	1.1413	0.0	0.1288	31.2018	0%
Average	0.6323	0.0	0.0536	31.113	26.7%

Table 41: Results of the models with the focal-R-MSE loss with $\beta = 2$ and $\theta = 1$ for three lead month SSTA and MHW forecasts.

Location	MSE↓	CSI↑	CSI 80↑	Training Time↓	PUR↓
BOP	0.3450	0.0	0.0	26.2805	20%
BP	0.6225	0.0	0.0	25.0737	100%
CI	0.6128	0.0	0.0333	26.5760	0%
CR	0.5608	0.0	0.0	26.6553	100%
CS	0.3387	0.0	0.0	25.3281	80%
F	0.8349	0.0	0.1000	27.4149	0%
HG	0.4613	0.0	0.0	23.9966	40%
OP	0.6114	0.0	0.0	28.9686	100%
R	0.5715	0.0	0.0	26.0939	40%
SI	0.6143	0.0	0.0	27.1667	100%
T	1.0632	0.0	0.0081	28.0358	0%
W	1.1438	0.0	0.0397	24.7594	0%
Average	0.6484	0.0	0.0151	26.3625	48.3%

Table 42: Results of the models with the balanced MSE loss with optimized σ for three lead month SSTA and MHW forecasts.

Location	MSE↓	CSI↑	CSI 80↑	Training Time↓	PUR↓
BOP	0.4532	0.0	0.0	25.4122	100%
BP	0.6744	0.0	0.0	25.8747	100%
CI	1.0443	0.0417	0.1489	26.6697	0%
CR	0.5555	0.0	0.0	25.2941	100%
CS	0.3751	0.0	0.0	25.7201	100%
F	2.0951	0.2128	0.2920	26.5994	0%
HG	0.5513	0.0	0.0	26.8769	100%
OP	0.9148	0.1974	0.2679	24.5715	0%
R	0.6861	0.0	0.0	25.8642	80%
SI	0.9149	0.2317	0.2847	24.9348	20%
T	2.6808	0.1488	0.2045	25.8794	0%
W	1.3342	0.0	0.0	26.3002	100%
Average	1.0233	0.0694	0.0998	25.8331	58.3%

Table 43: Results of the models with the scaling-weighted MSE loss with $\alpha = 1.5$, $\beta = 0.5$, $w_{90\%} = 1.5$, and $w_{80\%} = 1.25$ for three lead month SSTA and MHW forecasts.

Location	MSE↓	CSI↑	CSI 80↑	Training Time↓	PUR↓
BOP	0.5440	0.1286	0.2590	39.5022	
BP	0.7200	0.0	0.0714	38.9915	
CI	0.6768	0.0	0.0588	40.6756	
CR	0.5420	0.0	0.2877	38.4012	
CS	0.3256	0.0652	0.2721	38.1835	
F	1.1251	0.1358	0.2595	38.7145	0%
HG	0.6555	0.0921	0.2460	38.9647	
OP	0.6243	0.1957	0.2479	38.8838	
R	0.6325	0.0506	0.2921	38.9228	
SI	0.7525	0.2029	0.2517	38.8128	
T	1.1235	0.0471	0.2209	39.0596	
W	1.1102	0.1215	0.2889	38.5404	
Average	0.7360	0.0866	0.2297	38.9710	0%

Table 44: Results of the models with the scaling-weighted MSE loss with $\alpha = 2$, $\beta = 0.5$, $w_{90\%} = 1.5$, and $w_{80\%} = 1.25$ for three lead month SSTA and MHW forecasts.

Location	MSE↓	CSI↑	CSI 80↑	Training Time↓	PUR↓
BOP	0.5167	0.2241	0.2743	29.4121	
BP	0.7908	0.0263	0.1538	29.7531	
CI	0.6844	0.1200	0.2195	29.5277	
CR	0.5194	0.1757	0.3214	29.7048	
CS	0.3011	0.2121	0.3517	29.9427	
F	0.9411	0.3535	0.4538	29.6311	0%
HG	0.6719	0.1765	0.2713	29.9946	
OP	0.6525	0.2254	0.3115	29.4866	
R	0.5853	0.1792	0.4350	29.5298	
SI	0.6548	0.2346	0.3020	29.7061	
T	1.0160	0.2212	0.3681	29.6716	
W	1.0517	0.2222	0.3927	29.7749	
Average	0.6988	0.1976	0.3213	29.6779	0%

Table 45: Results of the models with the scaling-weighted MSE loss with $\alpha = 2$, $\beta = 1$, $w_{90\%} = 1.5$, and $w_{80\%} = 1.25$ for three lead month SSTA and MHW forecasts.

Location	MSE↓	CSI↑	CSI 80↑	Training Time↓	PUR↓
BOP	0.8963	0.1429	0.2771	24.4695	
BP	1.4682	0.0714	0.0806	24.3445	
CI	1.1323	0.0455	0.0957	24.4202	
CR	1.0557	0.1224	0.2593	24.5512	
CS	0.4999	0.1712	0.3254	24.4688	
F	1.4537	0.2447	0.3623	24.7630	0%
HG	1.0358	0.1074	0.1949	24.5973	
OP	1.1068	0.1753	0.2000	24.6275	
R	0.9274	0.1748	0.3397	24.7184	
SI	1.4973	0.1405	0.2368	24.8660	
T	2.1083	0.1373	0.2317	24.1534	
W	1.8007	0.0938	0.1687	24.7994	
Average	1.2485	0.1356	0.231	24.5649	0%

A.2.3 Six Lead Month Forecasts

Table 46: Results of the six-lag models for six lead month SSTA and MHW forecasts.

Location	MSE↓	CSI↑	CSI 80↑
BOP	0.4797	0.0800	0.2188
BP	1.1322	0.0556	0.0753
CI	1.1939	0.0	0.0594
CR	0.6796	0.1500	0.2276
CS	0.5333	0.2000	0.2331
F	1.4574	0.1193	0.2157
HG	0.6668	0.2059	0.1953
OP	0.9675	0.0164	0.1058
R	0.8115	0.2203	0.2652
SI	0.9592	0.0339	0.1750
T	1.3399	0.1571	0.2487
W	1.9929	0.1111	0.2386
Average	1.0178	0.1125	0.1882

Table 47: Results of the base models for six lead month SSTA and MHW forecasts.

Location	MSE↓	CSI↑	CSI 80↑	Training Time↓	PUR↓
BOP	0.3499	0.0	0.0375	22.2124	100%
BP	0.6106	0.0	0.0	23.0696	100%
CI	0.6230	0.0	0.0	23.2094	100%
CR	0.5644	0.0	0.0	22.8684	100%
CS	0.3754	0.0	0.0	22.0390	100%
F	0.8735	0.0	0.0	22.6347	80%
HG	0.5588	0.0	0.0	23.4015	100%
OP	0.6072	0.0	0.0	22.7006	100%
R	0.7069	0.0	0.0	22.5721	100%
SI	0.6128	0.0	0.0	22.5788	100%
T	1.2498	0.0	0.0	23.4525	100%
W	1.3500	0.0	0.0	22.8589	60%
Average	0.7163	0.0	0.0	22.8932	95%

Table 48: Results of the models with the MAE loss for six lead month SSTA and MHW forecasts.

Location	MSE↓	CSI↑	CSI 80↑	Training Time↓	PUR↓
BOP	0.4878	0.0	0.0	18.2453	
BP	0.5970	0.0	0.0	18.3938	
CI	0.6201	0.0	0.0	18.3550	
CR	0.5787	0.0	0.0	18.3447	
CS	0.3835	0.0	0.0	18.2798	
F	0.8901	0.0	0.0	18.2918	100%
HG	0.5623	0.0	0.0	18.1040	
OP	0.6062	0.0	0.0	18.2433	
R	0.7484	0.0	0.0	18.6339	
SI	0.6186	0.0	0.0	18.0005	
T	1.2724	0.0	0.0	18.0751	
W	1.4942	0.0	0.0	18.1270	
Average	0.7383	0.0	0.0	18.2578	100%

Table 49: Results of the models with the Huber loss with $\delta = 0.5$ for six lead month SSTA and MHW forecasts.

Location	MSE↓	CSI↑	CSI 80↑	Training Time↓	PUR↓
BOP	0.5002	0.0	0.0851	21.0768	
BP	0.6397	0.0	0.0	20.7108	
CI	0.7652	0.0	0.0727	21.9564	
CR	0.6393	0.0	0.0190	20.9529	
CS	0.4719	0.0	0.0417	20.7544	
F	1.0741	0.0	0.0392	22.0080	0%
HG	0.6639	0.0	0.1167	21.0887	
OP	0.7010	0.0238	0.1205	20.7983	
R	0.8109	0.0139	0.0643	21.1487	
SI	0.7582	0.0	0.1047	20.9167	
T	1.6308	0.0	0.0312	21.0592	
W	1.6290	0.0417	0.0764	21.0578	
Average	0.857	0.0066	0.0643	21.1274	0%

Table 50: Results of the models with the weighted MSE loss with $w_{90\%} = 1.5$ and $w_{80\%} = 1.25$ for six lead month SSTA and MHW forecasts.

Location	MSE↓	CSI↑	CSI 80↑	Training Time↓	PUR↓
BOP	0.4598	0.0	0.0	26.3108	100%
BP	0.6117	0.0	0.0	26.9528	100%
CI	0.6207	0.0	0.0	25.4601	80%
CR	0.5620	0.0	0.0	26.4343	100%
CS	0.3746	0.0	0.0	26.6167	100%
F	0.8802	0.0	0.0	25.6504	100%
HG	0.5579	0.0	0.0	28.1599	100%
OP	0.6074	0.0	0.0	24.3975	100%
R	0.7024	0.0	0.0	26.4807	100%
SI	0.6127	0.0	0.0	25.4115	100%
T	1.2449	0.0	0.0	26.0454	100%
W	1.4165	0.0	0.0	26.0530	100%
Average	0.7209	0.0	0.0	26.1644	99.2%

Table 51: Results of the models with the focal-R-MSE loss with $\beta = 2$ and $\theta = 1$ for six lead month SSTA and MHW forecasts.

Location	MSE↓	CSI↑	CSI 80↑	Training Time↓	PUR↓
BOP	0.1506	0.0714	0.4271	24.7791	
BP	0.3848	0.1600	0.3000	25.6488	
CI	0.2587	0.1765	0.3824	26.4069	
CR	0.2317	0.0980	0.4174	25.7978	
CS	0.1243	0.2286	0.4821	25.4496	
F	0.3132	0.3611	0.5752	26.4808	0%
HG	0.2348	0.2273	0.3832	25.1393	
OP	0.2776	0.4103	0.4557	25.7948	
R	0.2263	0.2162	0.5814	25.4148	
SI	0.2277	0.4595	0.4646	25.4777	
T	0.3975	0.3780	0.5714	25.4651	
W	0.5148	0.2500	0.4786	25.1732	
Average	0.2785	0.2531	0.4599	25.5857	0%

Table 52: Results of the models with the balanced MSE loss with optimized σ for six lead month SSTA and MHW forecasts.

Location	MSE↓	CSI↑	CSI 80↑	Training Time↓	PUR↓
BOP	0.4496	0.0	0.0	26.4039	
BP	0.6568	0.0	0.0	25.0939	
CI	0.6523	0.0	0.0	25.2148	
CR	0.5569	0.0	0.0	26.3515	
CS	0.3713	0.0	0.0	26.2046	
F	0.8360	0.0	0.0	25.7762	100%
HG	0.5527	0.0	0.0	24.6710	
OP	0.6071	0.0	0.0	27.0505	
R	0.6972	0.0	0.0	26.6746	
SI	0.6204	0.0	0.0	25.9011	
T	1.2264	0.0	0.0	26.9230	
W	1.3363	0.0	0.0	25.8432	
Average	0.7136	0.0	0.0	26.009	100%

Table 53: Results of the models with the scaling-weighted MSE loss with $\alpha = 1.5$, $\beta = 0.5$, $w_{90\%} = 1.5$, and $w_{80\%} = 1.25$ for six lead month SSTA and MHW forecasts.

Location	MSE↓	CSI↑	CSI 80↑	Training Time↓	PUR↓
BOP	0.4987	0.0278	0.1769	37.9092	0%
BP	0.6212	0.0	0.0192	37.7647	60%
CI	0.8057	0.0	0.0492	41.2355	0%
CR	0.5372	0.0	0.2420	37.7452	0%
CS	0.3194	0.0	0.0	37.8731	60%
F	1.3560	0.0385	0.1475	37.5851	0%
HG	0.7554	0.0	0.1937	37.6303	0%
OP	0.6160	0.0	0.0	37.9519	60%
R	0.6387	0.0	0.1494	37.3635	0%
SI	0.8267	0.1765	0.2296	37.4251	0%
T	1.3847	0.0	0.1125	37.9493	0%
W	1.7337	0.0247	0.1049	37.6366	0%
Average	0.8411	0.0223	0.1187	38.0058	15%

Table 54: Results of the models with the scaling-weighted MSE loss with $\alpha = 2$, $\beta = 0.5$, $w_{90\%} = 1.5$, and $w_{80\%} = 1.25$ for six lead month SSTA and MHW forecasts.

Location	MSE↓	CSI↑	CSI 80↑	Training Time↓	PUR↓
BOP	0.6385	0.0400	0.2370	30.1771	
BP	1.1459	0.0513	0.1529	30.3373	
CI	0.9405	0.0	0.0484	30.2619	
CR	0.6230	0.0968	0.2722	29.8960	
CS	0.3960	0.0541	0.2837	30.2367	
F	1.7772	0.0588	0.1705	30.2279	0%
HG	0.8125	0.0877	0.1927	29.9996	
OP	0.8793	0.1304	0.2078	30.3161	
R	0.7621	0.0390	0.2686	30.3375	
SI	0.9132	0.2121	0.2556	32.0875	
T	1.5985	0.0	0.0748	30.3832	
W	1.9870	0.0488	0.1313	30.2562	
Average	1.0395	0.0682	0.1913	30.3764	0%

Table 55: Results of the models with the scaling-weighted MSE loss with $\alpha = 2$, $\beta = 1$, $w_{90\%} = 1.5$, and $w_{80\%} = 1.25$ for six lead month SSTA and MHW forecasts.

Location	MSE↓	CSI↑	CSI 80↑	Training Time↓	PUR↓
BOP	0.9550	0.0706	0.1783	24.9321	
BP	1.4473	0.0750	0.0978	24.7257	
CI	1.3214	0.0	0.0449	24.9797	
CR	1.2793	0.0450	0.1703	25.1403	
CS	0.5889	0.2041	0.2961	24.9296	
F	1.6813	0.0778	0.2000	25.0409	0%
HG	1.0547	0.0938	0.1824	25.4127	
OP	1.2532	0.1333	0.2182	24.9969	
R	1.7950	0.0874	0.1488	25.2995	
SI	1.3298	0.1892	0.2158	25.0253	
T	3.2646	0.0737	0.1133	24.7305	
W	2.3590	0.1143	0.1685	24.8168	
Average	1.5275	0.0970	0.1695	25.0025	0%

A.2.4 Summary of the Results

Table 56: 12 selected locations with the corresponding results of monthly SSTA and MHW forecasts (Part 1). In each cell for a location and a lead time, the three lines show the models with different loss functions that outperformed the persistence or fixed-lag model in terms of the MSE for SSTA forecasts, the CSI for MHW forecasts, and the CSI 80 for suspected MHW forecasts, with the PUR not greater than 20%.

Location	One lead month
BOP	MSE, MAE, WMSE, FR
	BMSE, SWMSE1, SWMSE2
BP	MSE, MAE, Huber, WMSE, FR
	FR, BMSE, SWMSE1, SWMSE2
CI	MSE, MAE, WMSE, FR, SWMSE1
	Huber, SWMSE1, SWMSE2
	BMSE, SWMSE2
CR	MSE, MAE, WMSE, FR
	BMSE
	BMSE
CS	MSE, WMSE, FR
F	MSE, MAE, WMSE, FR
	BMSE, SWMSE2
	MSE, MAE, WMSE, FR, BMSE, SWMSE1, SWMSE2
HG	MSE, MAE, WMSE, FR
	MSE, MAE, Huber, WMSE, FR, BMSE, SWMSE1, SWMSE2
OP	MSE, MAE, WMSE, FR
	WMSE, FR, SWMSE1, SWMSE2
	MSE, MAE, Huber, WMSE, FR, BMSE, SWMSE1, SWMSE2
R	MSE, MAE, WMSE, FR
SI	MSE, MAE, WMSE, FR
	Huber, FR, BMSE, SWMSE1, SWMSE2
	MAE, WMSE, BMSE, SWMSE1, SWMSE2
T	BMSE, SWMSE2
	MAE, WMSE, FR, BMSE, SWMSE1, SWMSE2
W	BMSE
	BMSE

Table 57: 12 selected locations with the corresponding results of monthly SSTA and MHW forecasts (Part 2).

Location	Two lead months
BOP	MSE, WMSE, FR SWMSE1, SWMSE2
BP	MSE, Huber, WMSE, FR, SWMSE1, SWMSE2 BMSE, SWMSE1, SWMSE3 BMSE, SWMSE1, SWMSE2
CI	MSE, Huber, WMSE, FR, SWMSE1, SWMSE2 Huber, BMSE, SWMSE1, SWMSE2, SWMSE3 BMSE, SWMSE1, SWMSE2, SWMSE3
CR	MSE, WMSE, FR
CS	MSE, WMSE, FR
F	MSE, WMSE, FR SWMSE2 BMSE, SWMSE1, SWMSE2
HG	MSE, Huber, WMSE, FR SWMSE1, SWMSE2
OP	MSE, Huber, WMSE, FR, SWMSE1 BMSE, SWMSE1, SWMSE2, SWMSE3 MSE, Huber, WMSE, FR, BMSE, SWMSE1, SWMSE2, SWMSE3
R	MSE, WMSE, FR
SI	MSE, Huber, WMSE, FR BMSE, SWMSE2 BMSE, SWMSE1, SWMSE2
T	MSE, WMSE, FR BMSE, SWMSE1 BMSE, SWMSE1, SWMSE2, SWMSE3
W	MSE, Huber, WMSE, FR, SWMSE1 SWMSE2

Table 58: 12 selected locations with the corresponding results of monthly SSTA and MHW forecasts (Part 3).

Location	Three lead months
BOP	MSE, WMSE, FR SWMSE1, SWMSE3
BP	Huber, SWMSE1, SWMSE2, SWMSE3
CI	MSE, Huber, WMSE, FR, SWMSE1, SWMSE2, SWMSE3 BMSE BMSE
CR	
CS	MSE, WMSE, SWMSE1 SWMSE3 SWMSE3
F	MSE, Huber, WMSE, FR BMSE, SWMSE3 SWMSE3
HG	Huber, WMSE
OP	Huber, SWMSE1, SWMSE2 Huber, BMSE, SWMSE1, SWMSE2, SWMSE3 BMSE, SWMSE1, SWMSE2, SWMSE3
R	MSE, WMSE, SWMSE1
SI	MSE, Huber, SWMSE1 BMSE, SWMSE1, SWMSE2, SWMSE3 BMSE, SWMSE1, SWMSE2
T	MSE, WMSE, FR, SWMSE1
W	MSE, Huber, WMSE, FR, SWMSE1, SWMSE2

Table 59: 12 selected locations with the corresponding results of monthly SSTA and MHW forecasts (Part 4).

Location	Six lead months
BOP	Huber, WMSE SWMSE2
BP	Huber SWMSE3 SWMSE2, SWMSE3
CI	Huber, WMSE, SWMSE1, SWMSE2 Huber
CR	Huber, SWMSE1, SWMSE2 SWMSE1, SWMSE2
CS	Huber, SWMSE2 SWMSE3 SWMSE2, SWMSE3
F	Huber, SWMSE1
HG	Huber
OP	Huber, SWMSE2 SWMSE2, SWMSE3 Huber, SWMSE2, SWMSE3 Huber, SWMSE1, SWMSE2
R	SWMSE2
SI	Huber, SWMSE1, SWMSE2 SWMSE1, SWMSE2, SWMSE3 SWMSE1, SWMSE2, SWMSE3
T	WMSE
W	Huber, WMSE, SWMSE1, SWMSE2 SWMSE3

A.3 Example Scatter Plots

A.3.1 One Lead Month Forecasts

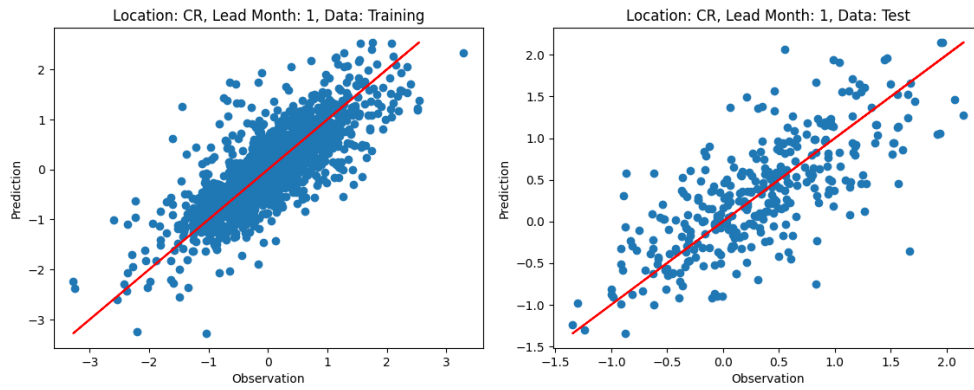


Figure 7: SSTA observation and prediction scatter plots of the persistence model for one lead month forecasts at Cape Reinga, on the training and test data respectively.

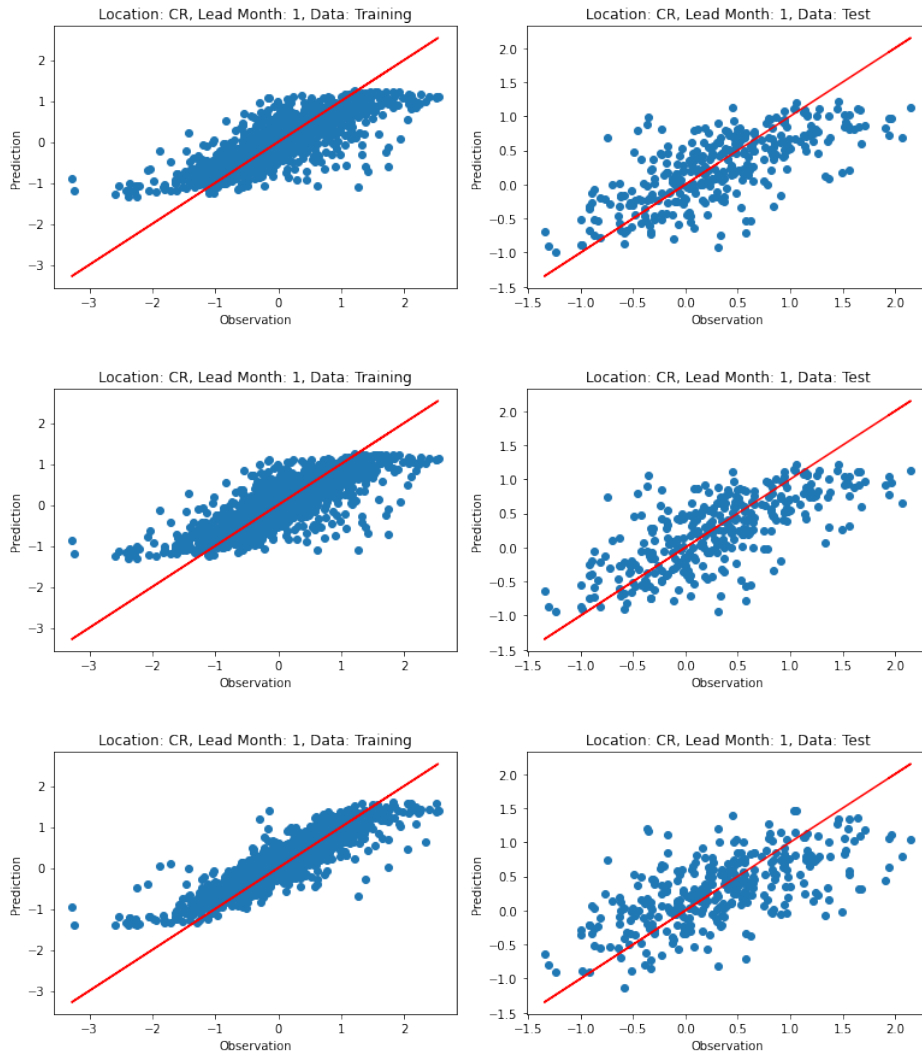


Figure 8: SSTA observation and prediction scatter plots of the last model for one lead month forecasts at Cape Reinga, on the training and test data respectively. The corresponding loss functions from top to bottom are the MSE, the MAE, and the Huber.

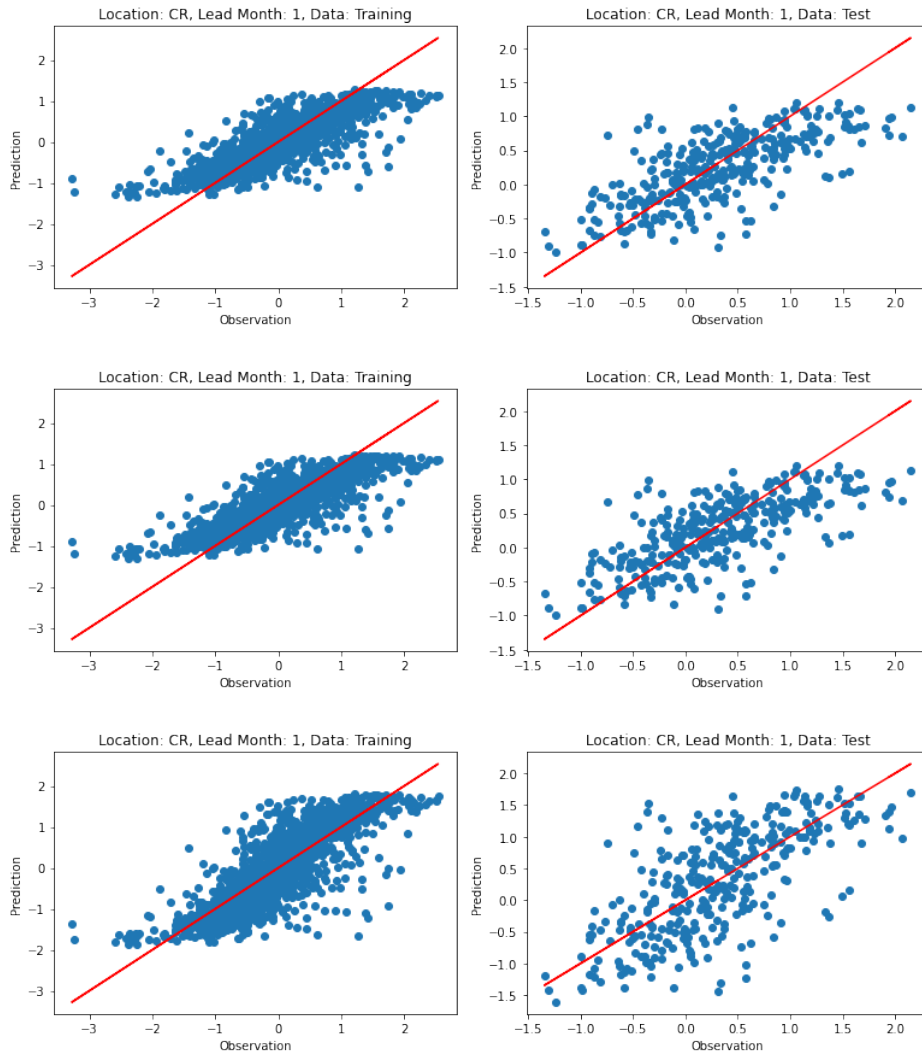


Figure 9: SSTA observation and prediction scatter plots of the last model for one lead month forecasts at Cape Reinga, on the training and test data respectively. The corresponding loss functions from top to bottom are the weighted MSE, the focal-R, and the balanced MSE.

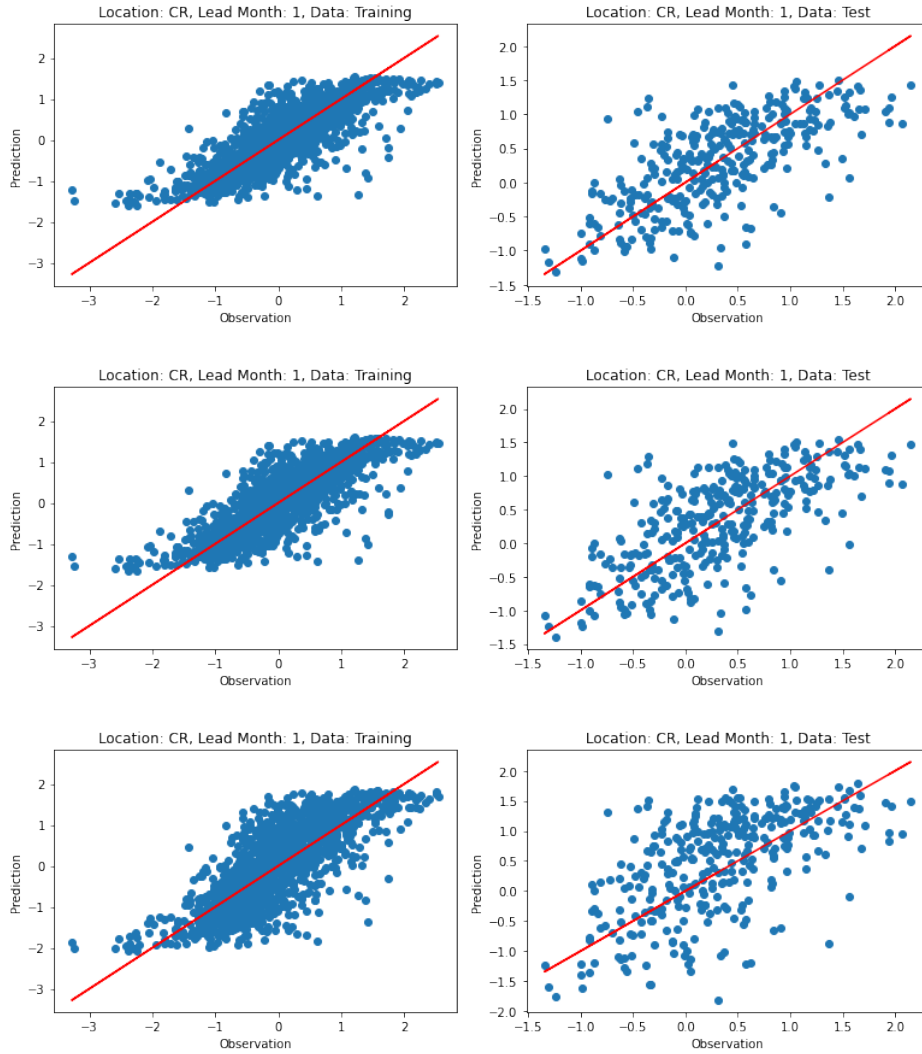


Figure 10: SSTA observation and prediction scatter plots of the last model for one lead month forecasts at Cape Reinga, on the training and test data respectively. The corresponding loss function is our proposed scaling-weighted MSE, from top to bottom with the hyperparameters $\alpha = 1.5, \beta = 0.5$, $\alpha = 2, \beta = 0.5$, and $\alpha = 2, \beta = 1$ respectively.

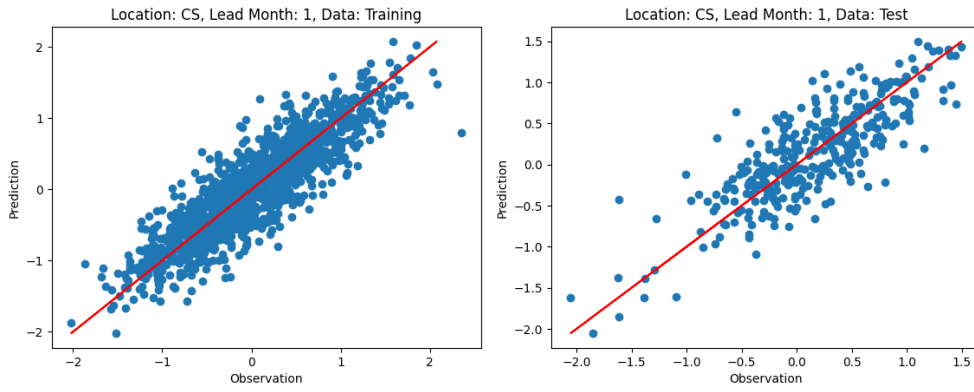


Figure 11: SSTA observation and prediction scatter plots of the persistence model for one lead month forecasts at Cook Strait, on the training and test data respectively.

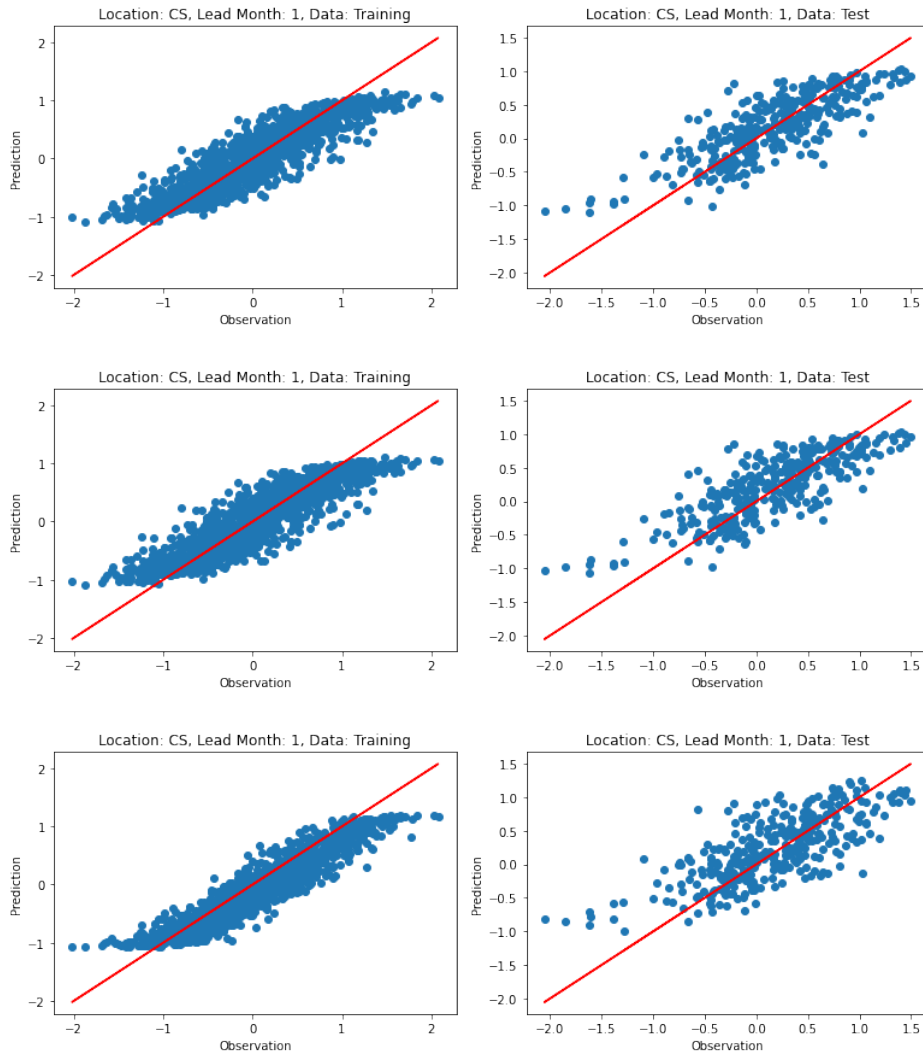


Figure 12: SSTA observation and prediction scatter plots of the last model for one lead month forecasts at Cook Strait, on the training and test data respectively. The corresponding loss functions from top to bottom are the MSE, the MAE, and the Huber.

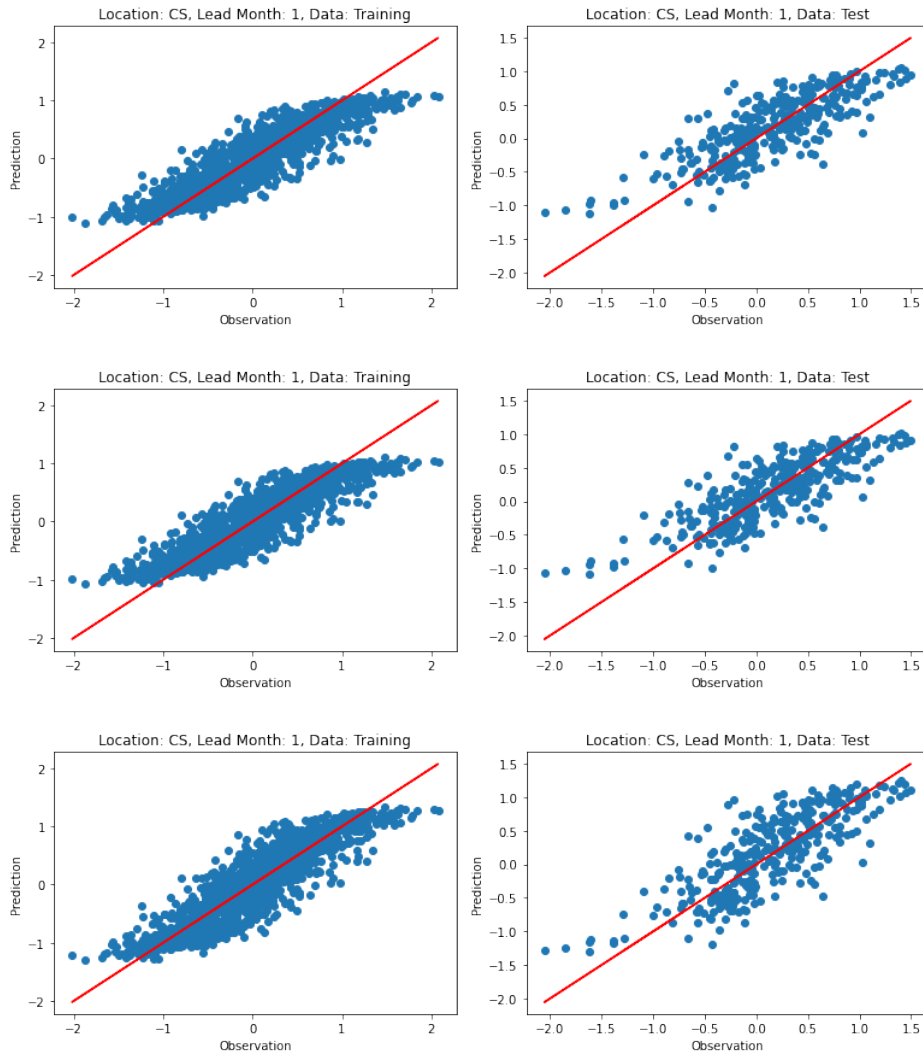


Figure 13: SSTA observation and prediction scatter plots of the last model for one lead month forecasts at Cook Strait, on the training and test data respectively. The corresponding loss functions from top to bottom are the weighted MSE, the focal-R, and the balanced MSE.

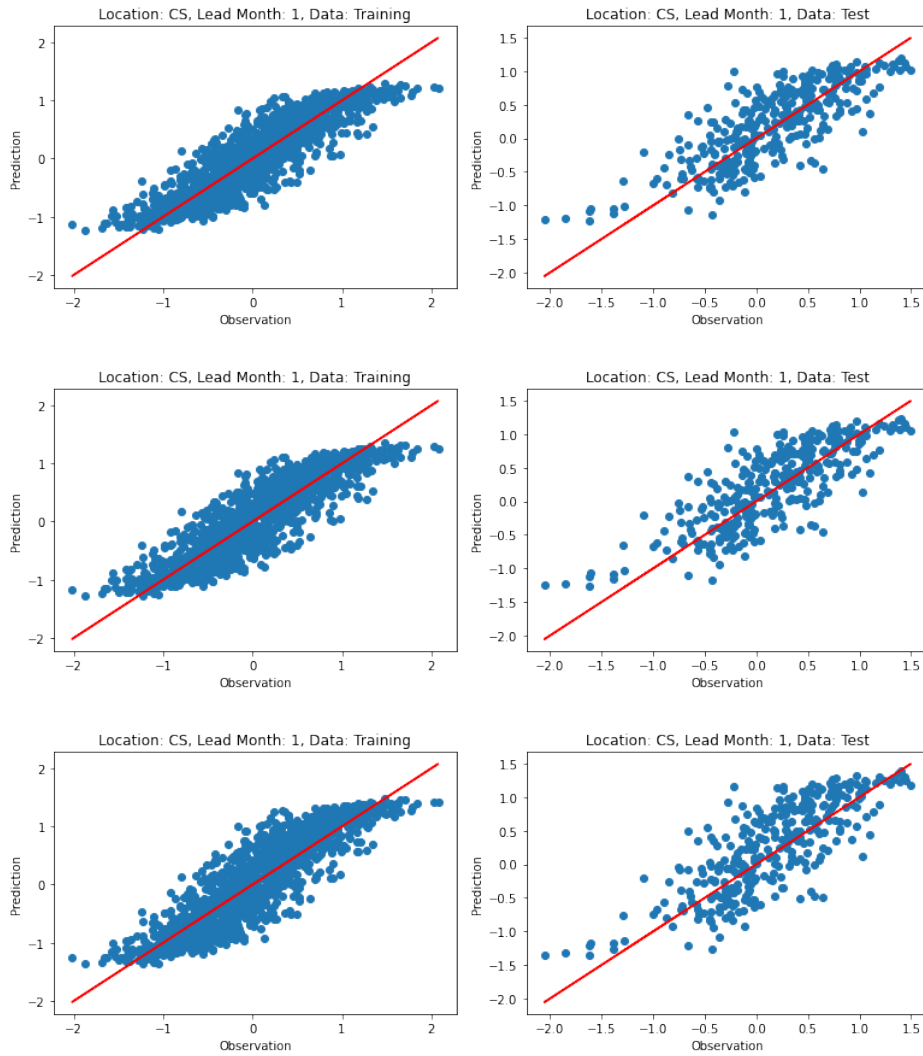


Figure 14: SSTA observation and prediction scatter plots of the last model for one lead month forecasts at Cook Strait, on the training and test data respectively. The corresponding loss function is our proposed scaling-weighted MSE, from top to bottom with the hyperparameters $\alpha = 1.5, \beta = 0.5, \alpha = 2, \beta = 0.5$, and $\alpha = 2, \beta = 1$ respectively.

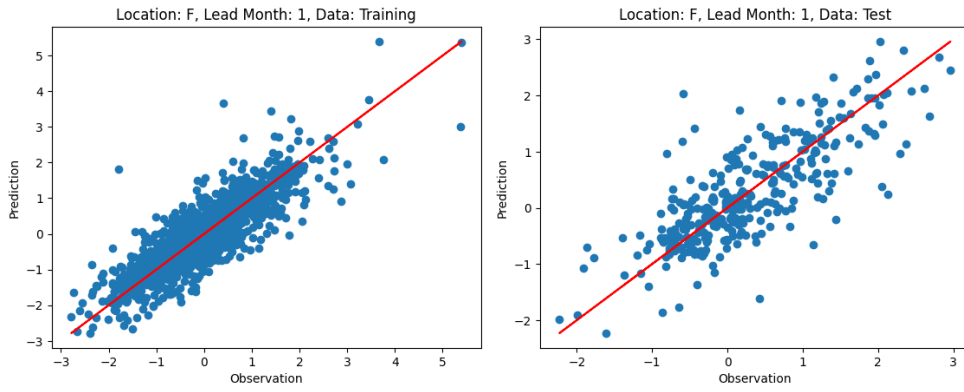


Figure 15: SSTA observation and prediction scatter plots of the persistence model for one lead month forecasts at Fiordland, on the training and test data respectively.

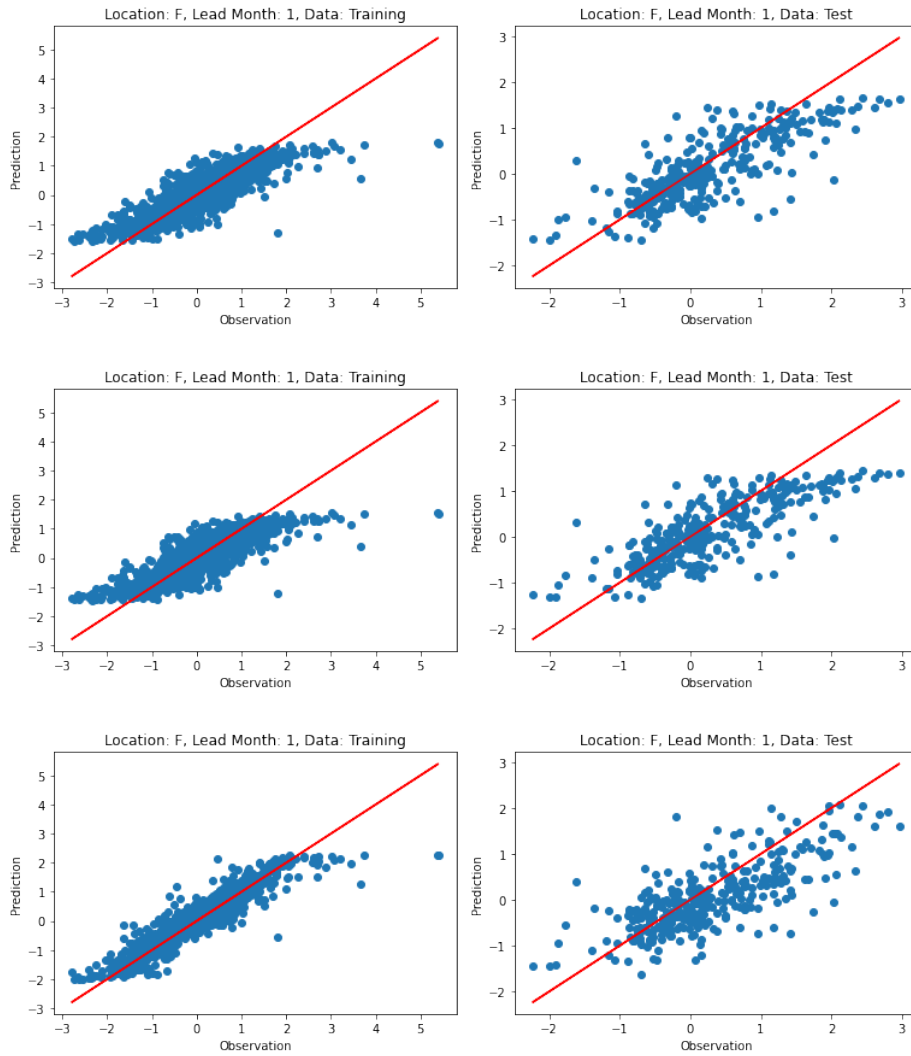


Figure 16: SSTA observation and prediction scatter plots of the last model for one lead month forecasts at Fiordland, on the training and test data respectively. The corresponding loss functions from top to bottom are the MSE, the MAE, and the Huber.

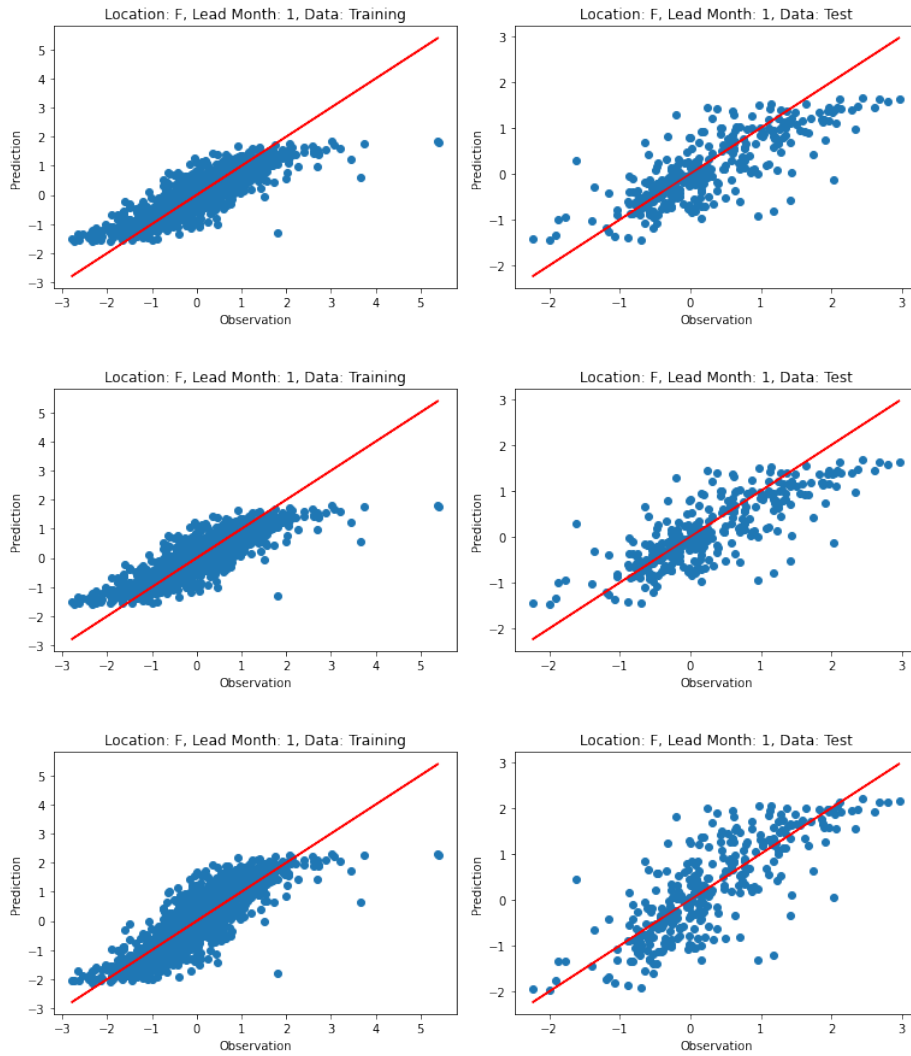


Figure 17: SSTA observation and prediction scatter plots of the last model for one lead month forecasts at Fiordland, on the training and test data respectively. The corresponding loss functions from top to bottom are the weighted MSE, the focal-R, and the balanced MSE.

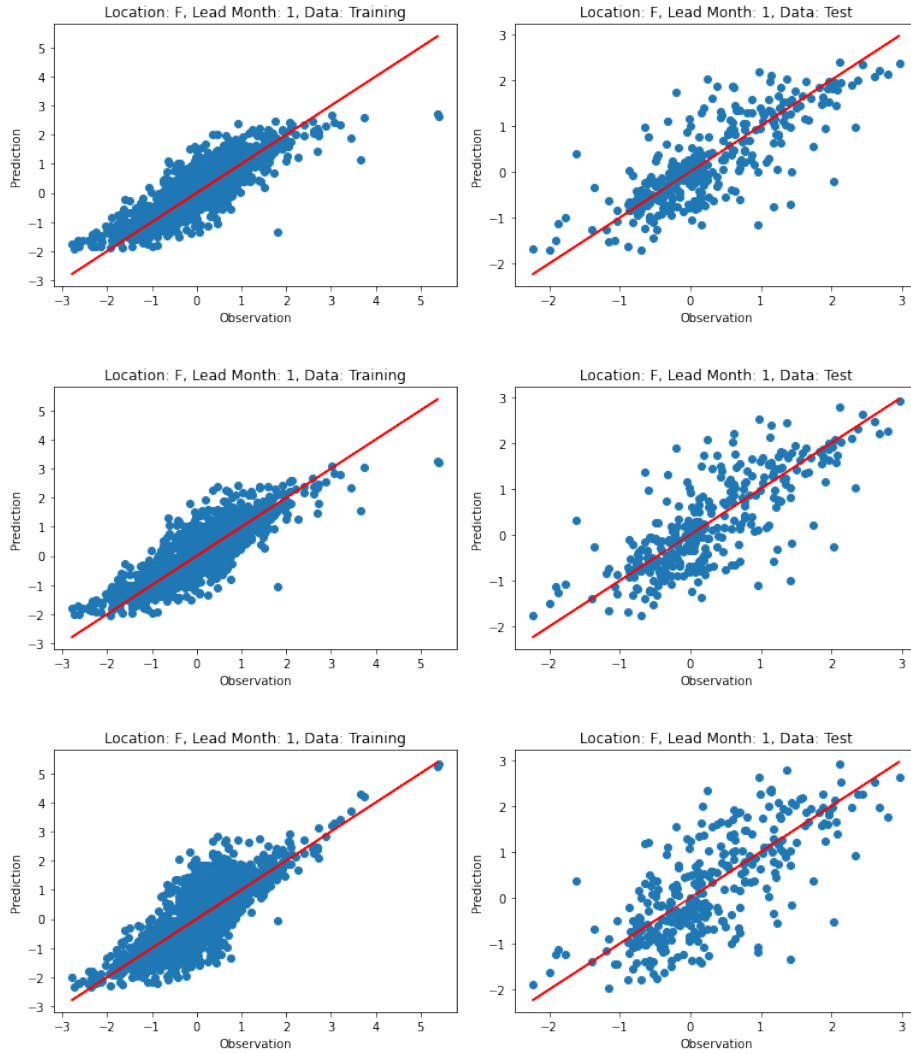


Figure 18: SSTA observation and prediction scatter plots of the last model for one lead month forecasts at Fiordland, on the training and test data respectively. The corresponding loss function is our proposed scaling-weighted MSE, from top to bottom with the hyperparameters $\alpha = 1.5, \beta = 0.5, \alpha = 2, \beta = 0.5,$ and $\alpha = 2, \beta = 1$ respectively.

A.3.2 Two Lead Month Forecasts

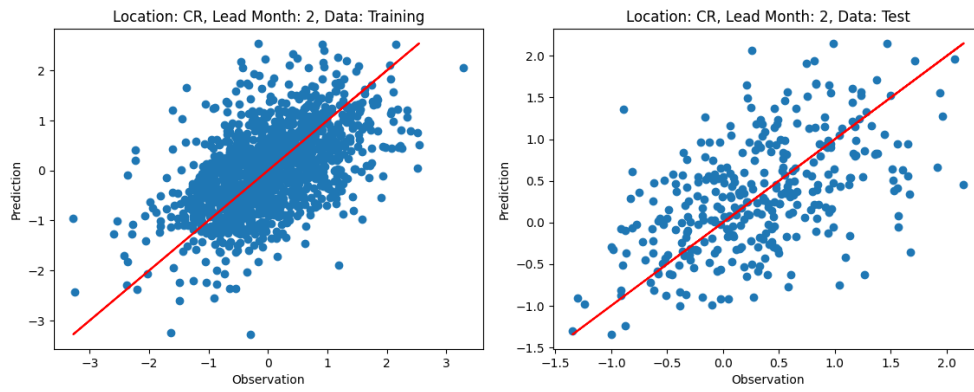


Figure 19: SSTA observation and prediction scatter plots of the two-lag model for two lead month forecasts at Cape Reinga, on the training and test data respectively.

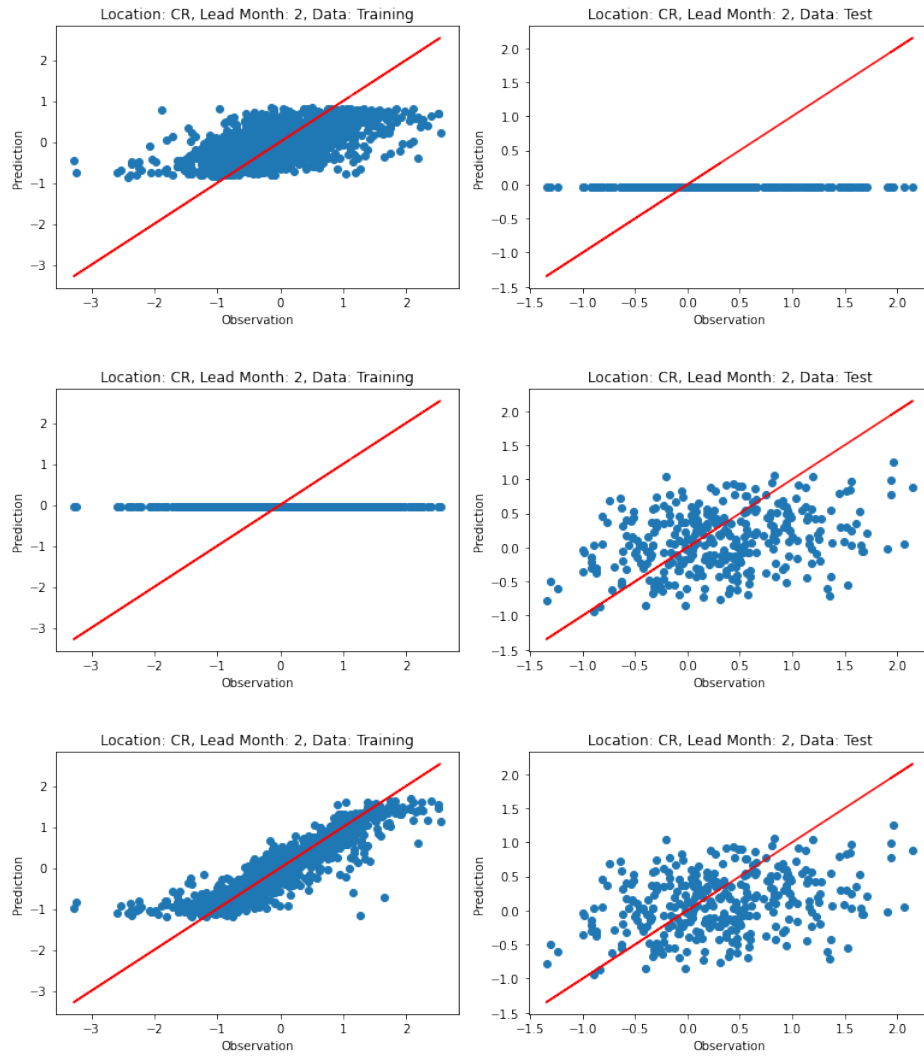


Figure 20: SSTA observation and prediction scatter plots of the last model for two lead month forecasts at Cape Reinga, on the training and test data respectively. The corresponding loss functions from top to bottom are the MSE, the MAE, and the Huber.

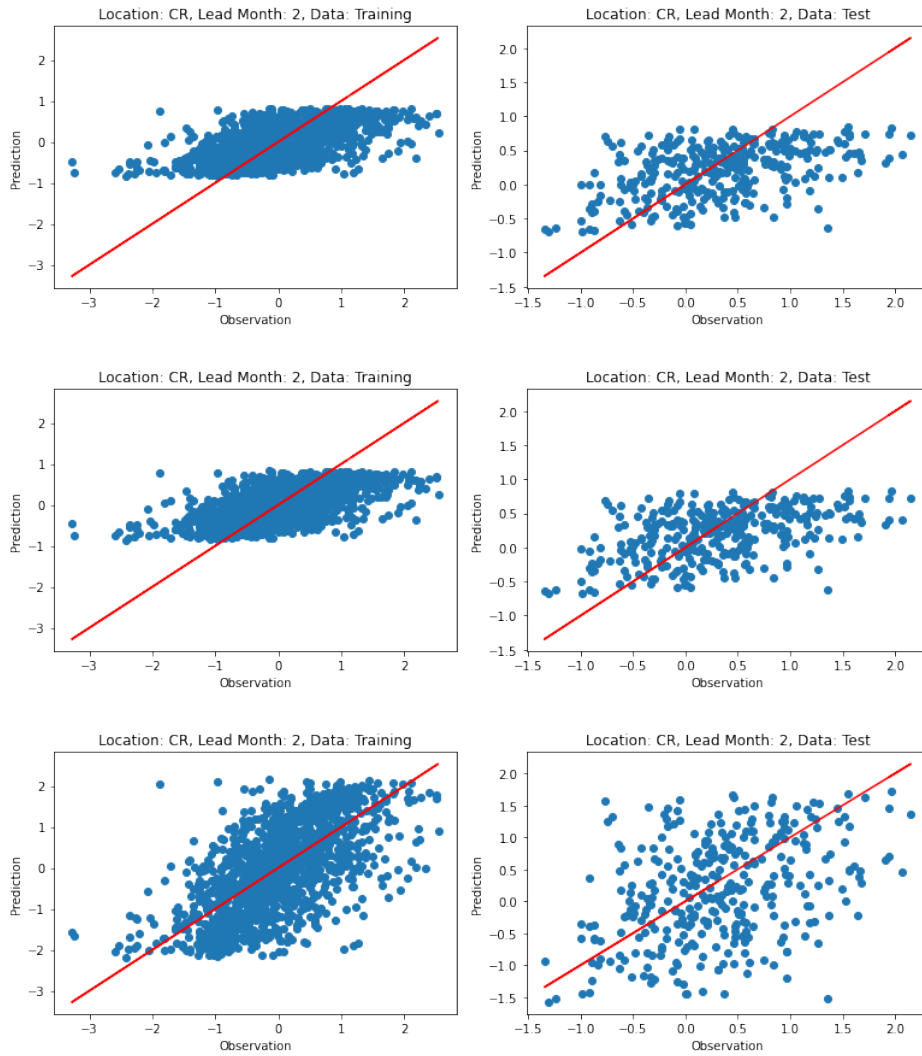


Figure 21: SSTA observation and prediction scatter plots of the last model for two lead month forecasts at Cape Reinga, on the training and test data respectively. The corresponding loss functions from top to bottom are the weighted MSE, the focal-R, and the balanced MSE.

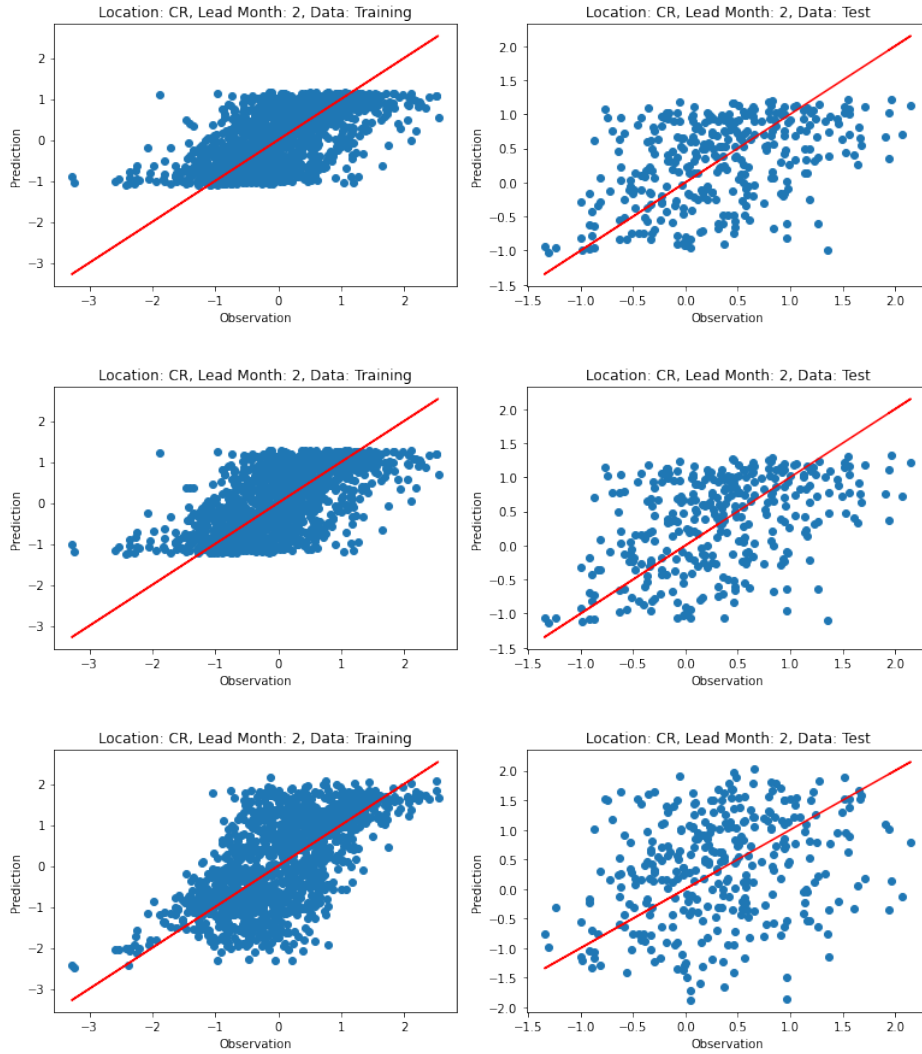


Figure 22: SSTA observation and prediction scatter plots of the last model for two lead month forecasts at Cape Reinga, on the training and test data respectively. The corresponding loss function is our proposed scaling-weighted MSE, from top to bottom with the hyperparameters $\alpha = 1.5$, $\beta = 0.5$, $\alpha = 2$, $\beta = 0.5$, and $\alpha = 2$, $\beta = 1$ respectively.

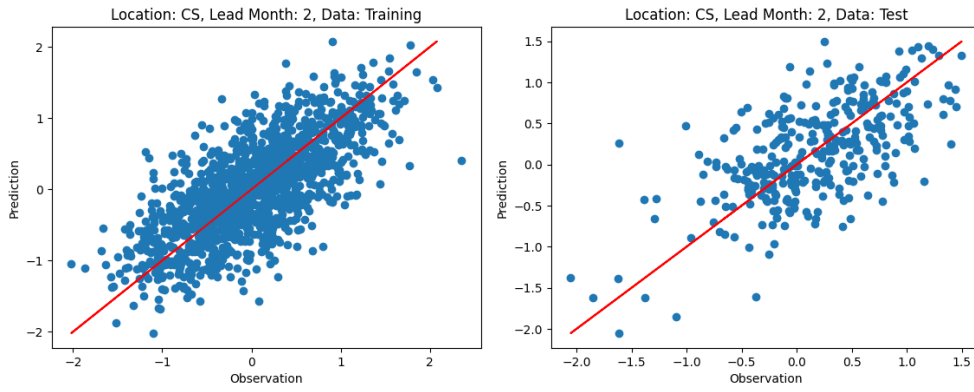


Figure 23: SSTA observation and prediction scatter plots of the two-lag model for two lead month forecasts at Cook Strait, on the training and test data respectively.

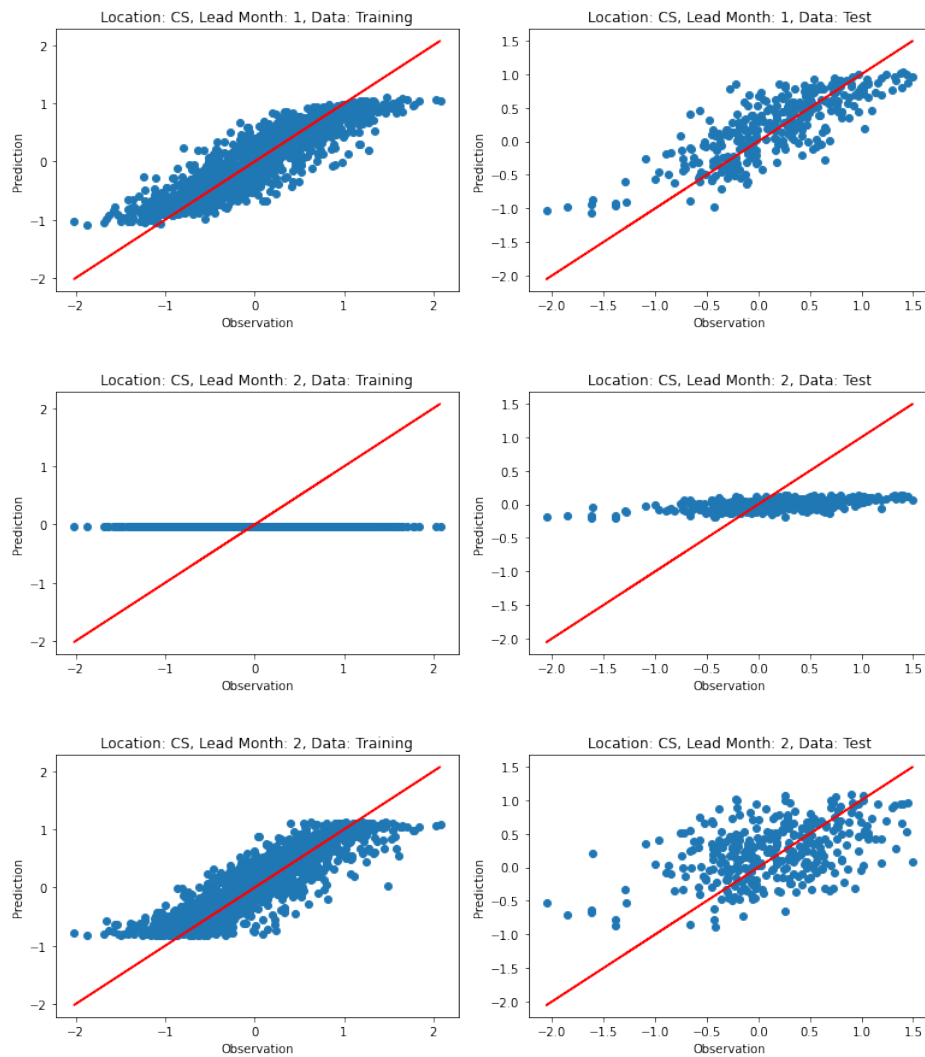


Figure 24: SSTA observation and prediction scatter plots of the last model for two lead month forecasts at Cook Strait, on the training and test data respectively. The corresponding loss functions from top to bottom are the MSE, the MAE, and the Huber.

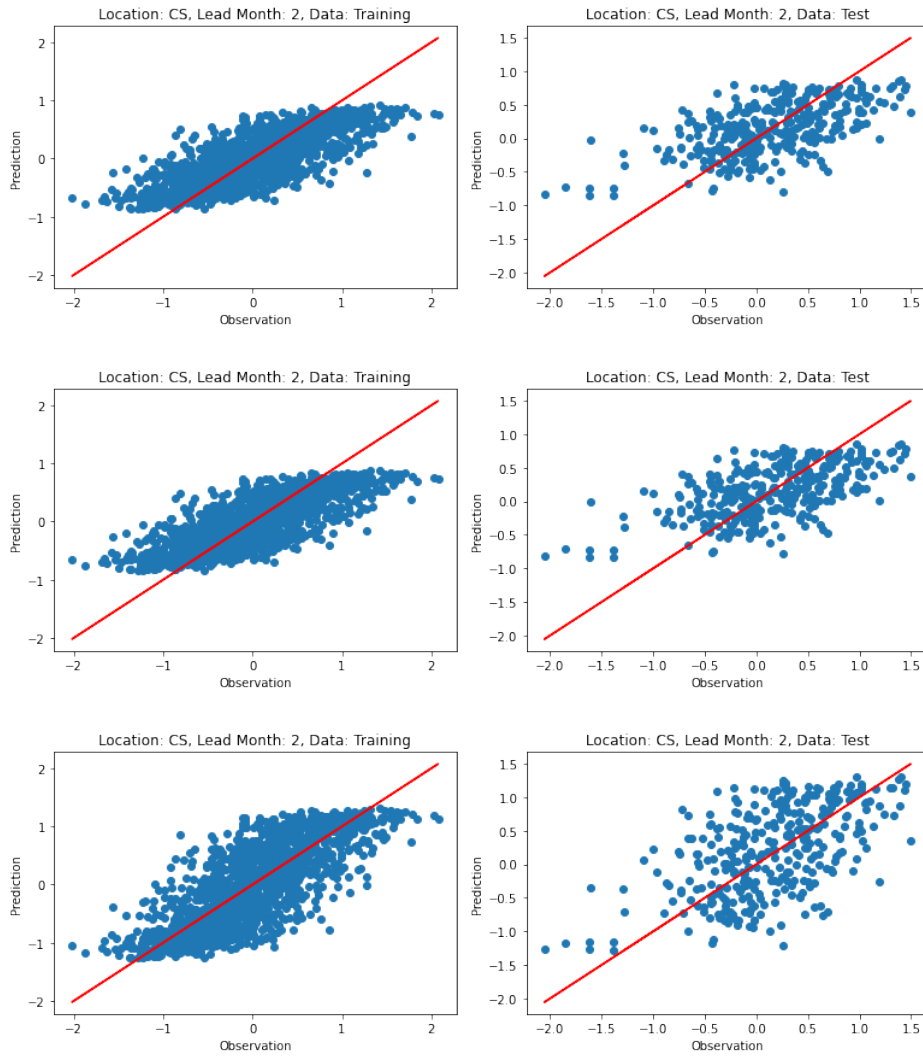


Figure 25: SSTA observation and prediction scatter plots of the last model for two lead month forecasts at Cook Strait, on the training and test data respectively. The corresponding loss functions from top to bottom are the weighted MSE, the focal-R, and the balanced MSE.

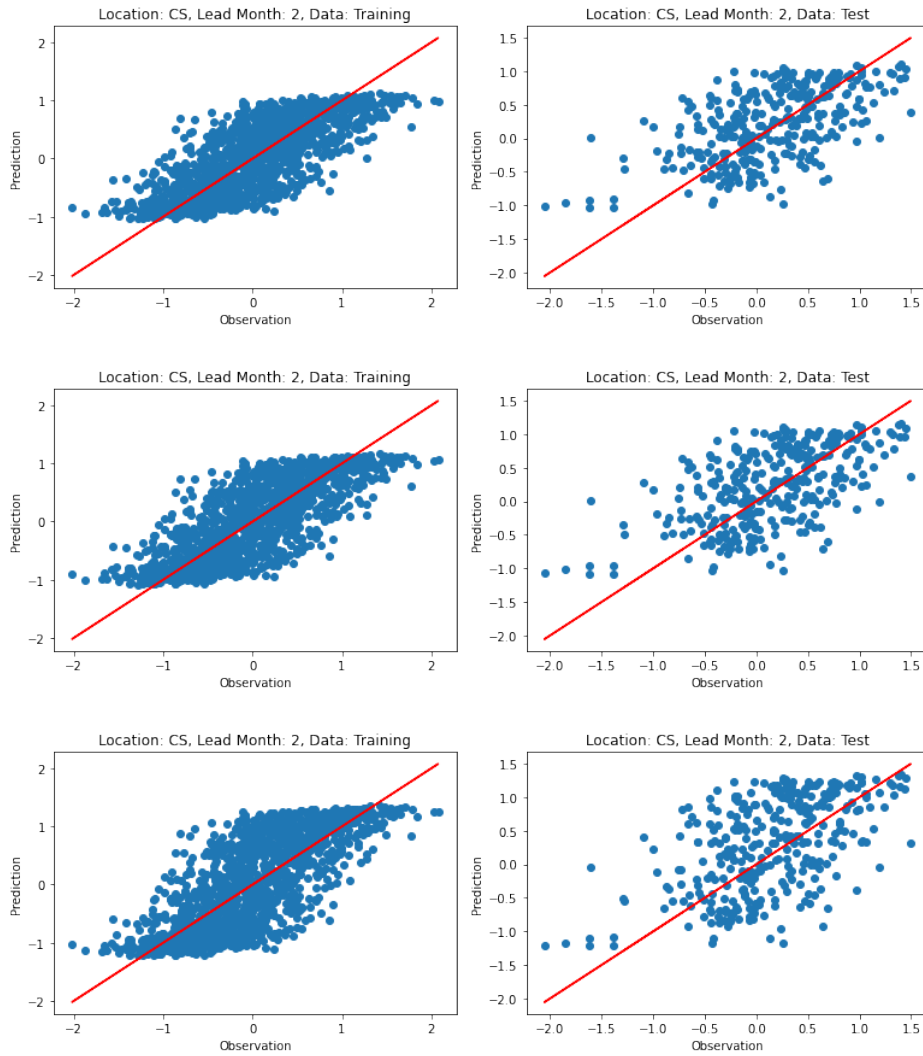


Figure 26: SSTA observation and prediction scatter plots of the last model for two lead month forecasts at Cook Strait, on the training and test data respectively. The corresponding loss function is our proposed scaling-weighted MSE, from top to bottom with the hyperparameters $\alpha = 1.5, \beta = 0.5, \alpha = 2, \beta = 0.5,$ and $\alpha = 2, \beta = 1$ respectively.

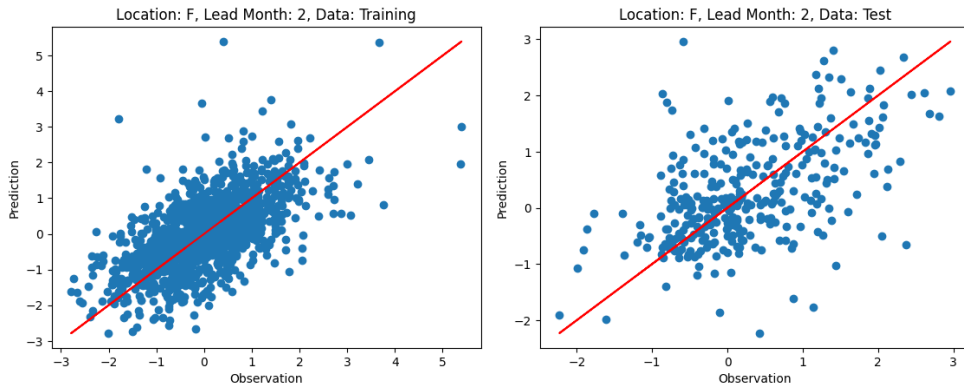


Figure 27: SSTA observation and prediction scatter plots of the two-lag model for two lead month forecasts at Fiordland, on the training and test data respectively.

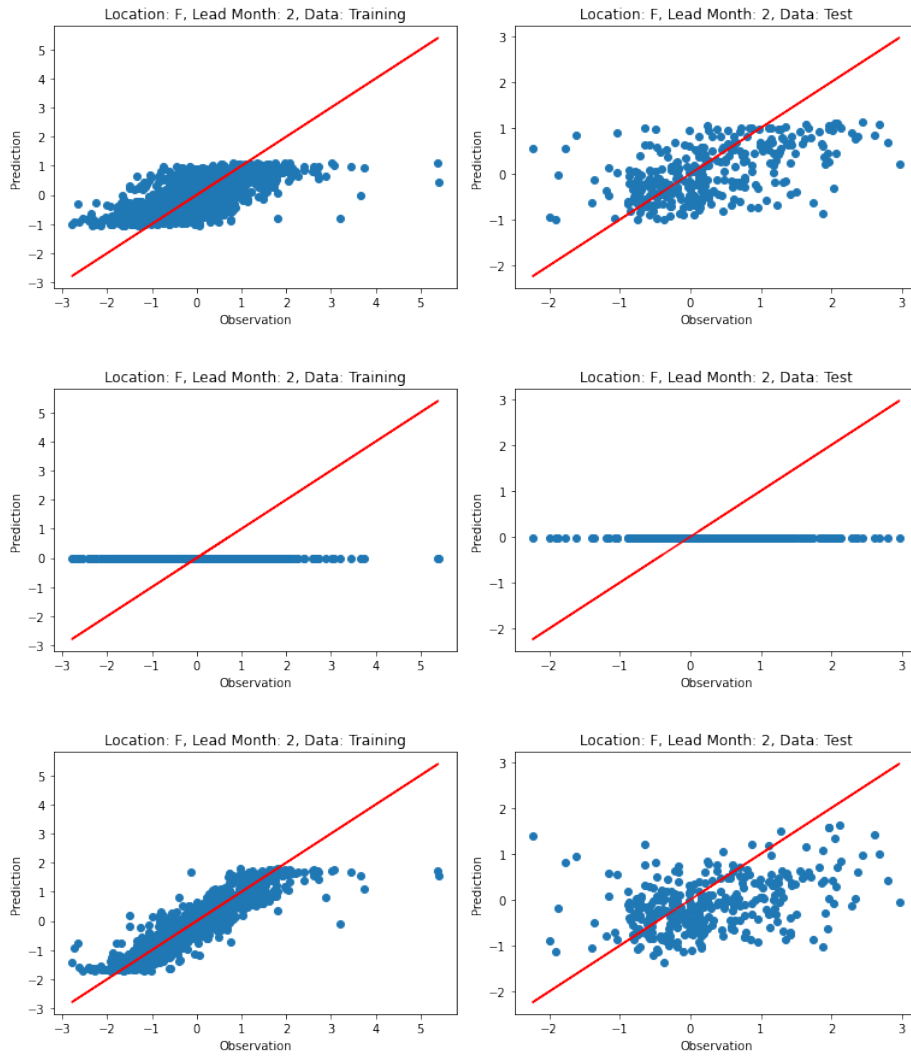


Figure 28: SSTA observation and prediction scatter plots of the last model for two lead month forecasts at Fiordland, on the training and test data respectively. The corresponding loss functions from top to bottom are the MSE, the MAE, and the Huber.

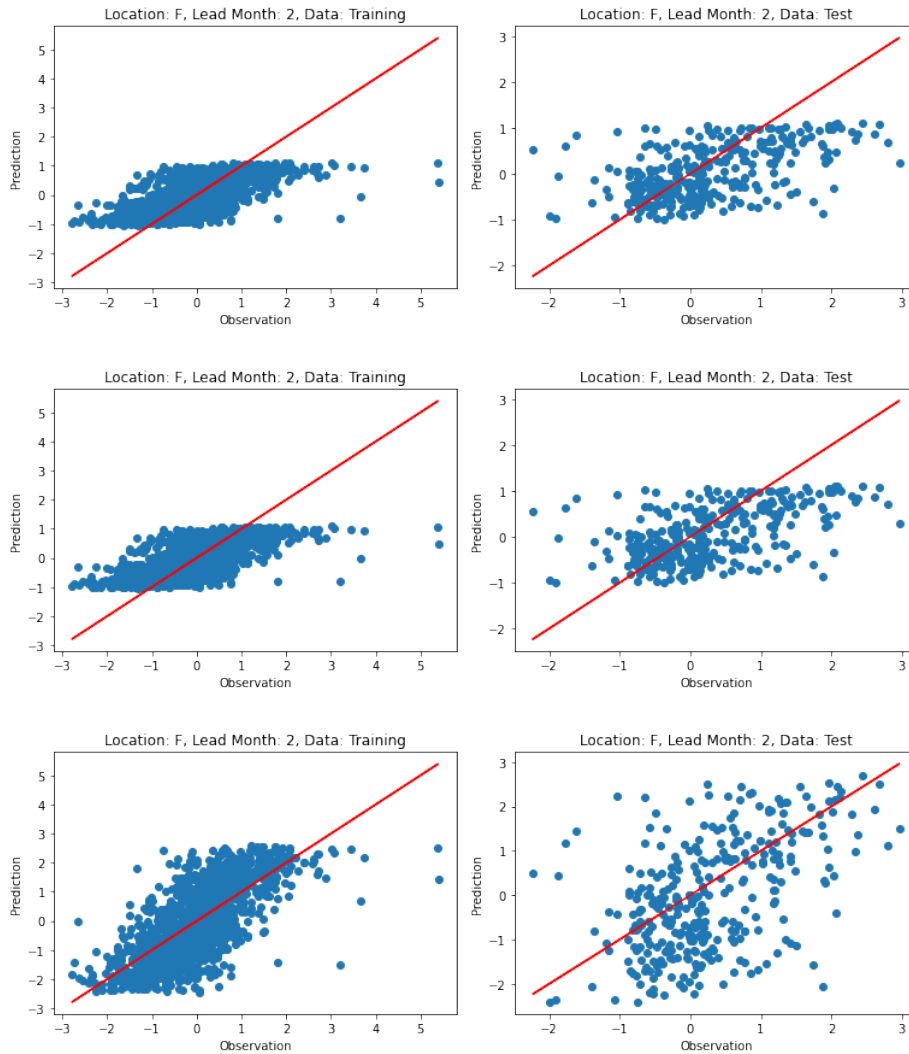


Figure 29: SSTA observation and prediction scatter plots of the last model for two lead month forecasts at Fiordland, on the training and test data respectively. The corresponding loss functions from top to bottom are the weighted MSE, the focal-R, and the balanced MSE.

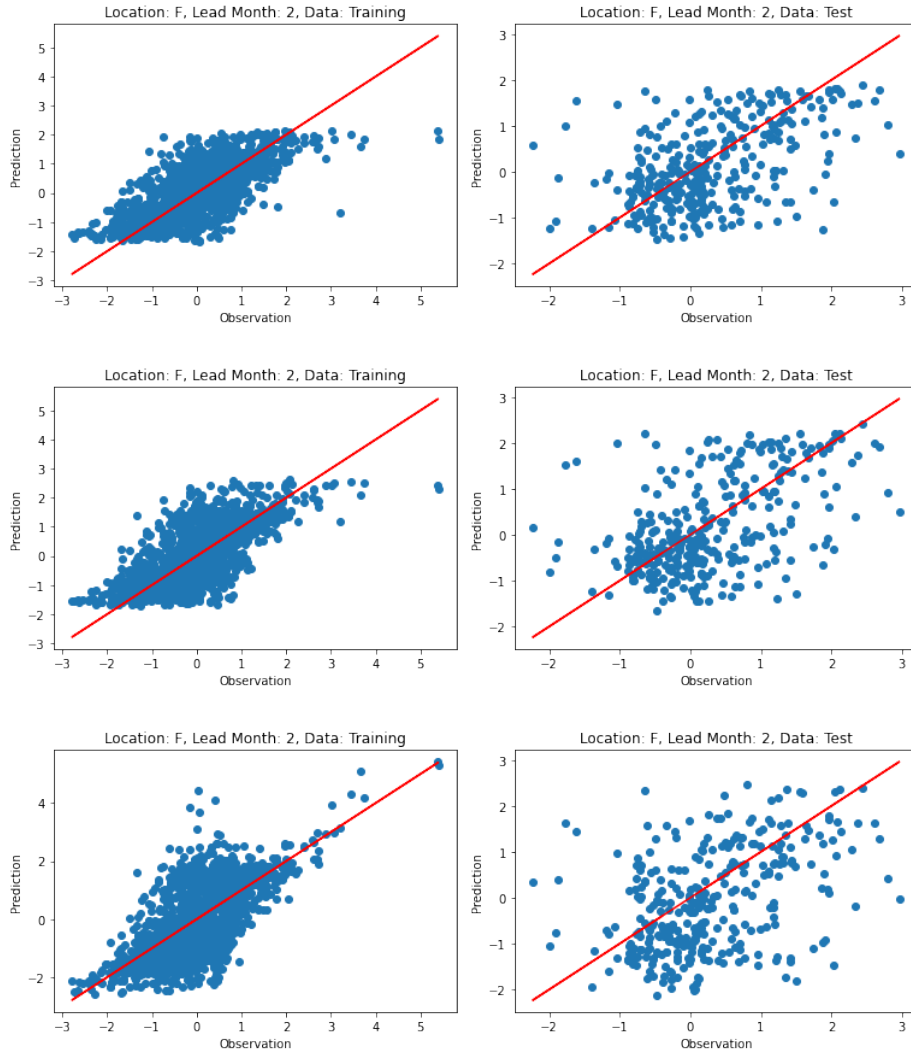


Figure 30: SSTA observation and prediction scatter plots of the last model for two lead month forecasts at Fiordland, on the training and test data respectively. The corresponding loss function is our proposed scaling-weighted MSE, from top to bottom with the hyperparameters $\alpha = 1.5, \beta = 0.5, \alpha = 2, \beta = 0.5,$ and $\alpha = 2, \beta = 1$ respectively.

A.3.3 Three Lead Month Forecasts

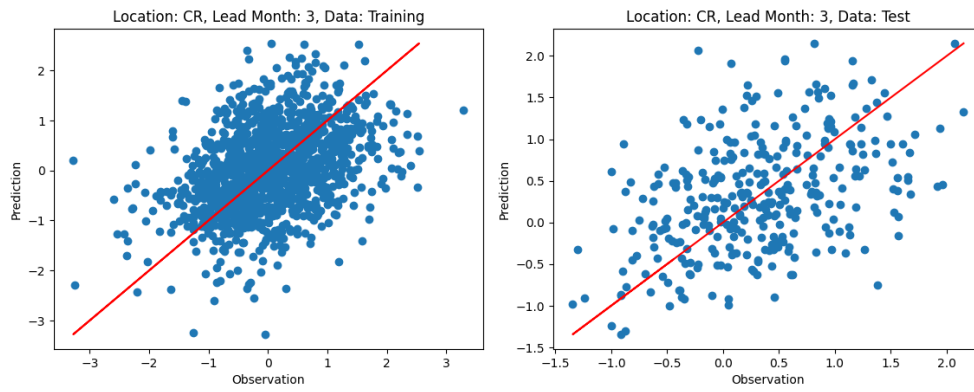


Figure 31: SSTA observation and prediction scatter plots of the three-lag model for three lead month forecasts at Cape Reinga, on the training and test data respectively.

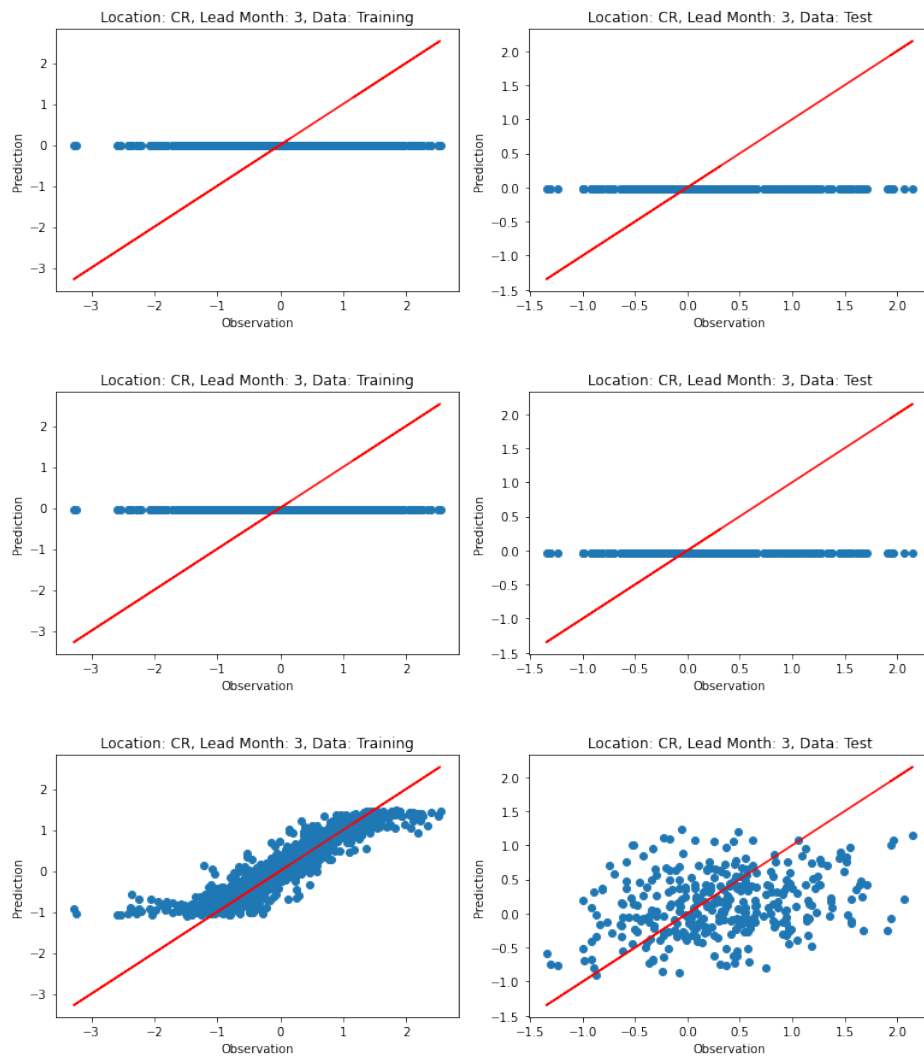


Figure 32: SSTA observation and prediction scatter plots of the last model for three lead month forecasts at Cape Reinga, on the training and test data respectively. The corresponding loss functions from top to bottom are the MSE, the MAE, and the Huber.

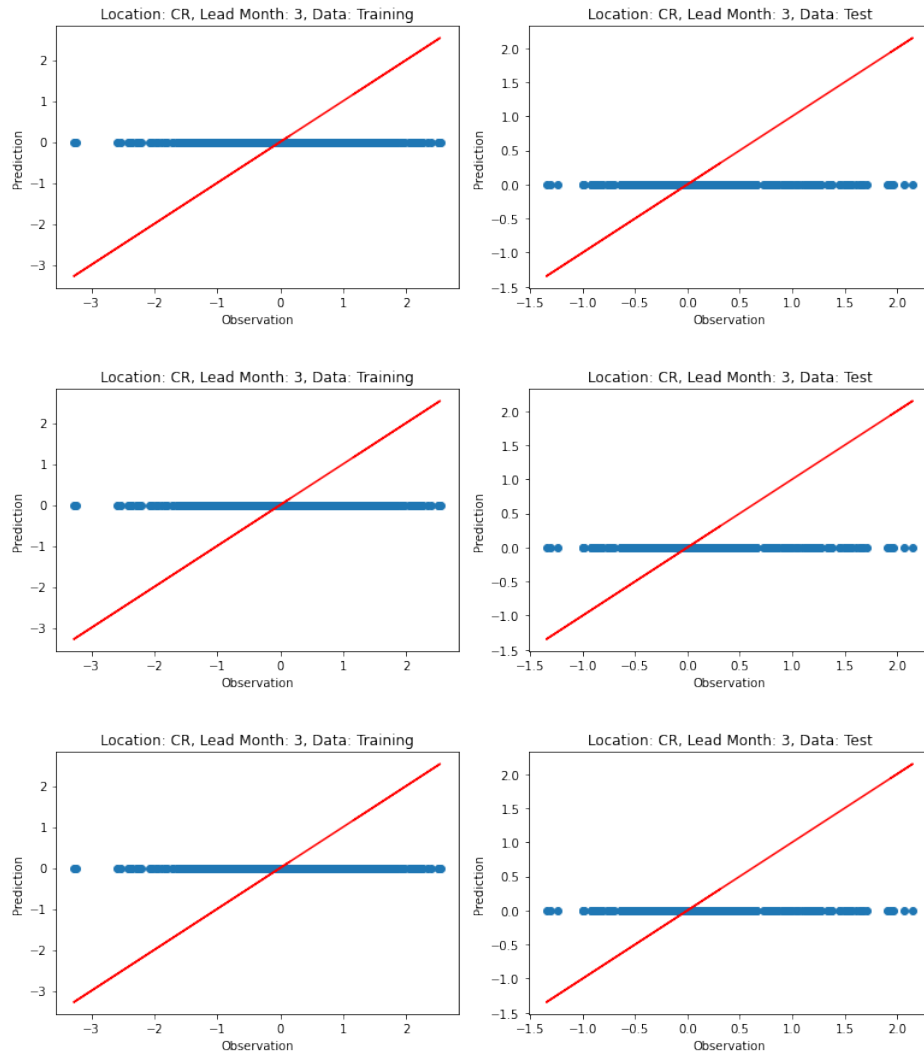


Figure 33: SSTA observation and prediction scatter plots of the last model for three lead month forecasts at Cape Reinga, on the training and test data respectively. The corresponding loss functions from top to bottom are the weighted MSE, the focal-R, and the balanced MSE.

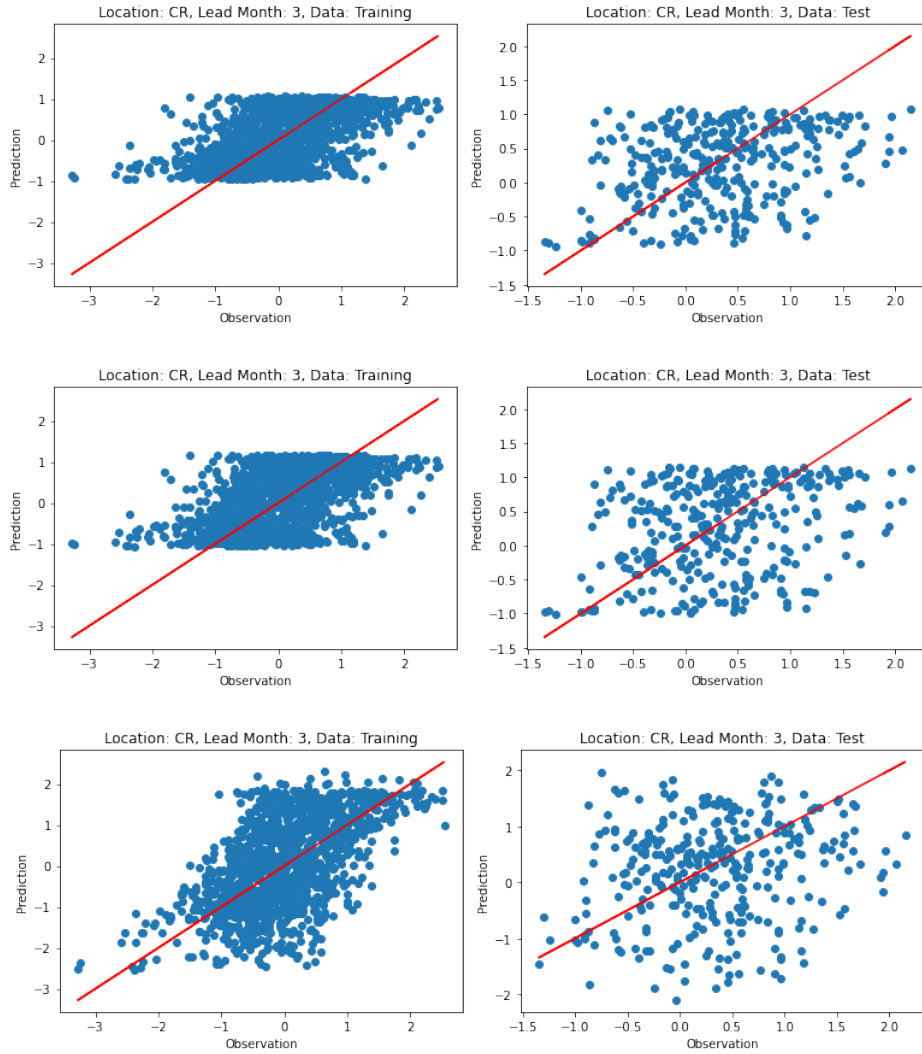


Figure 34: SSTA observation and prediction scatter plots of the last model for three lead month forecasts at Cape Reinga, on the training and test data respectively. The corresponding loss function is our proposed scaling-weighted MSE, from top to bottom with the hyperparameters $\alpha = 1.5$, $\beta = 0.5$, $\alpha = 2$, $\beta = 0.5$, and $\alpha = 2$, $\beta = 1$ respectively.

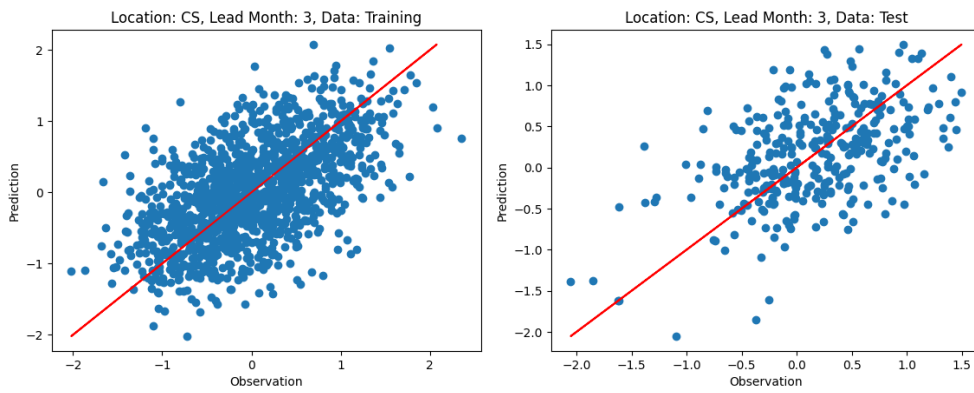


Figure 35: SSTA observation and prediction scatter plots of the three-lag model for three lead month forecasts at Cook Strait, on the training and test data respectively.

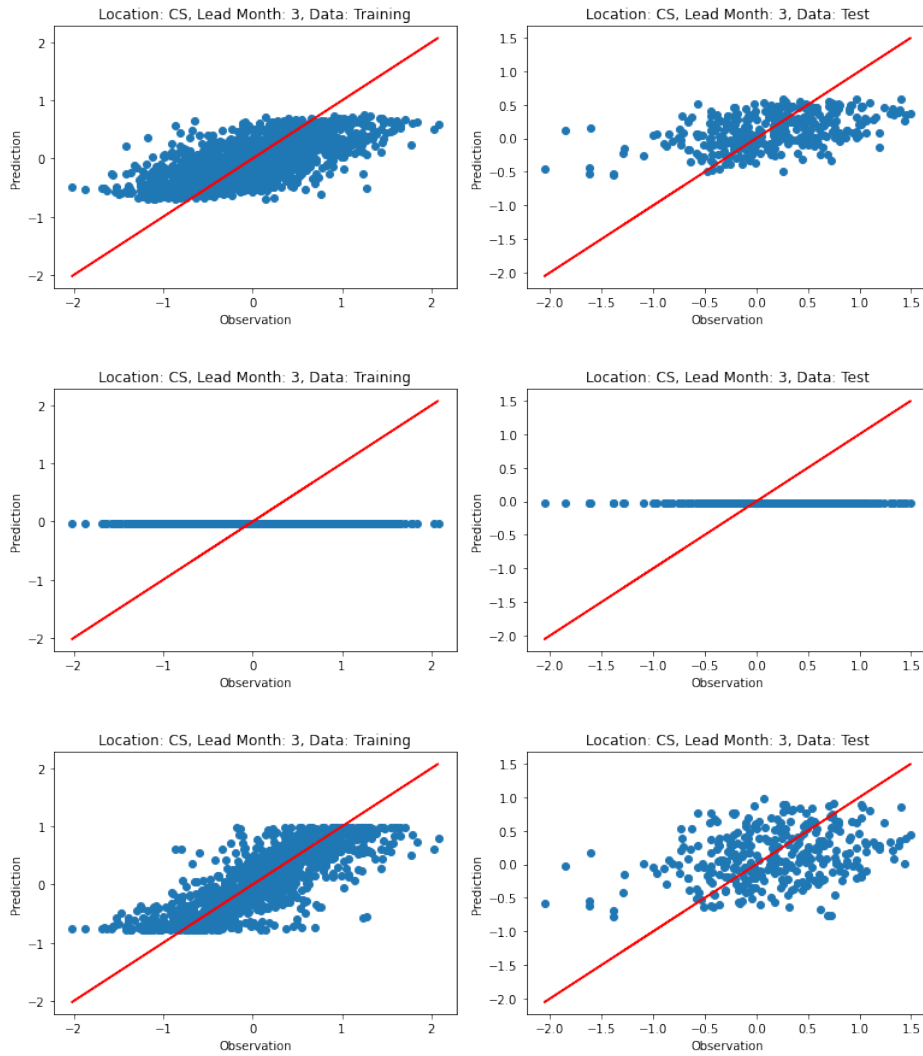


Figure 36: SSTA observation and prediction scatter plots of the last model for three lead month forecasts at Cook Strait, on the training and test data respectively. The corresponding loss functions from top to bottom are the MSE, the MAE, and the Huber.

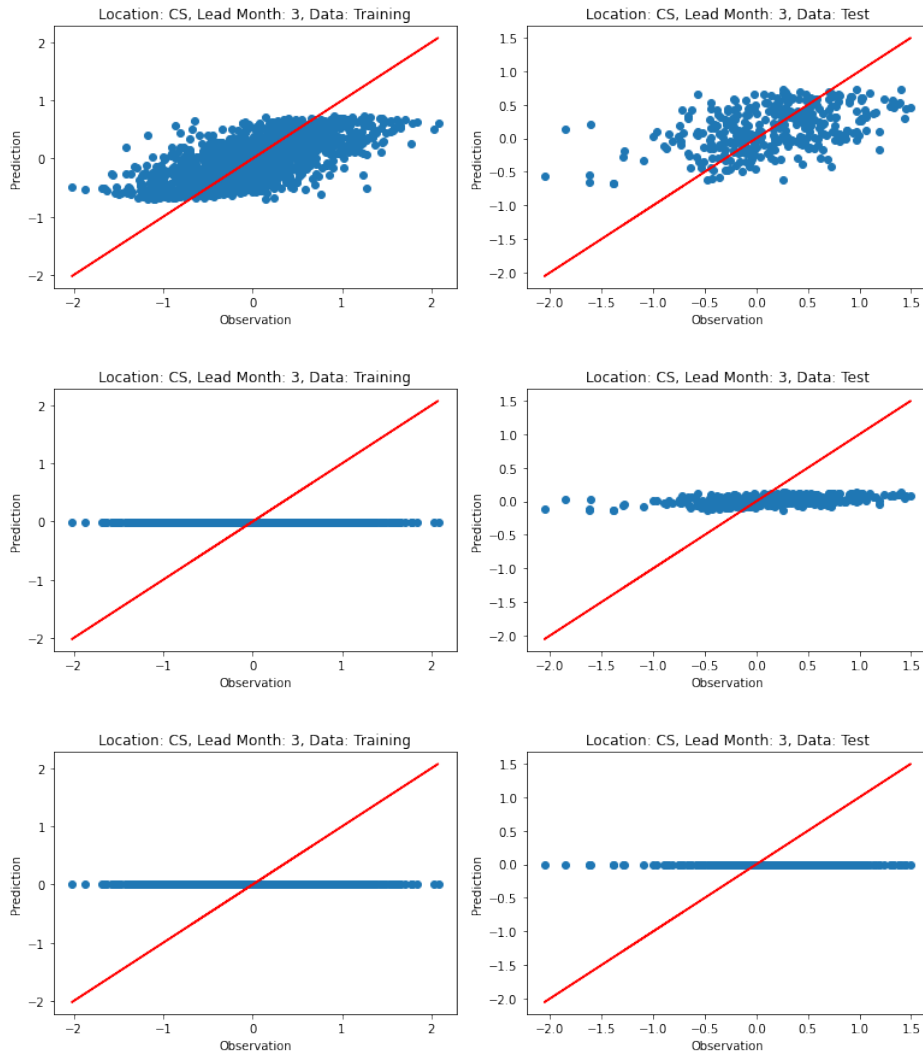


Figure 37: SSTA observation and prediction scatter plots of the last model for three lead month forecasts at Cook Strait, on the training and test data respectively. The corresponding loss functions from top to bottom are the weighted MSE, the focal-R, and the balanced MSE.

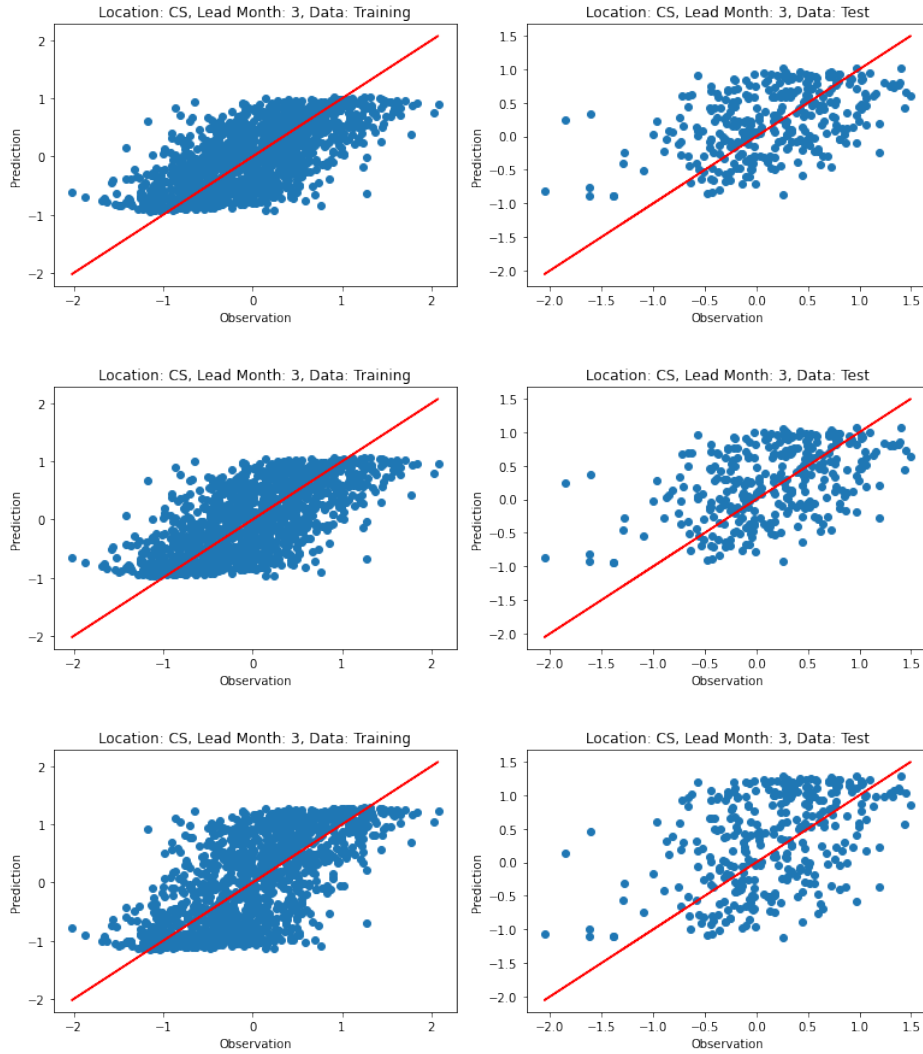


Figure 38: SSTA observation and prediction scatter plots of the last model for three lead month forecasts at Cook Strait, on the training and test data respectively. The corresponding loss function is our proposed scaling-weighted MSE, from top to bottom with the hyperparameters $\alpha = 1.5$, $\beta = 0.5$, $\alpha = 2$, $\beta = 0.5$, and $\alpha = 2$, $\beta = 1$ respectively.

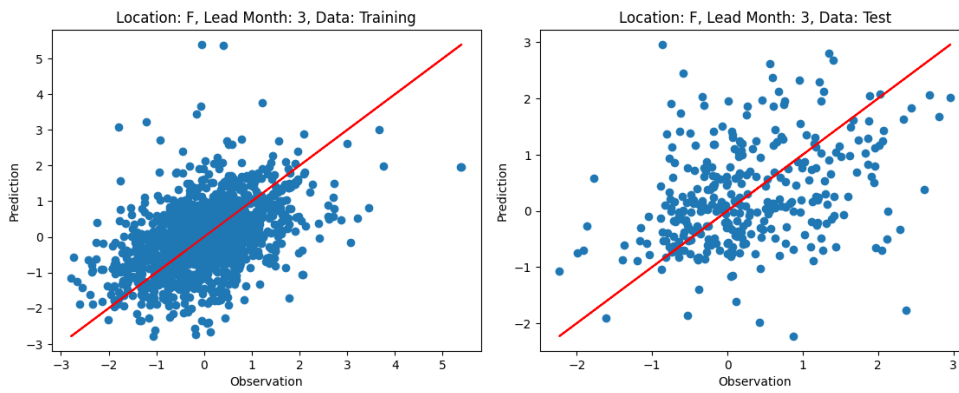


Figure 39: SSTA observation and prediction scatter plots of the three-lag model for three lead month forecasts at Fiordland, on the training and test data respectively.

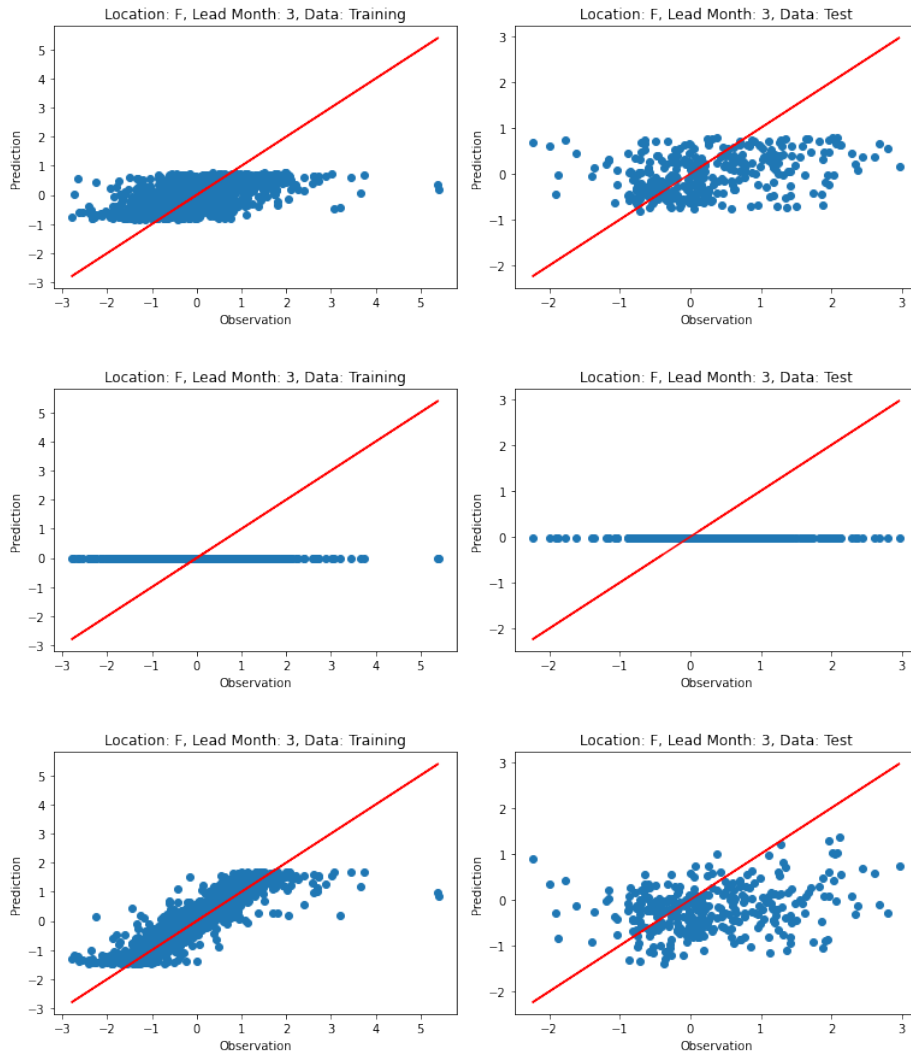


Figure 40: SSTA observation and prediction scatter plots of the last model for three lead month forecasts at Fiordland, on the training and test data respectively. The corresponding loss functions from top to bottom are the MSE, the MAE, and the Huber.

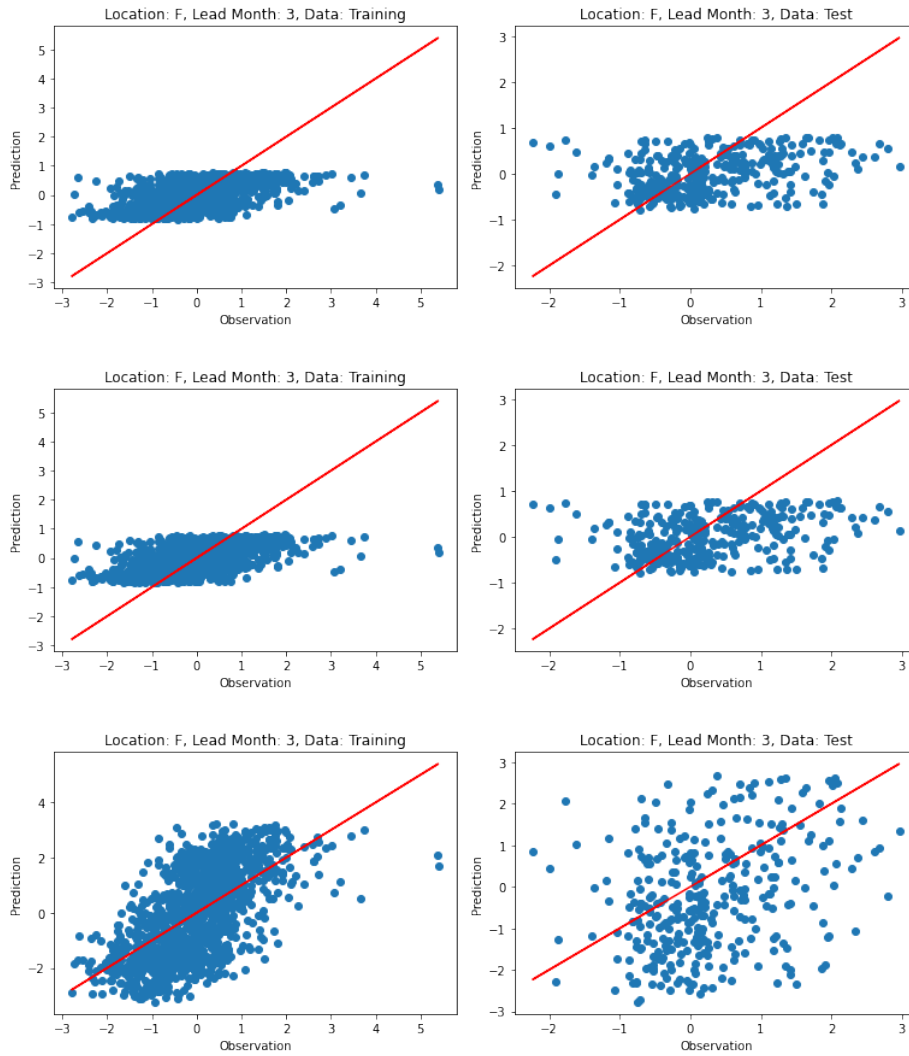


Figure 41: SSTA observation and prediction scatter plots of the last model for three lead month forecasts at Fiordland, on the training and test data respectively. The corresponding loss functions from top to bottom are the weighted MSE, the focal-R, and the balanced MSE.

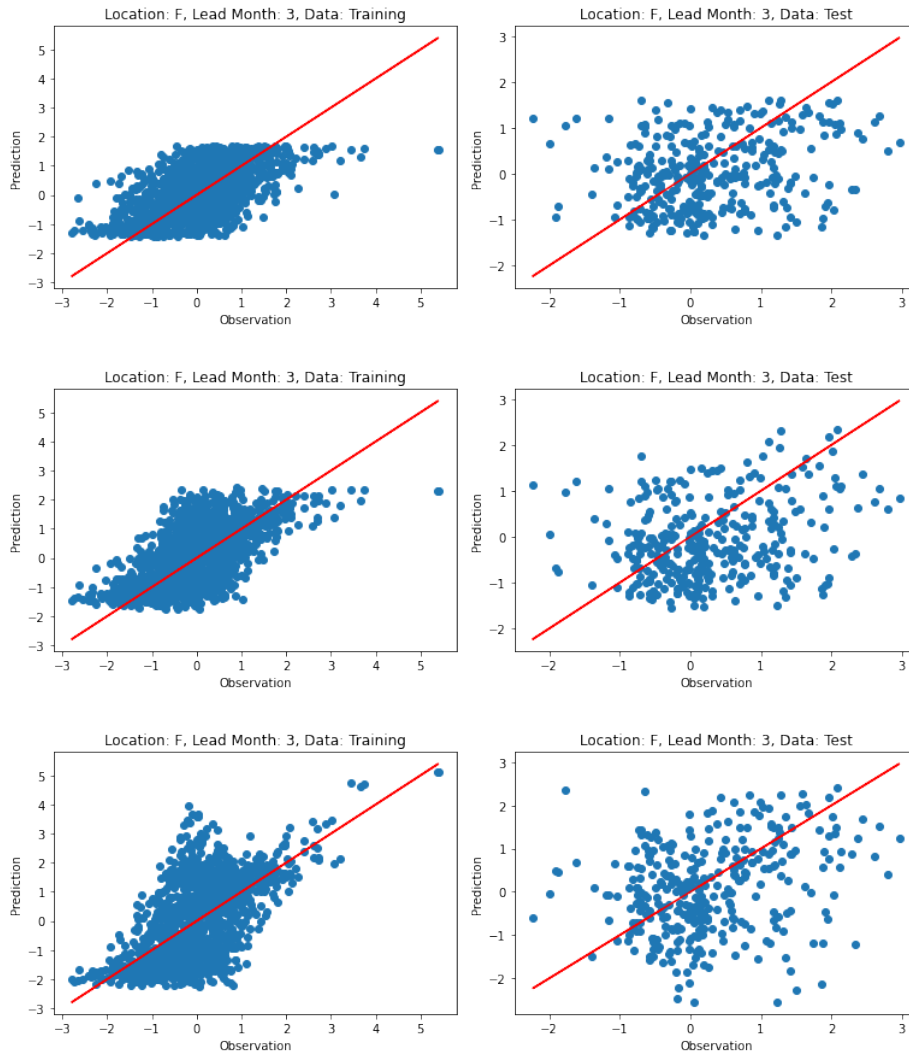


Figure 42: SSTA observation and prediction scatter plots of the last model for three lead month forecasts at Fiordland, on the training and test data respectively. The corresponding loss function is our proposed scaling-weighted MSE, from top to bottom with the hyperparameters $\alpha = 1.5, \beta = 0.5, \alpha = 2, \beta = 0.5$, and $\alpha = 2, \beta = 1$ respectively.

A.3.4 Six Lead Month Forecasts

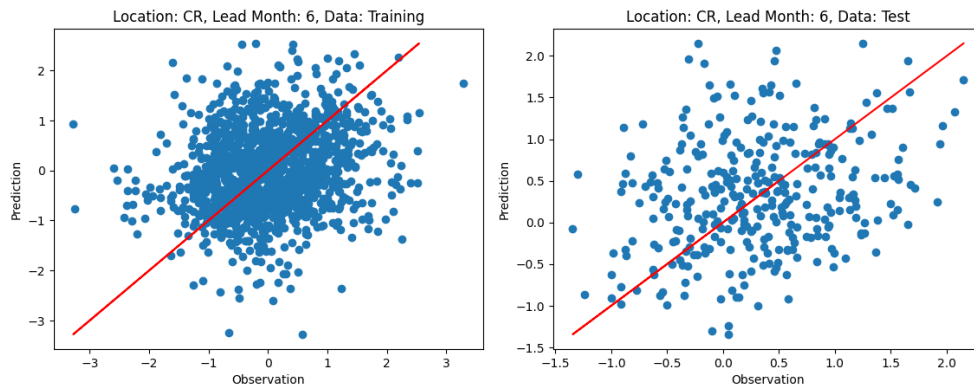


Figure 43: SSTA observation and prediction scatter plots of the six-lag model for six lead month forecasts at Cape Reinga, on the training and test data respectively.

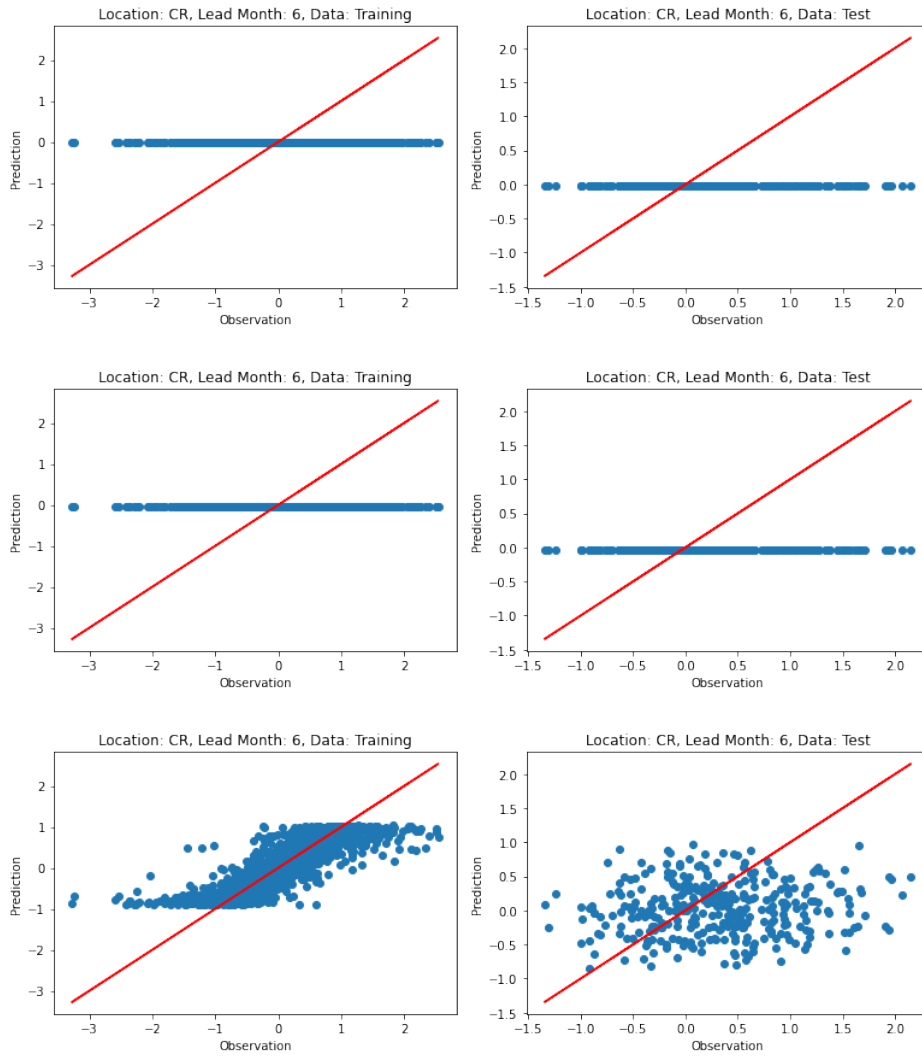


Figure 44: SSTA observation and prediction scatter plots of the last model for six lead month forecasts at Cape Reinga, on the training and test data respectively. The corresponding loss functions from top to bottom are the MSE, the MAE, and the Huber.

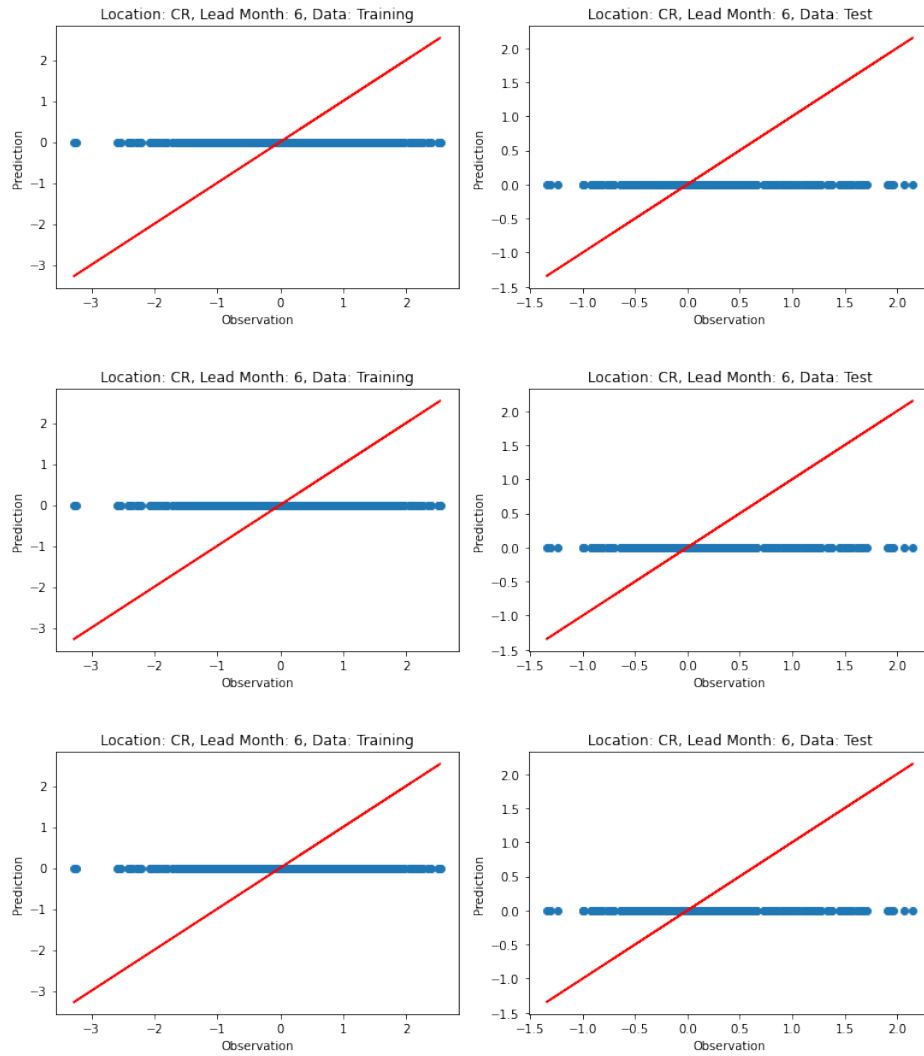


Figure 45: SSTA observation and prediction scatter plots of the last model for six lead month forecasts at Cape Reinga, on the training and test data respectively. The corresponding loss functions from top to bottom are the weighted MSE, the focal-R, and the balanced MSE.

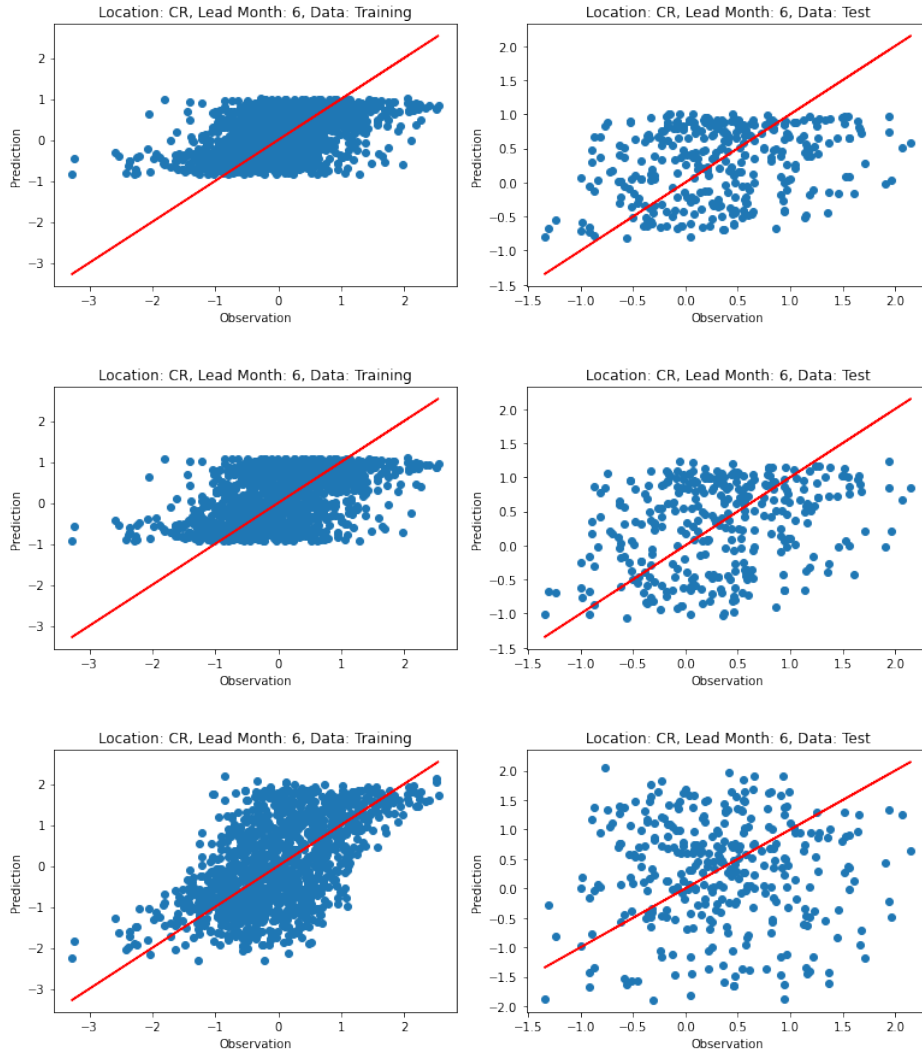


Figure 46: SSTA observation and prediction scatter plots of the last model for six lead month forecasts at Cape Reinga, on the training and test data respectively. The corresponding loss function is our proposed scaling-weighted MSE, from top to bottom with the hyperparameters $\alpha = 1.5$, $\beta = 0.5$, $\alpha = 2$, $\beta = 0.5$, and $\alpha = 2$, $\beta = 1$ respectively.



Figure 47: SSTA observation and prediction scatter plots of the six-lag model for six lead month forecasts at Cook Strait, on the training and test data respectively.

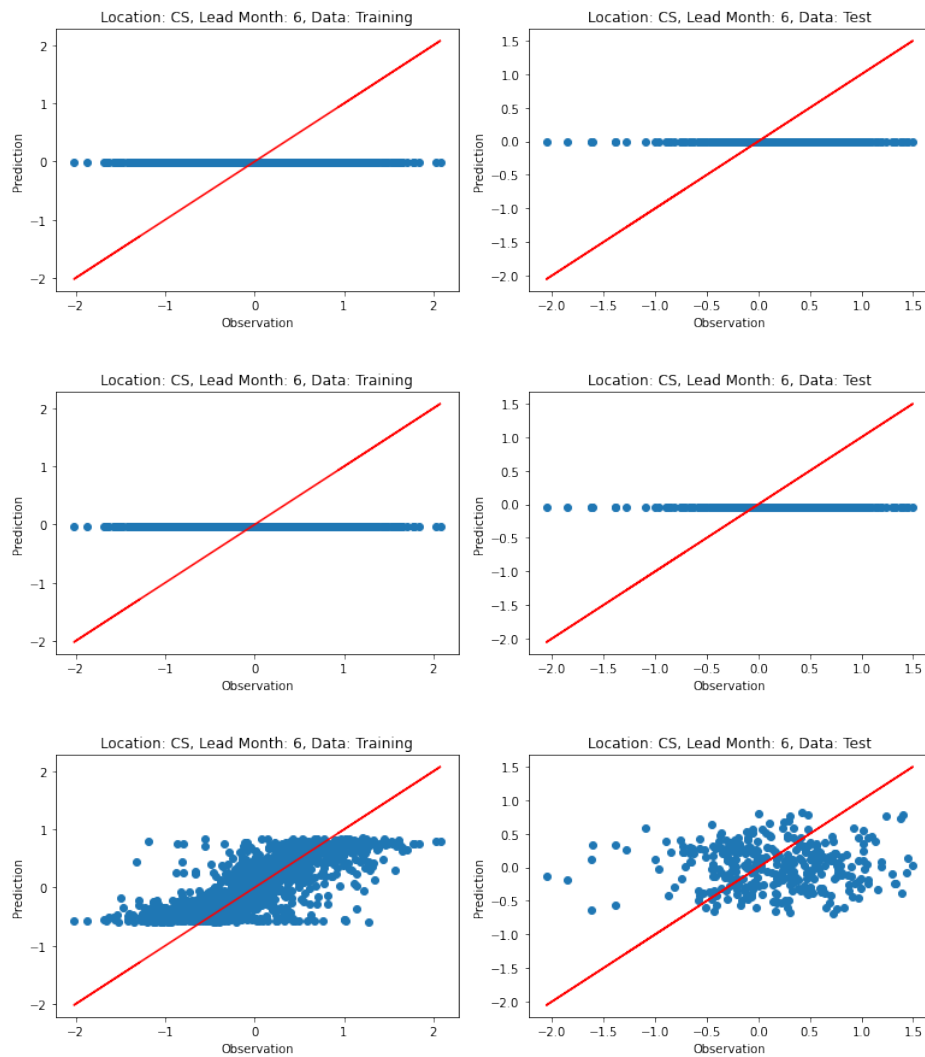


Figure 48: SSTA observation and prediction scatter plots of the last model for six lead month forecasts at Cook Strait, on the training and test data respectively. The corresponding loss functions from top to bottom are the MSE, the MAE, and the Huber.

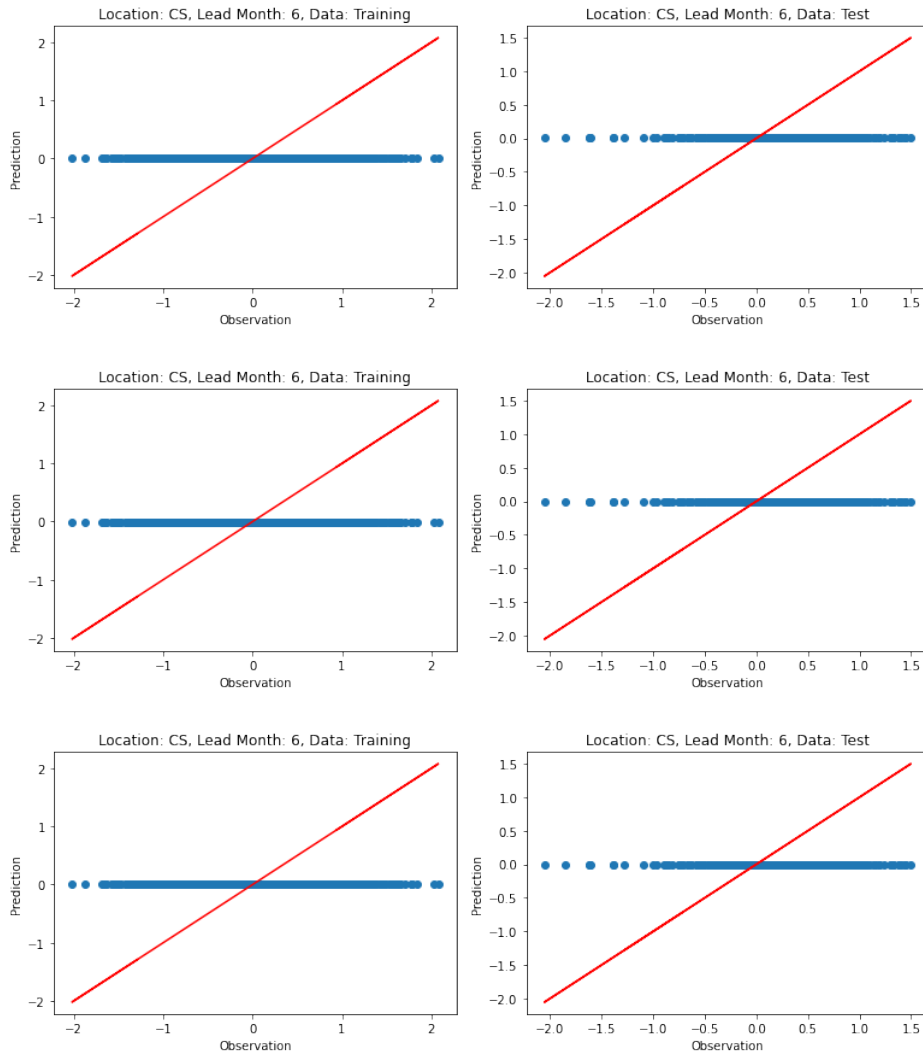


Figure 49: SSTA observation and prediction scatter plots of the last model for six lead month forecasts at Cook Strait, on the training and test data respectively. The corresponding loss functions from top to bottom are the weighted MSE, the focal-R, and the balanced MSE.

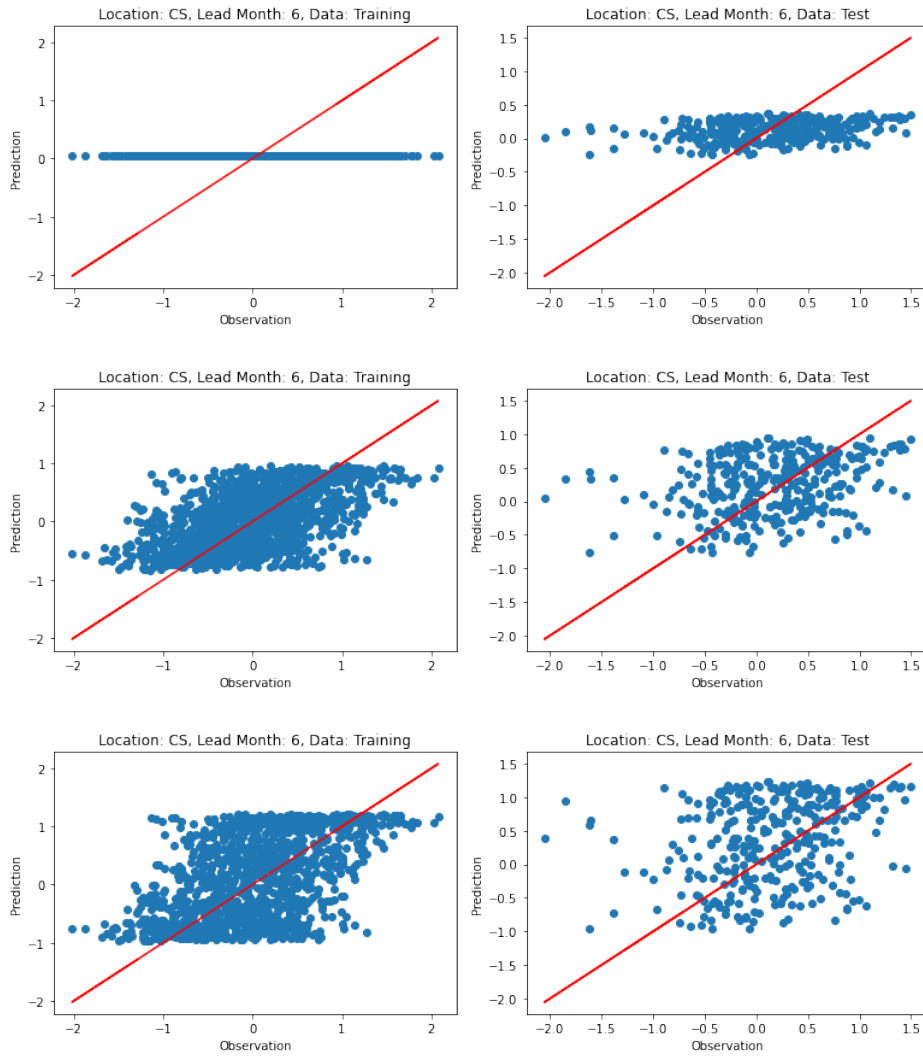


Figure 50: SSTA observation and prediction scatter plots of the last model for six lead month forecasts at Cook Strait, on the training and test data respectively. The corresponding loss function is our proposed scaling-weighted MSE, from top to bottom with the hyperparameters $\alpha = 1.5, \beta = 0.5, \alpha = 2, \beta = 0.5$, and $\alpha = 2, \beta = 1$ respectively.

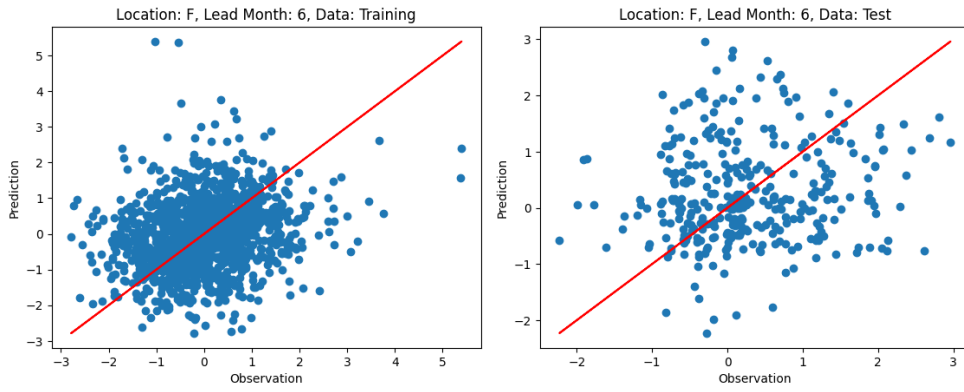


Figure 51: SSTA observation and prediction scatter plots of the six-lag model for six lead month forecasts at Fiordland, on the training and test data respectively.

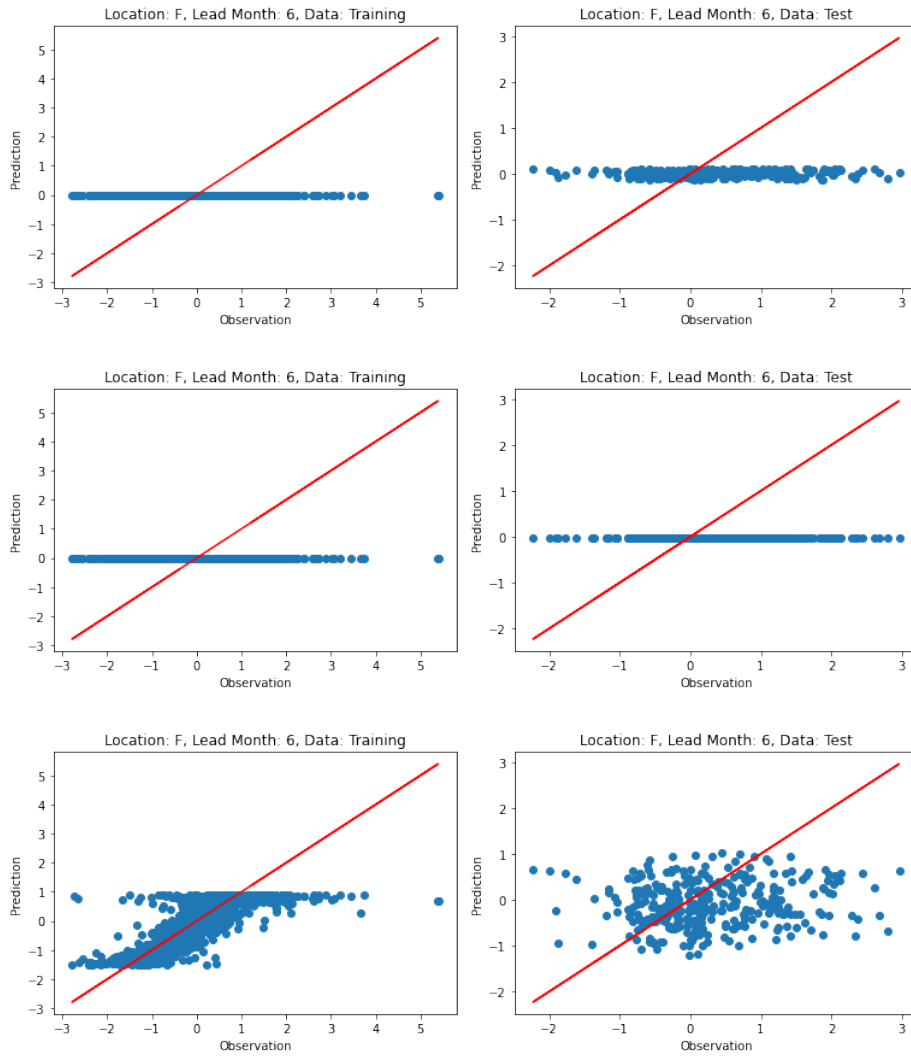


Figure 52: SSTA observation and prediction scatter plots of the last model for six lead month forecasts at Fiordland, on the training and test data respectively. The corresponding loss functions from top to bottom are the MSE, the MAE, and the Huber.

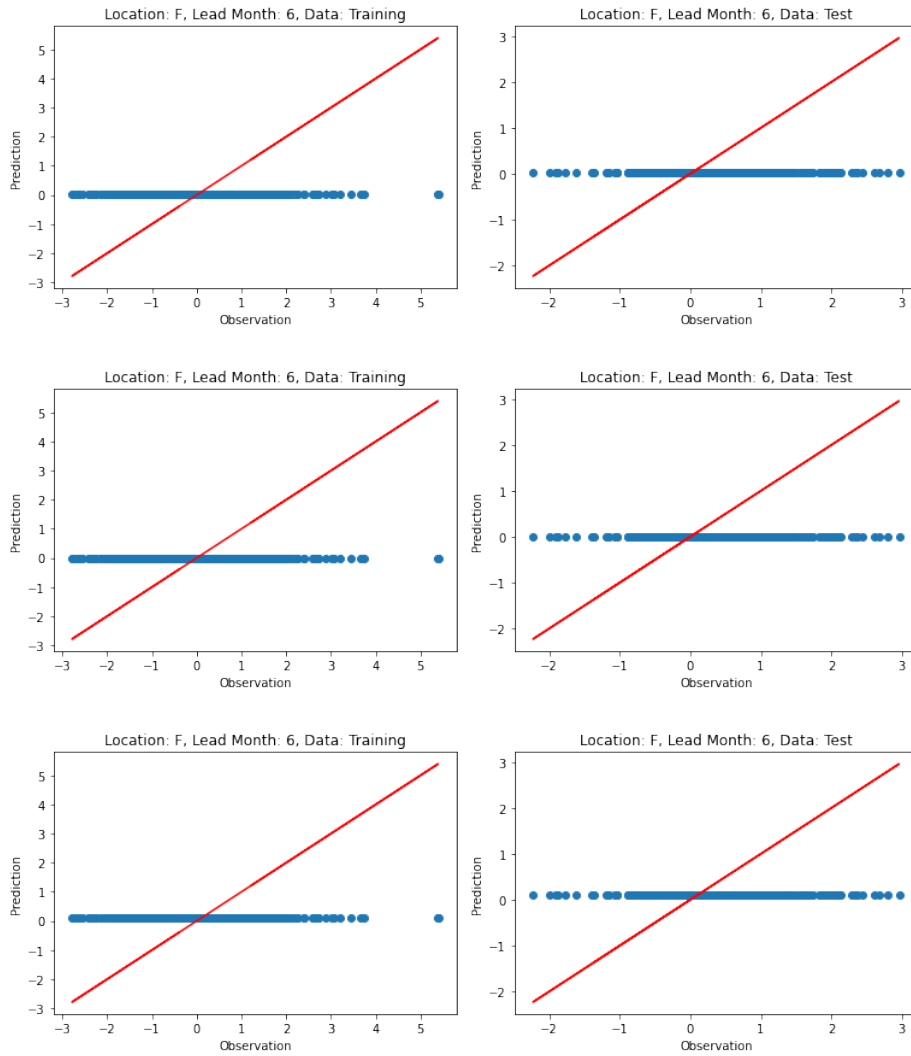


Figure 53: SSTA observation and prediction scatter plots of the last model for six lead month forecasts at Fiordland, on the training and test data respectively. The corresponding loss functions from top to bottom are the weighted MSE, the focal-R, and the balanced MSE.

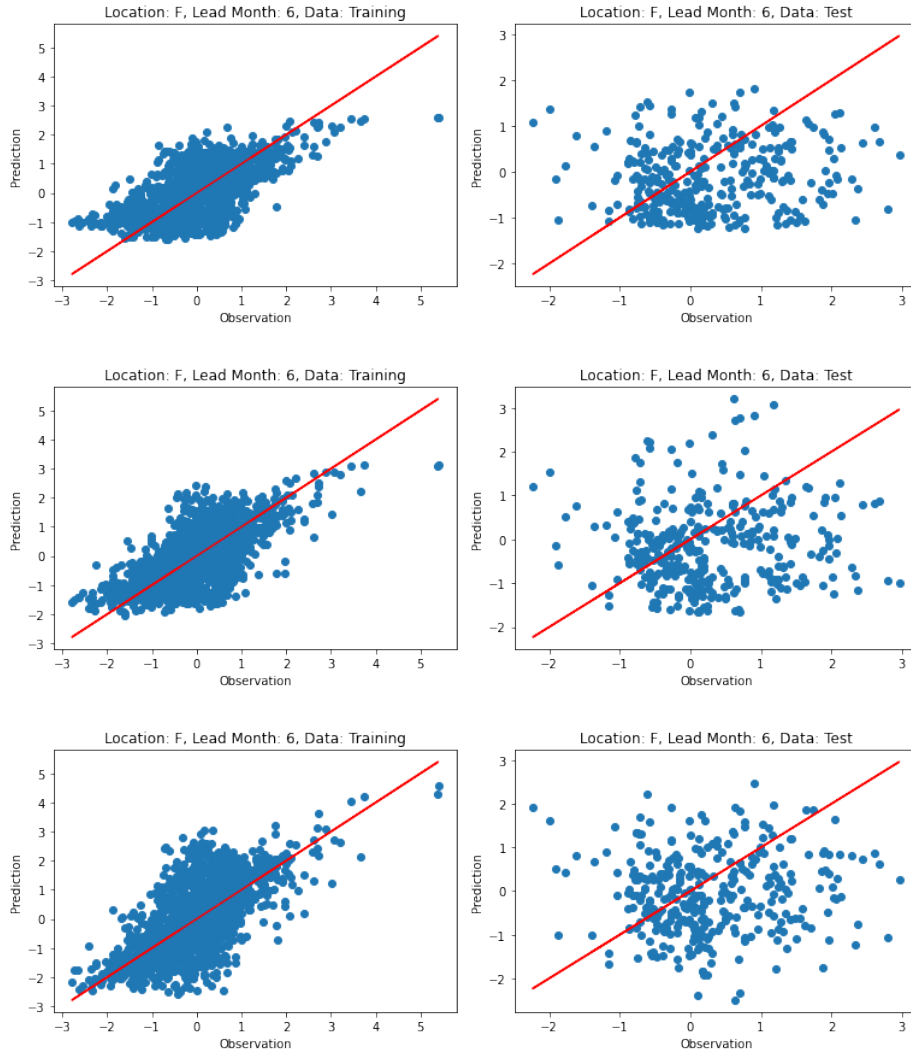


Figure 54: SSTA observation and prediction scatter plots of the last model for six lead month forecasts at Fiordland, on the training and test data respectively. The corresponding loss function is our proposed scaling-weighted MSE, from top to bottom with the hyperparameters $\alpha = 1.5$, $\beta = 0.5$, $\alpha = 2$, $\beta = 0.5$, and $\alpha = 2$, $\beta = 1$ respectively.

A.4 Data Availability

The preprocessed SSTA sequences are stored in the NumPy array files and accessible at <https://drive.google.com/drive/folders/1Nf2CyGK7LpgEgRpCBL0sGqcGcY3Ib040?usp=sharing>.

A.5 Code and Results Availability

The code and results are presented in Jupyter Notebooks and accessible at https://drive.google.com/drive/folders/1z0Hx_BwZL45RnTWCMt3VNZ6bgMugLNQk?usp=sharing.